The Deep and Transient Universe: New Challenges and Opportunities

Scientific prospects of the *SVOM* mission

J. Wei, B. Cordier, et al.
(Version of 05-10-2016, for full list of contributors see overleaf)

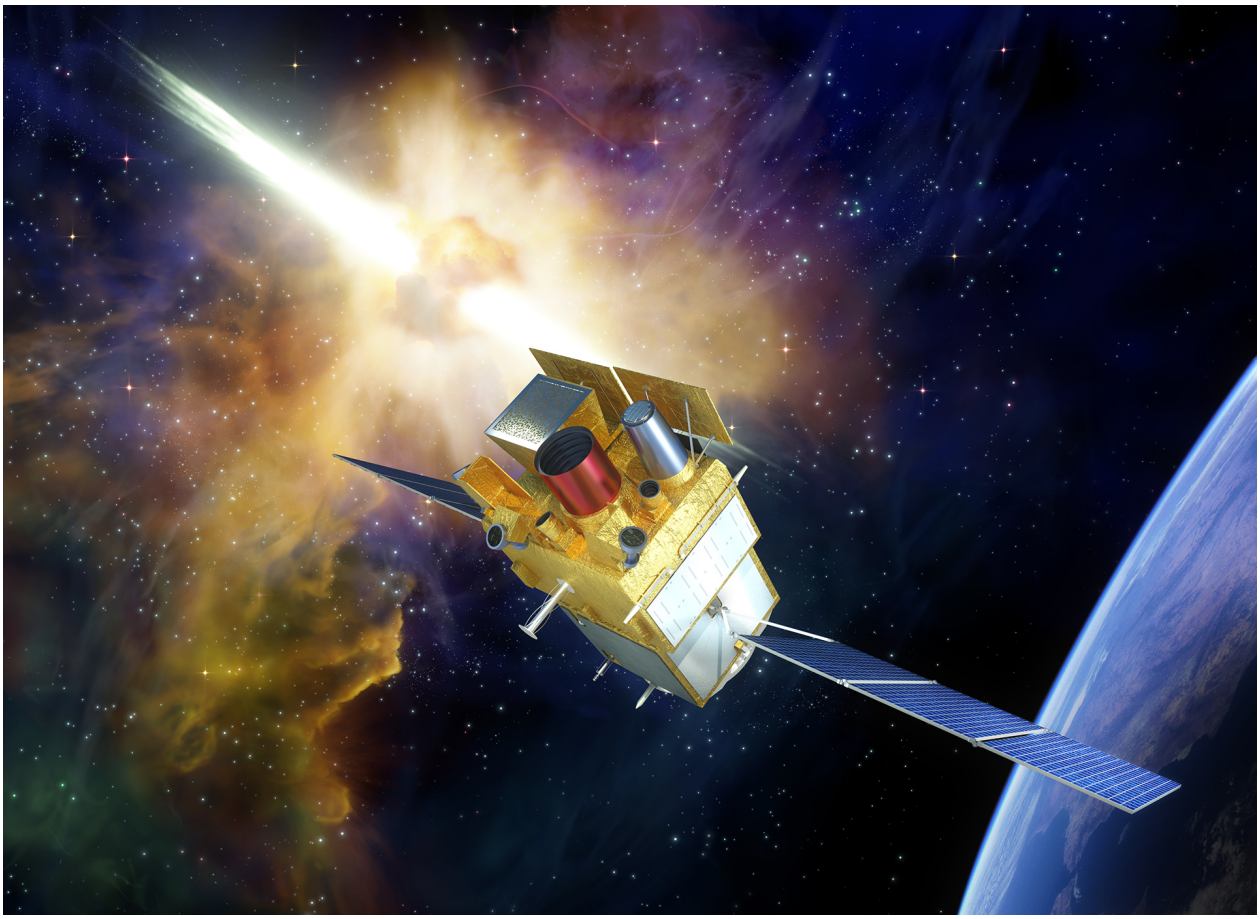

Frontispiece : Artist view of the *SVOM* satellite

Principal Investigators

J. Wei, National Astronomical Observatories/Chinese Academy of Science
20A Datun Road, Beijing, 100012, China

B. Cordier, CEA Saclay, DSM/IRFU/Service d'Astrophysique
91191 Gif-sur-Yvette, France
email: wjy@nao.cas.cn & bertrand.cordier@cea.fr

Contributors

S. Antier, CEA, Saclay, France
P. Antilogus, LPNHE, Paris, France
J.-L. Atteia, IRAP, Toulouse, France
A. Bajat, IRAP, Toulouse, France
S. Basa, LAM, Marseille, France
V. Beckmann, APC, Paris, France
M.G. Bernardini, LUPM, Monpellier, France
S. Boissier, LAM, Marseille, France
L. Bouchet, IRAP, Toulouse, France
V. Burwitz, MPI, Garching, Germany
A. Claret, CEA, Saclay, France
Z.-G. Dai, NJU, Nanjing, China
F. Daigne, IAP, Paris, France
J. Deng, NAOC, Beijing, China
D. Dornic, CPPM, Marseille, France
H. Feng, DEP, Tsinghua University, Beijing, China
T. Foglizzo, CEA, Saclay, France
H. Gao, BNU, Beijing, China
N. Gehrels, NASA, Greenbelt, USA
O. Godet, IRAP, Toulouse, France
A. Goldwurm, APC, Paris, France
F. Gonzalez, CNES, Toulouse, France
L. Gosset, CEA, Saclay, France
D. Götz, CEA, Saclay, France
C. Gouiffes, CEA, Saclay, France
F. Grise, Obs. astron. de Strasbourg, France
A. Gros, CEA, Saclay, France
J. Guilet, MPA, Garching, Germany
X. Han, NAOC, Beijing, China
M. Huang, NAOC, Beijing, China
Y.-F. Huang, NJU, Nanjing, China
M. Jouret, CNES, Toulouse, France
A. Klotz, IRAP, Toulouse, France
O. La Marle, CNES, Toulouse, France
C. Lachaud, APC, Paris, France
E. Le Floch, CEA, Saclay, France
W. Lee, UNAM, Mexico, Mexico
N. Leroy, LAL, Orsay, France
L.-X. Li, KIAA, PKU, Beijing, China
S. C. Li, SECM, Shanghai, China
Z. Li, Dept. of Astronomy, PKU, Beijing, China
E.-W. Liang, GXU-NAOC, Nanning, China
H. Lyu, Guangxi University, Nanning, China
K. Mercier, CNES, Toulouse, France
G. Migliori, CEA, Saclay, France
R. Mochkovitch, IAP, Paris, France
P. OBrien, Dept. of Astronomy, UL, Leicester, UK
J. Osborne, Dept. of Astronomy, UL, Leicester, UK
J. Paul, CEA, Saclay, France
E. Perinati, IAAT, Tübingen, Germany
P. Petitjean, IAP, Paris, France
F. Piron, LUPM, Montpellier, France
Y. Qiu, NAOC, Beijing, China
A. Rau, MPE, Garching, Germany
J. Rodriguez, CEA, Saclay, France
S. Schanne, CEA, Saclay, France
N. Tanvir, University of Leicester, UK
E. Vangioni, IAP, Paris, France
S. Vergani, GEPI, Meudon, France
F.-Y. Wang, NJU, Nanjing, China
J. Wang, NAOC, Beijing, China
X.-G. Wang, GXU-NAOC, Nanning, China
X.-Y. Wang, NJU, Nanjing, China
A. Watson, UNAM, Mexico, Mexico
N. Webb, IRAP, Toulouse, France
J. J. Wei, PMO, Nanjing, China
R. Willingale, Dept. of Astron., UL, Leicester, UK
C. Wu, NAOC, Beijing, China
X.-F. Wu, PMO, Nanjing, China
L.-P. Xin, NAOC, Beijing, China
D. Xu, NAOC, Beijing, China
S. Yu, SECM, Shanghai, China
W.-F. Yu, SHAO, Shanghai, China
Y.-W. Yu, CCNU, Wuhan, China
B. Zhang, UNLV, Las Vegas, USA
S.-N. Zhang, IHEP, Beijing, China
Y. Zhang, SECM, Shanghai, China
X.L. Zhou, NAOC, Beijing, China

Contents

1 Context **6**
- 1.1 Time-domain astrophysics: the discovery space after *Swift* . . . 6
- 1.2 The astronomical panorama in 2020 . . . 6

2 *SVOM* Mission **9**
- 2.1 The *SVOM* mission profile . . . 9
- 2.2 The *SVOM* instruments . . . 11
  - 2.2.1 The soft gamma-ray imager ECLAIRs onboard *SVOM* . . . 12
  - 2.2.2 The gamma-ray spectrometer GRM onboard *SVOM* . . . 12
  - 2.2.3 Combined ECLAIRs and GRM spectroscopy between 4 keV and 5 MeV . . . 13
  - 2.2.4 The ground-based visible telescope array GWAC . . . 13
  - 2.2.5 The X-ray telescope MXT onboard *SVOM* . . . 14
  - 2.2.6 The visible telescope VT onboard *SVOM* . . . 15
  - 2.2.7 The ground-based visible/infrared telescope F-GFT . . . 15
  - 2.2.8 The ground-based visible telescope C-GFT . . . 16
- 2.3 The *SVOM* science ground segment . . . 17
- 2.4 *SVOM*: a highly versatile astronomy satellite . . . 18

3 *SVOM* Advances on GRB Science (*SVOM* core program) **19**
- 3.1 Classical long GRBs: physical mechanisms . . . 19
- 3.2 Classical long GRBs: characterization of the population . . . 22
- 3.3 The diversity of long GRBs: X-ray flashes, underluminous and ultralong GRBs . . . 24
- 3.4 Short GRBs . . . 25
- 3.5 GRBs as particle accelerators . . . 28
- 3.6 *SVOM* and the high-redshift universe . . . 30
  - 3.6.1 GRBs to probe reionization . . . 31
  - 3.6.2 The galaxy luminosity function in the era of reionization . . . 33
  - 3.6.3 The escape fraction of ionizing radiation . . . 34
  - 3.6.4 Catching PopIII stars . . . 34
- 3.7 The cosmic Star Formation Rate evolution . . . 35
- 3.8 Studies of GRB host galaxies . . . 37
  - 3.8.1 GRBs as probes of star-forming processes and physical conditions in very young stellar environments . . . 37
  - 3.8.2 Absorptions in afterglow spectra . . . 39
- 3.9 Cosmology and fundamental physics . . . 40
  - 3.9.1 Could GRBs be used as standard rulers ? . . . 40
  - 3.9.2 Variation of fundamental constants . . . 42

4 *SVOM* Advances on Rapid Follow-Up Observations (*SVOM* ToO program) **43**
- 4.1 Introduction . . . 43
- 4.2 Search for *SVOM* counterparts to multi-wavelength triggers . . . 44
- 4.3 Search for *SVOM* counterparts to multi-messenger triggers . . . 44
  - 4.3.1 Gravitational waves . . . 45
  - 4.3.2 Neutrinos . . . 45
  - 4.3.3 High Energy Photons . . . 46

5 *SVOM* Advances on Observatory Science (*SVOM* general program) 48
5.1 Active Galactic Nuclei 48
5.2 Ultra Luminous X-ray Sources and Tidal Disruption Events 49
5.3 Galactic sources 50
5.3.1 Accreting systems 50
5.3.2 Pulsars and magnetars 51
5.3.3 Flaring stars 52
5.4 Exoplanets and Solar System bodies 53
5.5 Additional science opportunities 53

EXECUTIVE SUMMARY

To take advantage of the astrophysical potential of Gamma-Ray Bursts (GRBs), Chinese and French astrophysicists have engaged the *SVOM* mission (Space-based multi-band astronomical Variable Objects Monitor), aiming to:

- permit the detection of all known types of GRBs,
- provide fast, reliable GRB positions,
- measure from visible to MeV the spectral shape of the GRB prompt emission,
- measure from visible to MeV the temporal properties of the GRB prompt emission,
- quickly identify the afterglows of detected GRBs at X-ray and visible wavelengths, including those which are highly redshifted (z>5),
- measure from visible to X-rays the spectral shape of the early and late GRB afterglow,
- measure from visible to X-rays the temporal evolution of the early and late GRB afterglow.

Major advances in GRB studies resulting from the synergy between space and ground observations, the *SVOM* mission implements space and ground instrumentation. The space segment includes:

- a wide field-of-view hard X-ray imager and spectrometer,
- a wide field-of-view soft gamma-ray spectrometer,
- a narrow field-of-view low-energy X-ray telescope,
- a narrow field-of-view visible/near infrared (NIR) telescope. The ground segment includes:
- two follow-up telescopes (one of which featuring efficient NIR capabilities),
- an array of wide field-of-view visible cameras.

The scientific objectives of the mission put a special emphasis on two categories of GRBs: very distant GRBs at z>5 which constitute exceptional cosmological probes, and faint/soft nearby GRBs which allow probing the nature of the progenitors and the physics at work in the explosion. These goals have a major impact on the design of the mission: the on-board hard X-ray imager is sensitive down to 4 keV and computes on line image and rate triggers, and the follow-up telescopes on the ground are sensitive in the NIR.

At the beginning of the next decade, *SVOM* will be the main provider of GRB positions and spectral parameters on very short time scale. The *SVOM* instruments will operate simultaneously with a wide range of powerful astronomical devices. This rare instrumental conjunction, combined with the relevance of the scientific topics connected with GRB studies, warrants a remarkable scientific return for *SVOM*.

In addition, the *SVOM* instrumentation, primarily designed for GRB studies, composes a unique multi-wavelength observatory with rapid slew capability that will find multiple applications for the whole astronomy community beyond the specific objectives linked to GRBs. For example, the *SVOM* mission has been conceived to promptly scrutinize the celestial fields where sources have been detected by wide field-of-view astronomical devices such as the upgraded generation of gravitational wave detectors (advanced Virgo/LIGO) and high-energy neutrino detectors (KM3NeT, IceCube).

The following pages list the scientific themes that will benefit from observations made with *SVOM*, whether they are specific GRB topics, or more generally all the issues that can take advantage of the multi-wavelength capabilities of *SVOM*.

1 Context

1.1 Time-domain astrophysics: the discovery space after *Swift*

Astronomy is truly undergoing a revolution in terms of our ability to monitor the time-variability of the Universe in a continuous way using new facilities coupled with fast computers. The opening up of the temporal domain is transforming our knowledge of how the Universe evolves, particularly for objects which are undergoing explosive change, such as a supernova or a Gamma-ray Burst (GRB), e.g. Kumar & Zhang (2015). These explosive events can release enormous amounts of power both in electromagnetic radiation and in non-electromagnetic forms such as neutrinos and gravitational-waves and test our understanding of the laws of physics under the most extreme conditions.

Observing facilities which are currently on-line enable the sky to be monitored fairly continuously in real-time over large areas and across the electromagnetic spectrum, capturing the temporal behaviour of the Universe in a way previously unattainable. Examples facilities include the LOFAR radio telescope (van Haarlem et al., 2013), the Pan-STARRs optical facility (Chambers et al. in preparation) and the *Swift* (Gehrels et al., 2004) and *Fermi* high-energy satellites. Non-electromagnetic facilities are also now observing, particularly the Advanced LIGO-VIRGO gravitational-wave observatory (LIGO Scientific Collaboration et al., 2015), which recently found its first source (Abbott et al., 2016b), and the IceCube neutrino experiment (Aartsen et al., 2015a). The data from all these facilities have already opened up the temporal domain, but are just a foretaste of what is to come.

Many of the previously developed theories have come under intense strain by new observational results, such as the highly variable emission seen at late times in GRBs, the discovery of extremely luminous supernovae and the unexplained fast radio bursts (Lorimer et al., 2007). Theoretical models predict a variety of exotic explosions and stellar mergers, together with their multiple signatures across the electromagnetic spectrum. Theory also predicts that some will be accompanied by gravitational wave, neutrino and high-energy particle emission. The provision of *SVOM* in the next decade will coincide with the multi-messenger era and will provide a critical element of the era of time-domain astronomy both by finding transients and by following-up those from other facilities.

In the period when *SVOM* will fly, the number of transients found will increase by several orders of magnitude as even more powerful facilities come on-line, in particular the Large Synoptic Survey Telescope (LSST, LSST Science Collaboration et al. 2009) and the Square Kilometre Array (SKA). The sheer grasp of the new facilities, which will produce thousands of alerts per day from variable or transient sources, mean we will require super-computers to process the data in real-time and smart algorithms to broker which transients to focus on with follow-up facilities. The importance of the temporal domain has been recognised in recent reports by the Chinese Space and Technology Roadmap (Guo & Wu, 2010), the European Union ASTRONET group (Bode, 2015) and the USA National Research Council Decadal Survey (Committee for a Decadal Survey of Astronomy and Astrophysics, 2010).

While we can confidently predict the importance of *SVOM* data based on current observations, time domain experiments often make their most startling discoveries in unexpected and serendipitous ways. This has certainly been the experience from the *Swift* mission and Pan-STARRSs, for example. The power of *SVOM* combined with the grasp of the future facilities will without doubt stimulate a new revolution in astronomy.

1.2 The astronomical panorama in 2020

The astronomical panorama of the next decade will be shaped by new instruments developed to address various outstanding questions raised by present day astrophysics. This panorama encompasses large radio, infrared, visible and gamma-ray telescopes, advanced gravitational wave interferometers and neutrino detectors of the km^3 class (Fig. 1), as well as simulations with powerful computers. These instruments will revolutionize our understanding of astrophysics in fields as diverse as the first ages and the reionization of the universe, the nature of the dark universe (dark matter and dark energy), the demography and role

of black holes, exoplanets and planetary formation, and fundamental physical processes. Young fields, like Time Domain Astronomy and Multi-Messenger Astrophysics are also expected to grow very fast, bringing new discoveries.

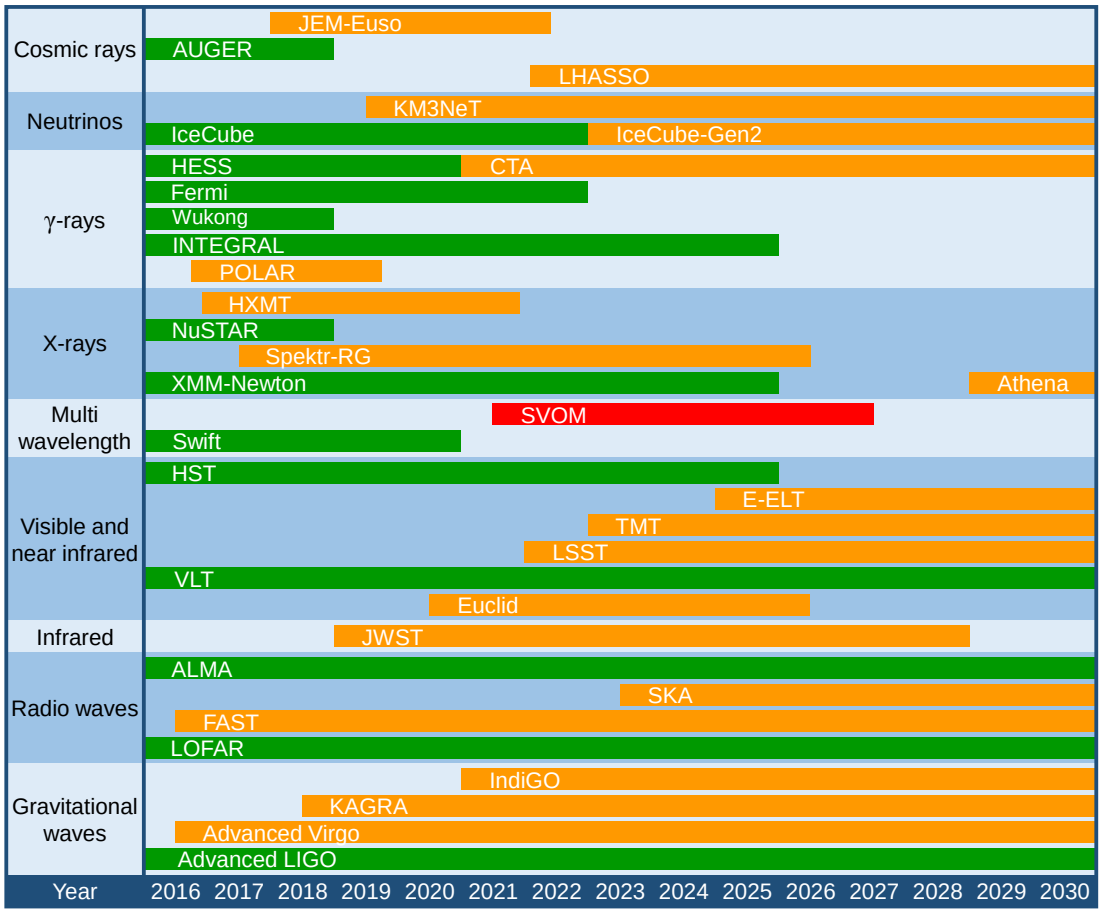

Figure 1: The observational panorama in the *SVOM* era.

In this panorama, *SVOM* is expected to offer two unique capabilities, which are currently being provided by *Swift*: monitoring the hard X-ray sky for high-energy transients and doing multi-wavelength follow-up of self-triggered high-energy transients and remarkable transients detected with other facilities (upon ToO request). We have selected below some topics that will undoubtedly benefit from a close collaboration between *SVOM* and other astronomical facilities.

A universe of black holes: *SVOM* will provide crucial information on transient black hole (BH) activity. The follow-up of a majority of *SVOM* detected transients with large optical and radio telescopes on the ground, will permit measuring the history of stellar mass BH formation up to redshift z=10 and compare it with the star formation rate. *SVOM* will also increase the statistics on Tidal Disruption Events (TDEs), providing a better understanding of dormant massive BHs at the center of galaxies, while the optical to gamma-ray energy coverage of *SVOM* will permit a better understanding of the physics at work in Active Galactic Nuclei (AGNs), especially blazars.

The sources of gravitational waves: *SVOM* will benefit from the operation of advanced gravitational wave (GW) detectors to explore the zoo of transient GW sources. These studies can elucidate the origin of short GRBs, identify which GRBs are coming from binary mergers and constrain their beaming

angle. *SVOM* will also help GW detectors to identify low significance signals from binary mergers.

The epoch of reionization: GRBs provide unique glimpses into the epoch of reionization ($z \geq 6$), for instance they permit studying small high redshift galaxies, which cannot be observed by other means. They also have the potential to constrain the contribution of massive stars to the reionization of the universe and tell us if the first stars (population III) produce GRBs. These studies, which rely on early measures of the optical spectra of GRBs beyond z=6, emphasize the need to recognize high-z GRBs quickly, a task that will be eased by sensitive follow-up with *SVOM* narrow-field instruments.

Physics of relativistic jets: The physics of accretion/ejection is a fundamental problem in astrophysics. High-energy galactic transients, GRBs and AGNs offer complementary ways to capture the dynamic of this process. With built-in multi-wavelength capabilities and a close collaboration with radio and VHE telescopes on Earth, *SVOM* will observe transient activity from galactic and extragalactic relativistic jets, providing insight into their nature, origin, acceleration mechanism and radiation processes, with impacts on our understanding of the origin of VHE cosmic-rays. *SVOM* observations will benefit from complementary observations of GRB jets. Polarimetry of the prompt emission (e.g. POLAR) will bring crucial insight into the magnetic field configuration of GRB jets, while km^3 neutrino detectors (ICECUBE, KM3Net) may provide unique clues on the nature and energy content of relativistic jets (hadronic vs leptonic or magnetically dominated).

GRB progenitors: Our understanding of GRB progenitors will make great progress with *SVOM*. The low energy threshold of *SVOM* will permit the detection of nearby XRFs, clarifying the connection between "core-collapse GRBs" and SNIbc. The frequency of orphan afterglows detected with the LSST will permit measuring the true GRB rate and establishing meaningful comparison with the rate of SNIbc. Regarding short GRBs, they will benefit from a double diagnostic: GW interferometers will be crucial for the identification of "merger GRBs" among *SVOM* triggers, while optical observations with VT will permit the early detection of optical afterglows and searches for kilonova emission.

Galactic monsters: The low energy threshold of ECLAIRs will permit the detection of thousands of transients from flare stars, white dwarves (novae), galactic neutron stars (X-ray bursters and magnetars) and active black holes (microquasars), and their detailed follow-up with MXT and VT. *SVOM* observations, will permit powerful diagnostic of many important physical processes at work in stellar flares, nuclear burning on neutron stars and white dwarves, accretion/ejection or the origin of magnetar activity, especially if they are part of multi-wavelength campaigns involving ground based radio, NIR and VHE telescopes.

Other transients: In the next decade, many astronomical instruments will monitor the sky for transients. In the visible sky, LSST will detect each year dozens of orphan GRB afterglows and thousands of luminous supernovae and tidal disruption events, and much closer to us, thousands of gravitational lensing events in our galaxy. In radio, we anticipate the detection of thousands of fast radio bursts. For the most interesting events, *SVOM* may act as a follow-up machine combining X-ray and optical sensitivity, fast response (hours) and high availability.

In conclusion, it is clear that the highest benefit of *SVOM* will be obtained in collaboration with the large astronomical facilities existing in the 2020 decade. These collaborations will go in both directions: large facilities observing *SVOM* high-energy transients, and *SVOM* observing remarkable transients discovered by other facilities, with its narrow field telescopes. The scientific outcome anticipated from such collaborations fully justifies efforts to establish strong collaborations well in advance.

2 *SVOM* Mission

2.1 The *SVOM* mission profile

The *SVOM* satellite will be launched by a Chinese launcher LM-2C from Xichang and will be inserted into a Low Earth Orbit with an inclination of 30^o, an altitude of 625 km and an orbital period of ∼96 min. With these parameters the satellite passes through the South Atlantic Anomaly several times per day, inducing an overall dead-time of 13 to 17%.

SVOM (Fig. 2) carries two wide field of view (FoV) high-energy instruments: a coded-mask gamma-ray imager (ECLAIRs), and a gamma-ray spectrometer (GRM), and two narrow field telescopes: a Microchannel X-ray Telescope (MXT) and a Visible-band Telescope (VT). The *SVOM* ground segment includes additional instruments: a wide angle optical camera (GWAC) monitoring a part of the ECLAIRs FoV in real-time, and two 1-m-class robotic follow-up telescopes (the GFTs).

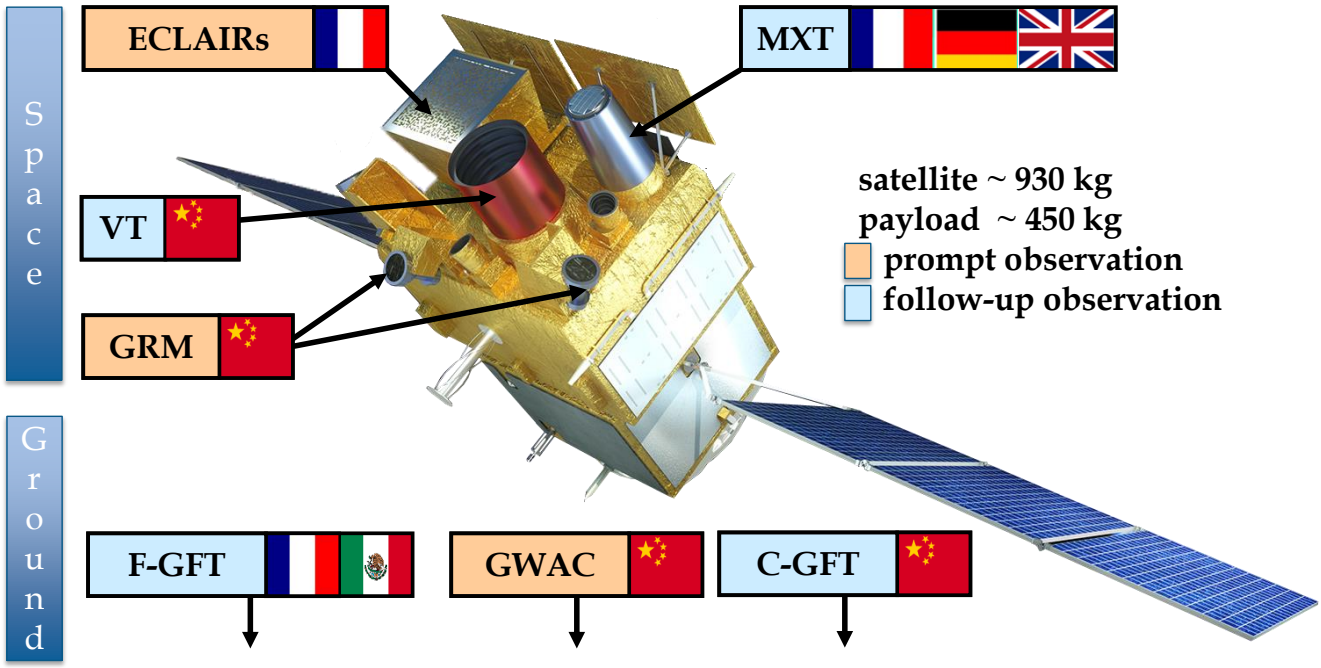

Figure 2: View of the *SVOM* space-based and ground-based instruments.

In order to facilitate redshift measurements of the GRBs detected by *SVOM*, the satellite attitude will follow a predefined orientation, called B1 attitude law. Most of the year the optical axis of the *SVOM* instruments will be pointed 45^o offset from the anti-solar direction. This pointing includes avoidance periods in order to exclude the Sco-X1 source and the galactic plane from the ECLAIRs field of view. An additional constraint favors areas of the sky observable by large telescopes located in Chile, Hawaï and Canary Island. This strategy ensures that *SVOM* GRBs will be detected towards the night hemisphere, quickly observable from ground by large telescopes, and optimizes the chances to detect the GRB counterparts and host galaxies. More details on the *SVOM* pointing strategy can be found in Cordier et al. (2008).

As a consequence of the Low-Earth Orbit combined with a roughly anti-solar attitude law, the Earh occults each orbit the FoV of the *SVOM* instruments. The mean duty cycle is about 65% for ECLAIRs and 50% for the narrow-FoV instruments MXT and VT.

Most often the *SVOM* pointing follows the B1 attitude law (Fig. 3), waiting for a GRB. When ECLAIRs triggers on a GRB event, it communicates its position to the spacecraft, which slews autonomously within minutes to the source for rapid follow-up observations of the GRB afterglow emission

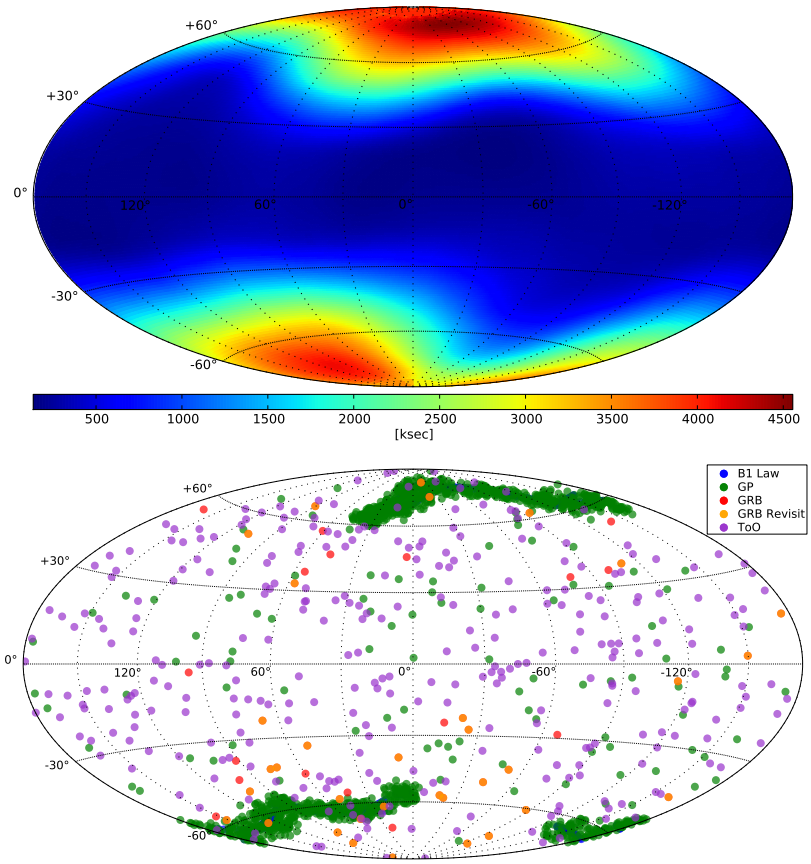

Figure 3: Scenario of 1 year of observation following the B1 attitude law, simulating 65 GRBs, and one ToO per day. (Up) Sky exposure in ksec and in galactic coordinates for the ECLAIRs telescope (wide FoV). (Bottom) Map in galactic coordinates of the *SVOM* pointing direction for the same scenario, corresponding to the targets observed by the VT and MXT (narrow FoV).

with the MXT in X-rays and the VT in the visible band. The satellite stays pointed towards the source for 14 orbits (∼1 day). The GRB position and its main characteristics determined by ECLAIRs are also quickly sent to the ground using the *SVOM* VHF emitter. Refined positions of the X-ray counterpart detected by MXT are also down-linked via VHF. The VHF signal is received by one of the 40 to 50 ground stations, distributed on Earth under the satellite track. The system design ensures that 65% of the alerts are received within 30 s at the Science Centers, which forward them via internet (using the GCN and VOEvent networks) to the *SVOM* ground instruments (GWAC and GFTs) and to the scientific community.

The Core Program of the mission covers all *SVOM* observations related to the detection and characterization of the prompt and afterglow emission of GRBs. With an expected GRB rate of around 60-70 per year, the Core Program accounts for about 25% of the useful mission time.

The Target of Opportunity (ToO) program of *SVOM* manages unplanned observations of transient and variable sources programmed from the ground. All scientists will have the opportunity to apply for ToOs, evaluated by the PIs. Accepted observations are performed immediately by the *SVOM* ground instruments, and within some delay by the *SVOM* space instruments, depending on the availability of the satellite up-link stations. Observations are performed within 48 h for a standard ToO, and within 12 h for an exceptional ToO (e.g. galactic supernova or GW alert) using on request additional stations. The typical observation duration is 1 orbit (45 min useful time) for a standard ToO, and 14 orbits (∼10 h)

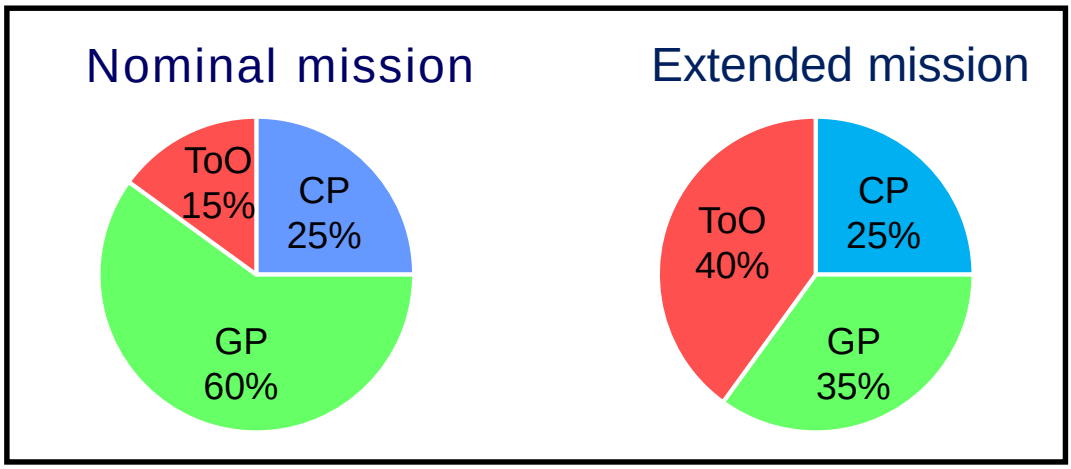

Figure 4: Allocated observation-time fraction for the three *SVOM* scientific programs : Core Program (CP), Target of Opportunity Program (ToO), General Program (GP). The extended mission (3 years after the launch) involves a higher ToO fraction and more GP time outside the B1 law (from 10% to 50%).

for an exceptional ToO. A significant portion of the useful time, 15% at the beginning of the mission, is foreseen for ToO observations.

The General Program (GP) of *SVOM* is devoted to pre-planned observations and complements the transient sky observations managed by the Core Program and ToOs. The GP is built taking into account the system requirements of the GRB program, in particular the pointing strategy that optimizes the ground follow-up of *SVOM* GRBs. Therefore the GP allows pointing at sources close (i.e. within 5^o to 10^o) to the B1 attitude law. In order to increase the scientific interest of the GP, it is foreseen to allow observations outside the B1 constraint during 10% of the GP useful time. The minimal duration of a GP observation is 1 orbit ($\sim$45 min). The GP is open to all scientists responding to *SVOM* calls for observation proposals, issued every year, and evaluated by a Time Allocation Committee based on their scientific merit.

In order to contribute to the opening-up of the time-domain astronomy scheduled for the next decade, an evolution of the *SVOM* time allocation is planned (Fig. 4), increasing the ToO-time from 15% to 40%, allowing for 5 instead of 1 ToO per day. In the same time the GP useful time permitted outside the B1 constraint increases from 10% to 50%.

The scientific products of the GRB Core Program and the ToOs are made public as soon as available. GP data remain restricted during 1 year to the PI of each accepted proposal, after which they become public.

2.2 The *SVOM* instruments

The *SVOM* spacecraft consists of two wide-field instruments: ECLAIRs and the Gamma-Ray Monitor (GRM) for the observation of the prompt emission and two narrow field instruments: the Micro-channel X-ray Telescope (MXT) and the Visible Telescope (VT) for the observation of the afterglow emission. *SVOM* has also two sets of ground dedicated-instruments: a wide-field instrument GWAC for the observation of the optical prompt emission, and narrow-field instruments GFT for the follow-up observations in the visible and near-infrared domain. This section describes individually each *SVOM* instrument.

2.2.1 The soft gamma-ray imager ECLAIRs onboard *SVOM*

The main goal of the hard X-ray coded-mask imager ECLAIRs [1], operating in the 4-150 keV energy range, is the detection and fast localization of hard X-ray transients onboard *SVOM*. Its low energy threshold of 4 keV will open to *SVOM* the realm of extragalactic soft X-ray transients, such as X-Ray Flashes or SN shock breakouts, which are still poorly explored.

Coded-mask imaging is very efficient to survey large fractions of the hard X-ray sky, as demonstrated by instruments such as *INTEGRAL*/ISGRI and *Swift*/BAT (Lebrun et al., 2003; Barthelmy et al., 2005). The ECLAIRs detection plane is made of 6400 pixels of CdTe (4×4 mm^2, 1-mm thick) and its read-out electronics. A 54×54 cm^2 coded mask with 40% open fraction is located 46 cm above the detection plane to define a FoV of 2 sr (zero coded FoV) and a point spread function of 52 arcmin (FWHM). A passive lateral Pb/Al/Cu-layer shield blocks the hard X-ray radiation originating from outside the FoV.

The on-board management and scientific trigger electronics (UGTS) configures the instrument and searches for new transient sources within reconstructed sky images of the ECLAIRs FoV, and alerts in near-real time the satellite about their localization. Hard X-ray transients are identified as count-rate excesses on the detection plane (monitored on time scales from 10 ms to about 10 s on 4 energy bands and in 9 detector zones) followed by their sky imaging, or directly as new sources in sky images constructed cyclically (on time scales from 10 s to about 1300 s). The UGTS stores each detected pixel-hit to mass memory, allowing detailed on-ground data analysis, among which offline searches of additional transients sources.

ECLAIRs has been optimized taking into account the limited resources (mass, power, volume) available on the *SVOM* spacecraft, which allow a sensitive area of 1000 cm^2 and a point source localization error (PSLE) better than 12 arcmin (for 90% of the sources at detection limit). Major challenges are the 4 keV energy-threshold and the on-board detection of transients on top of a strongly varying background (of about 3000 counts/s), modulated by the SAA passages and the Earth transit through the FoV every orbit. Detection-plane prototype measurements and simulations performed with the trigger software implemented suggest that those challenges are met by the instrument design (Antier et al., 2015; Godet et al., 2014a; Lacombe et al., 2014; Nasser et al., 2014; Schanne et al., 2014; Zhao et al., 2012), and predict a detection each year of 60 GRBs, several non-GRB extragalactic transients, dozens of AGNs and hundreds of galactic X-ray transients and persistent sources. Detailed descriptions of ECLAIRs are provided in a series of articles: Schanne et al. (2015); Godet et al. (2014a); Lacombe et al. (2014); Le Provost et al. (2014); Schanne et al. (2014).

2.2.2 The gamma-ray spectrometer GRM onboard *SVOM*

The Gamma-Ray Monitor[2] (GRM) will contribute to GRB-related studies including a) GRB physics of progenitor, jet mechanism and components, energy dissipation mechanism and radiation mechanism, b) Multi-messenger studies through gravitational waves, neutrinos and high-energy cosmic rays, c) Cosmology and fundamental physics. In addition GRM will contribute to Terrestrial Gamma-ray Flashes (TGFs) studies by taking advantage of its low Earth orbit, wide FoV and energy range up to several MeV.

GRM consists of three detection modules (GRDs), each made of a NaI(Tl) scintillating crystal, a photomultiplier and its readout electronics. Each GRD has an area of 200 cm^2, thickness of 1.5 cm, FoV of ± 60 degrees with respect to its symmetry axis, dead time <8 μs, temporal resolution <20 μs and energy resolution of 16% at 60 keV. A plastic scintillator in front of the NaI(Tl) crystal is used to distinguish low energy electrons from gamma-rays. The 3 GRD-modules point at different directions to form a combined FoV of 2 sr, matching the ECLAIRs one, within which a rough localization ($\sim \pm 5^o$) of transient sources can be achieved onboard. The energy range of the GRM is 15-5000 keV, extending towards high energies the range of ECLAIRs to measure E_{peak} for a large fraction of *SVOM* GRBs. We expect that GRM

[1] institutes: APC Paris, CNES Toulouse, IAP Paris, IRAP Toulouse, IRFU/CEA Saclay, LUPM Montpellier (France)
[2] institute: IHEP Beijing (China)

will detect >90 GRBs/yr. GRM has a good sensitivity to short/hard GRBs, similar to GBM on *Fermi*. GRM generates by itself onboard triggers, whose time and crude localization is transferred to ECLAIRs for trigger enhancement, and to ground facilities (e.g. GWAC, GW experiments) for joint observations.

A calibration detector (GCD) containing a ^{241}Am isotope is installed on the edge of each GRD for gain monitoring and energy calibration. In addition a charged particle monitor (GPM) will help to announce SAA entries and serve to protect the detection modules.

2.2.3 Combined ECLAIRs and GRM spectroscopy between 4 keV and 5 MeV

The combined ECLAIRs and GRM dataset will allow a complete study of each GRB's prompt high-energy emission, from 4 keV to a few MeV, including characterization of its spectral shape. Recent observations of prompt phases of GRBs in gamma-rays with *Fermi*/GBM have revealed a complexity in their spectral shape, going beyond a simple phenomenological Band function (two smoothly connected power laws, (Band et al., 1993)), with the necessity to include an additional hard power law (Ackermann et al., 2013a; Guiriec et al., 2010a; Ackermann et al., 2010; Abdo et al., 2009), whose extrapolation to low energy has also been observed in a few cases (Tierney et al., 2013), or a thermal emission component (Guiriec et al., 2011a, 2013). A GRB population simulation, based on the *Fermi/GBM* spectral catalog (Gruber et al., 2014a) and on specific GRBs with remarkable spectral characteristics, shows that the combination of ECLAIRs and GRM will constrain the spectral parameters (SED peak energy, spectral slopes, kT, etc.) with good precision, providing direct insights on the prompt emission mechanisms (e.g. Ghirlanda et al. 2003).

2.2.4 The ground-based visible telescope array GWAC

The Ground-based Wide Angle Camera system[3] (GWAC) of *SVOM* is designed to observe in the visible domain the prompt phase of *SVOM* GRBs. During this phase, in which most of the energy is emitted in γ-rays, observations of emission at other wavelengths, particularly in the visible, are believed to provide clues to the understanding of the jet composition, as well as the energy dissipation, particle acceleration and radiation mechanisms. Up to now, only in a few cases prompt emission has been observed from visible to γ-rays, e.g. in the naked-eye burst GRB080319B (Racusin et al., 2008) and GRB130427A (Vestrand et al., 2014) and a larger sample promises to revolutionize the understanding of GRB physics. To do so, simultaneous observations at high cadence in visible and γ-rays are needed throughout the prompt and into the early afterglow phase.

GWAC is designed to observe more than 12% of *SVOM* GRBs in the visible band from 5 min before to 15 min after the trigger. For a high observation efficiency, the total GWAC array will comprise 36 camera units, covering a total FoV of 5400 sq. deg. For a significant detection efficiency, the sensitivity (at 5σ for 10 s exposures) will reach a limiting magnitude M_V=15 under full Moon condition (M_V=16 for new Moon). Each camera unit will have an effective aperture size of 18 cm, a 4096×4096 E2V back-illuminated CCD, operating in the 0.5 to 0.85 μm band, and a FoV of 150 sq. deg, providing source localizations of 11 arcsec in 13 s exposure images. GWAC will be saturated for objects brighter than M_V=11.

A prototype version, the Mini-GWAC, is designed to observe bright GRBs, using 12 camera units covering about 5200 sq. deg, in which each camera has an aperture of 7 cm and a FoV of ∼440 sq. deg, reaching M_V=11.5 under full Moon (M_V=12.5 for new Moon), providing source localizations of 30 arcsec in 15 s exposure images.

Both GWAC and Mini-GWAC search for optical transients in real time around the trigger coordinates from ECLAIRs, GRM, MXT, VT, GFTs, and other instruments.

Considering their super-large FoV and short cadence exposures, GWAC and Mini-GWAC are powerful instruments for searching short-time scale optical transients, such as counterparts of gravitational wave events, early phases of supernovae, counterparts of neutrino events, flare stars, near-Earth objects, etc.

[3]institute: NAOC Beijing (China)

GWAC and Mini-GWAC have also the capability to detect optical transients by themselves without external triggers. Two 60 cm telescopes and several 30 cm telescopes will be setup beside to follow-up optical transient candidates detected by GWAC and Mini-GWAC, in order to check if they are real or false events, providing coordinates with ∼1 acrsec accuracy, and delivering multi-band light-curves for confirmed transients.

Both GWAC and Mini-GWAC have three observing modes. A first observing mode, designed for GRB prompt emission studies, points the cameras to the FoV of ECLAIRs and tracks the stars. In a second mode, designed to follow-up ToO requests, one or several cameras are pointed promptly to each accepted ToO target. In a third mode, an even larger FoV is surveyed, by scanning several areas cyclically with each camera.

The GWAC, Mini-GWAC and follow-up telescopes will be divided into two sets, each of which having 18 GWAC cameras, 6 Mini-GWAC cameras, one 60 cm telescope, and several 30 cm telescopes. As a baseline, one set will be setup at Ali observatory, China, the other one at CTIO, Chile.

2.2.5 The X-ray telescope MXT onboard *SVOM*

The Microchannel X-ray Telescope[4] (MXT) is a very light (∼35 kg), and compact (∼1.2 m) focusing X-ray telescope operating in the 0.2-10 keV energy range. With its sizable FoV for a pointed instrument (64×64 arcmin^2) and its sensitivity below the mCrab level, MXT will identify X-ray transients in non-crowded fields, localize them to sub-arcmin precision, and provide detailed X-ray spectra. The MXT subsystems are the optics based on square micro-channels, camera, carbon fiber structure, data processing unit, and radiator. For more details on the MXT instrument see Götz et al. (2014).

The optics of MXT uses a "Lobster Eye" geometry, as first defined by Angel (1979), and optimized for narrow-field use. Grazing incident X-rays are reflected within the square pores (40 μm side) of the square micro-pore optics plates (MPOs, 40 mm side, 1-2 mm thickness). The MPOs, produced by Photonis, are spherically slumped to a radius twice the focal length of MXT, and coated with Ir. The optics focal length is 1 m. Its front part is coated with 70 nm of Al for thermal insulation and to reduce the optical load on the detector. The MPO Point Spread Function (PSF) is composed by a central spot and two cross arms: about 50% of the incident X-rays are reflected twice and focused in the central PSF spot, X-rays reflected just once and focused in both PSF arms (2×22%), and the rest produces a diffuse patch. In the "Lobster Eye" geometry the vignetting is very low, reaching 10–15% at the edge of the FoV. Simulations indicate that the PSF reaches 4.5 arcmin FWHM at 1.5 keV.

The MXT camera uses a pnCCD developed by the MPE (Meidinger et al., 2006), with an active area of 256×256 pixels of 75 μm, and a reduced frame store area with 75×51 μm pixels. This CCD is fully depleted (450 μm depth) and has excellent low-energy response (45-48 eV FWHM at 277 eV), and energy resolution (123-131 eV FWHM at 5.9 keV), and is read-out rate every 100 ms. The detector is actively cooled to -65°C. A filter wheel allows to put a calibration source or additional optical/UV filters in front of the detector when needed. The GRB afterglow position is computed onboard in near real-time by the MXT Data Processing Unit.

The expected MXT effective area is 27 cm^2 at 1 keV for the central spot and 44 cm^2 including the PSF cross arms. Taking the expected background into account, this translates into a 5σ sensitivity in the 0.3–6 keV energy band of of 8×10^{-11} erg cm^{-2} s^{-1} for a 10 s observation, and $\sim10^{-12}$ erg cm^{-2} s^{-1} in 10 ks. The MXT throughput for 1 mCrab is ∼0.20 ct/s (for N_H=4.5×10^{21} cm^{-2}, assuming a photon index of 2.08).

The expected GRB afterglow localization performance, obtained by folding the entire *Swift/XRT* afterglow dataset through the MXT response, shows that MXT is well adapted to study GRB afterglows: 50% of the bursts will be localized better than 13 arcsec (statistical uncertainties only) within 5 min from

[4]institutes: CNES Toulouse, LAM Marseille, IRAP Toulouse, IRFU/CEA Saclay, OAS Strasbourg (France), IAAT Tübingen, MPE Garching (Germany), University of Leicester (UK)

trigger. This shows that despite a smaller effective area compared to *Swift*/XRT, most afterglows will remain detectable up to about 10^5 s after trigger.

2.2.6 The visible telescope VT onboard *SVOM*

The Visible Telescope[5] (VT) is a dedicated optical follow-up telescope onboard *SVOM*. Its main purpose is to detect and observe the optical afterglows of GRBs localized by ECLAIRs. It is a Ritchey-Chretien telescope with a 40 cm diameter and an f-ratio of 9. Its limiting magnitude is about M_V=22.5 for a 300 s integration time.

VT is designed to maximize the detection efficiency of GRB's optical afterglows. A dichroic beam splitter divides the light into two channels, in which the GRB afterglow is observed simultaneously, a blue channel with a wavelength from 0.4 to 0.65 μm and a red channel from 0.65 to 1 μm. Each channel is equipped with a 2K×2K CCD detector. The blue channel CCD is a normal thinned and back-illuminated one, while the red channel CCD is deep-depleted to obtain a high sensitivity at long wavelengths. The Quantum Efficiency (QE) of the red-channel CCD is over 50% at 0.9 μm, which gives VT the capability of detecting GRBs with redshifts larger than 6.5. The VT FoV is about 26×26 arcmin^2, covering the ECLAIRs error box in most cases.

In order to promptly provide GRB alerts with sub-arcsec accuracy, VT performs data processing onboard. After GRB localization by the coaligned MXT, lists of possible sources are extracted from successive VT sub-images, whose center and size is determined by the GRB position and error box provided by MXT. These lists are down-linked in near-real-time through the VHF network, to allow the ground software to produces finding charts and search the optical counterpart of the GRB, comparing the lists with existing catalogs. If a counterpart is identified, an alert is distributed to the world-wide astronomical community, to trigger observations by large ground-based telescopes in order to measure the spectroscopic redshift of the GRB.

In the *Swift* era, confirmed high-redshift GRBs are rare, in contrast to a theoretical predicted fraction of more than 5 to 7%. This is probably due to the fact that for most *Swift* GRBs the early-time optical follow-up images are not deep enough for a quick identification, such that faint GRBs cannot be spectroscopically observed in time by the large ground-based telescopes. This situation will be significantly improved by *SVOM*, thanks to the high sensitivity of VT, in particular at long wavelengths, and the generation of fast optical-counterpart alerts. Additionally, the anti-solar pointing strategy of *SVOM* allows GRBs to be observed by large ground-based spectroscopic telescopes at early times. Consequently more high-redshift GRBs are expected to be identified in the *SVOM* era.

2.2.7 The ground-based visible/infrared telescope F-GFT

The French-Ground Follow-up Telescope[6] (F-GFT) is a robotic 1-m class ground telescope dedicated to *SVOM*. It is designed to provide the redshift determination of GRBs, which is fundamental for their understanding and their use in cosmology, and which is currently only possible from ground. F-GFT measures the redshift photometrically with an accuracy of ∼10%, using broadband optical/infrared photometry, and additionaly provides sub-arcsec localization of GRBs. This information will be automatically delivered in less than 5 min (an order of magnitude quicker than current instruments), such that the most interesting GRBs (with high redshift, high extinction, etc) will be quickly identified and precisely localized, allowing rapid follow-up observations with the largest facilities (NOT, NTT, VLT, E-ELT, ALMA, etc) in order to obtain high-resolution afterglow spectra and very precise redshift determinations.

F-GFT is a collaboration between France and Mexico (UNAM and CONACyT). Mexico will host the F-GFT in the national observatory located in San Pedro Mártir, Baja California, which offers very good observing conditions (median seeing of 0.8 arcsec and about 80% of clear nights).

[5]institutes: NAOC Beijing, XIOPM Xian (China)

[6]institutes: CPPM Marseille, IRAP Toulouse, IRFU/CEA Saclay, LAM Marseille, OHP-OSU Pytheas (France), UNAM Mexico, UNAM Ensenada (Mexico)

SVOM sets strong constraints on the F-GFT technical specifications: very high availability for follow-up observations (∼90%), very good sensitivity (1.3 m mirror diameter), fast pointing speed (on target in less than 30 s), multiband photometry (from 0.4 to 1.7 μm, with at least two simultaneous bands), and FoV (13 arcmin in radius) covering the ECLAIRs trigger error box. The sensitivity reaches magnitude 20.5 in r band and 19.0 in J band (AB system, 60 s exposure time, SNR=5), which allows to detect more than ∼95% of the currently observed GRB dataset. Moreover ∼23% of the *SVOM* alerts will be immediately observable. Seventeen hours after the ECLAIRs trigger, despite this long delay and decrease in the GRB brightness, the F-GFT has still sufficient sensitivity to allow the detection of ∼65% of the GRBs in the infrared domain.

The unique combination of speed, FoV and sensitivity both in optical and infrared, permits the F-GFT to address a large number of scientific questions and provides a strong scientific return to the *SVOM* mission, in particular: a) the fast F-GFT response-time, allowing quick follow-up observations, will permit the study of the GRB prompt emission mechanism and the transition between the prompt and afterglow emission, a largely unexplored domain up to now in the visible and near infrared, which F-GFT will cover with a time resolution adapted to the fast variability of the emission in this phase; b) the unique sensitivity of F-GFT in the infrared will allow the search for highly obscured or redshifted GRBs (beyond redshift ∼6), invisible to the VT onboard *SVOM*, important for the study of the young Universe and the epoch of reionization; c) the sensitivity, availability and flexibility of the F-GFT will help searching for electromagnetic counterparts of high-energy neutrinos detected by ANTARES/KM3Net, or of gravitational wave events detected by advanced LIGO and Virgo.

2.2.8 The ground-based visible telescope C-GFT

The Chinese Ground Follow-up Telescope[7] (C-GFT) is based on an existing 1-m telescope located at Xinglong observatory, China, which is an f/8 Ritchey-Chretien system providing fast repointing through an altazimuth mount. It will be upgraded with a dichroic mirror system, 3 channels of SDSS g,r and i filters, a robotic control system, and a real-time data and communication system.

The 3 channels will be equipped with CMOS-CCD cameras with low read-out time, of size of 2K×2K, corresponding to a FoV of 21×21 arcmin^2, operating in the 0.4 to 0.95 μm band. The C-GFT sensitivity will reach mag(r)=19 (at 5σ, AB mag) for 100 s exposure time during new Moon nights.

The C-GFT robotic control system will point the telescope automatically to the ECLAIRs trigger sky position received from the CSC over *SVOM*net, and will also provide a user interface to change the pointing remotely. The real-time data processing system will search GRB counterparts in the 3 channel images, after CCD data reduction (bias, dark, and flat field correction), cosmic ray removal, and astrometric calibration. All detected GRB candidates will be provided with the parameters: sky localization (with accuracy of 0.5 arcsec), flux-calibrated magnitude, weight (or confidence) and finding chart. If no GRB candidate is found, upper limits will be provided. The data communication of C-GFT includes an instant data transfer network (based on the XMPP protocol) with VOEvent wrapped messages, transferring the detected GRB parameters. A no-instant data transfer network, based on FTP servers, permits large volume data transfers of FITS images, without stringent temporal requirements. The C-GFT telescope points towards the target, takes exposures, reads-out the data, processes it and reports the results all within respectively 5 min and 1 min after trigger reception. More than 20% of the ECLAIRs triggers will be observable by C-GFT.

In addition to the dedicated C-GFT at Xinglong observatory, two more 1-m telescopes will be set-up by the NAOC (National Astronomical Observatory of China) at Ali observatory, Tibet, western China, as a part of the LCOGT network. The NAOC will have access to ∼2500 h of observation time per year on LCOGT, which could be dedicated to follow-up *SVOM* GRBs via LCOGT ToO calls with a typical response time of about 15 min.

[7] institute: NAOC Beijing (China)

2.3 The *SVOM* science ground segment

The Chinese Science Center provides software tools for the General Program proposal writing and ToO generation. They include up-to-date instrument performances delivered by the Instrument Centers, observation footprint and SNR estimators, and information on source accessibility, background maps and catalogs etc. The Mission Center validates and coordinates the elaboration of observation requests made by the PIs for all observing programs of *SVOM*. The Control Center sends telecommands to be executed onboard the satellite. The Chinese Science Center[8] processes data of the Chinese instruments GRM and VT onboard *SVOM* and the ground-based C-GFT and GWAC. It also assists Instrument Scientists (ISs) of those instruments and Burst Advocates (BAs) on-duty on the Chinese side.

The French Science Center[9] processes data of the French instruments ECLAIRs and MXT onboard *SVOM* and the ground-based F-GFT. Three Instruments Centers, one for each French instrument, are connected to the French Science Center and host experts in charge of monitoring and calibration of the French instruments, as well as assistance to the BAs.

The VHF network collects the triggers generated onboard *SVOM* and sends them to the French Science Center, where the near real-time data analysis is performed locally or remotely by Chinese and French BAs. The Chinese and French GFTs point towards the GRBs detected by *SVOM* to produce results within 5 min. The GWAC collects data from -5 to +15 min around the trigger time.

All data are examined and possibly re-processed by BAs and ISs. BAs can request revisits of interesting GRBs. Data products are generated and re-processed as the pipelines improve throughout the mission lifetime, and will be made available by the Space Science Data Center. Data of the French instruments will also be made available by the French Science Center.

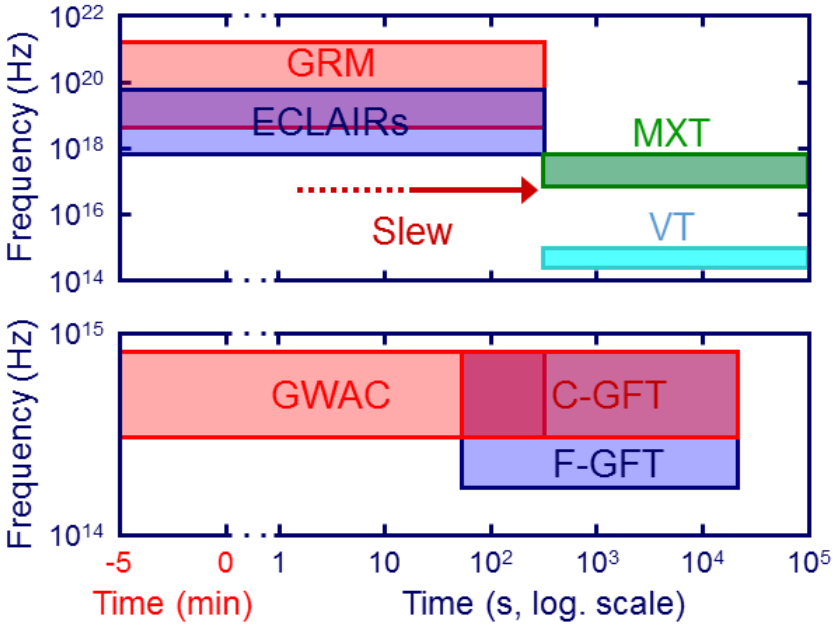

Figure 5: Spectral coverage of the GRB prompt emission and its afterglow with *SVOM* instruments, as a function of time (the burst is detected at time t = 0). The upper panel refers to space-born instruments (GRM, ECLAIRs, MXT, VT), the lower panel to ground-based instruments (GWAC, C-GFT, F-GFT).

[8]institute: NAOC Beijing (China)

[9]institutes: APC Paris, CNES Toulouse, CPPM Marseille, GEPI Paris, IAP Paris, IRAP Toulouse, IRFU/CEA Saclay, LAL Orsay, LAM Marseille, LUPM Montpellier (France)

2.4 *SVOM*: a highly versatile astronomy satellite

With built-in multi-wavelength capabilities, flexible operations and ground follow-up opening a large discovery space, *SVOM* will be a highly versatile Astronomy satellite. As depicted in Fig. 5, thanks to its unique instrumental combinations of wide-field (ECLAIRs + GRM + GWAC) and narrow-field (VT + MXT + C-GFT + F-GFT) instruments, *SVOM*, already well suited to permit fruitful GRB studies, should also effectively contribute in the new fields of Multi-Messenger Astrophysics.

3 *SVOM* Advances on GRB Science (*SVOM* core program)

Gamma-ray bursts (GRBs) are short and intense flashes of photons of energy observed mainly from $\sim$ 100 keV to $\sim$ 1 MeV, which are non-thermal, have significant variability, and typically last less than $\sim$ 100 s. This GRB prompt emission is followed by long-lasting afterglow emission in X-ray, optical, radio. Observations of afterglows enable us to localize positions of GRBs accurately, to discover their host galaxies, and to measure their redshifts. Due to their cosmological distances, the isotropic-equivalent luminosities of GRBs can reach very high values (upper bound $10^{54}\,\mathrm{erg\ s^{-1}}$) with a broad distribution of luminosities. Hence GRBs are the most powerful explosions in the universe, which are thought to be powered by the gravitational collapse of matter to form a black hole or a neutron star.

GRBs can be separated into two different types by their durations with a rough separation line of $\sim$ 2 s, since an obvious bimodal structure appears in the duration distribution (Kouveliotou et al., 1993). The number ratio of observed long GRBs with a duration > 2 s to short GRBs for < 2 s is roughly three to one. Generally, long GRBs tend to have a softer spectrum, while short GRBs are relatively harder. Long GRBs distribute in a very wide redshift range from 0.0085 to 9.4 and concentrate within $z \sim 1-2$, while short GRBs occur at closer distances with an average redshift of ~ 0.5 (Berger, 2014). There are several strong observational reasons for an association of long GRBs with the gravitational collapse of some massive stars (Woosley, 1993), while short GRBs are mostly likely associated with the mergers of binary compact stars (see e.g. Perna & Belczynski, 2002).

The above simple dichotomy for GRBs could still face some challenges. On one hand, the definition of GRB durations is actually instrument-dependent (see e.g. Qin et al., 2013), which could involve some selection biases. On the other hand, it is indeed very difficult to assign some GRBs that have a short prompt spike and subsequent extended ($\sim 10-100$ s) soft gamma-ray emission (e.g. GRBs 060505 and 060614) to the traditional short or long groups (Gal-Yam et al., 2006; Ofek et al., 2007). Additionally, several ultra-long GRBs with a duration longer than thousands of seconds have also been detected (Campana et al., 2011; Virgili et al., 2013), which could just be the long-duration tail of normal long GRBs (Zhang et al., 2014) or could indicate a distinct new kind of progenitors (Gendre et al., 2013; Levan et al., 2014b). Therefore, multiple observational criteria may in principle be needed for a more physical classification of GRBs (see e.g. Zhang, 2006; Lü et al., 2010).

SVOM is well designed to study the physics of the GRB phenomenon in all its diversity, thanks to an excellent spectral and temporal coverage of the prompt and afterglow emission combined with an optimized follow-up strategy aiming at the redshift determination for a large fraction of GRBs ($\sim 2/3$). The potential impact of *SVOM* in the study of long GRBs is discussed in sections 3.1, 3.2 and 3.3, the special case of short GRBs is presented in section 3.4. The synergy of *SVOM* with other instruments in the study of GRBs as cosmic accelerators is treated in section 3.5.

3.1 Classical long GRBs: physical mechanisms

The physical understanding of GRBs is especially challenging, due to their extreme properties. This quest is however highly motivating as it offers the possibility to improve our knowledge of the final fate of massive stars, to understand astrophysical relativistic jets from GRBs and other sources such as microquasars or blazars, and to study an extreme case of cosmic accelerator. In addition, the use of GRBs as probes of the distant universe can be improved by a better understanding of the progenitors, and/or GRB emission processes. A "standard" scenario for GRBs is now well accepted (e.g. Piran, 1999): an initial event such as the collapse of a massive star (long GRBs) or the coalescence of two compact objects (short GRBs, discussed below in section 3.4) leads to the formation of an accreting stellar mass compact source, most probably a black hole. This source releases a huge energy in the form of an ultra-relativistic jet. The prompt emission, which is non-thermal, is due to internal dissipation within the jet itself, for instance via internal shock waves (Rees & Mészáros, 1994). The afterglow is associated to the deceleration of the jet by the ambient medium (Mészáros & Rees, 1993), which leads to the propagation of a strong relativistic shock into the external medium (external shock) and of a reverse shock into the jet. Within

this theoretical framework, many questions remain open.

(1) Nature of GRB progenitors and central engines. While the production of GRBs seems to be due to a more or less universal process – the formation of short-lived relativistic ejecta emitted by accreting compact objects – their progenitors may be quite diverse. Classical long GRBs are associated with the collapse of some massive stars (collapsar model). However, the redshift distribution of *Swift* GRBs show that the cosmic GRB rate does not follow the star formation rate, the efficiency of GRB production appearing to be higher at high redshift (Daigne et al., 2006a). This shows that the production of a GRB depends on special conditions, which may be related to different properties of the progenitor: rotation, metallicity, binarity, etc. The progenitor stars should probably be very massive, typically heavier than $\sim 40 M_\odot$. Some may belong to the first generation of stars in the Universe (see discussion in section 3.6). A general picture is that the central iron core will collapse into a quickly spinning black hole. A high density transient accretion disk will form around the black hole, launching a pair of ultra-relativistic jets that move outward along the spin axis (Woosley, 1993; Ramirez-Ruiz et al., 2002; Zhang et al., 2003). However, many details of the process are still highly uncertain. First, how are the jets launched, by the Blandford-Znajek mechanism (Blandford & Znajek, 1977) or another mechanism? Second, although a few numerical approaches have been devoted to this question (MacFadyen & Woosley, 1999; Zhang et al., 2003), it is still uncertain whether the jet can penetrate through the stellar envelope of the progenitor while maintaining an ultra-relativistic speed and keeping to be highly collimated. Morover, the nature of the central object resulting from the collapse is also debated: the iron core may first collapse into a hyper-massive neutron star, which then spins down and collapses into a black hole at a later stage (supranova model, Vietri & Stella, 1999); it is also possible that the remnant object is not a black hole, but a millisecond magnetar (Kluźniak & Ruderman, 1998; Wheeler et al., 2000; Dai et al., 2006; Bucciantini et al., 2009), offering different mechanisms of energy injection with possible observable signatures (Dai et al., 2006; Zhang et al., 2006; Yu et al., 2015b).

The association of a GRB trigger with the detection of gravitational waves (GW) would provide a direct signature of the initial event leading to a GRB and the nature of the central object. Such an association is expected first for short GRBs (see section 3.4) as the GW emission from stellar collapses is expected to be weaker than in mergers (e.g. Fryer & New, 2011). Indirect signatures on the nature of the progenitor and the central engine can also be obtained from electromagnetic observations. Association or non-association of nearby GRBs with supernovae is an important clue (see section 3.2). Early spectroscopy of the afterglow can probe the immediate environment of the GRB and contribute to the identification of the progenitors of GRBs (e.g. Fox et al., 2008; Castro-Tirado et al., 2010). This necessitates accurate and rapid localizations. More generally, the density profile of the circumburst medium derived from the afterglow modelling can bring also valuable information on progenitors.

A broad spectral coverage of the prompt emission is necessary to investigate the existence of possible optical or X-ray precursors (a small fraction of long GRBs show a soft precursor emission before the main burst, Hu et al. 2014), which also puts some constraints on the central engine (e.g. lifetime). Finally, an extension of the sensitivity of GRB detectors into the X-ray domain is needed to study and characterize the population of soft GRBs and low-luminosity GRBs, which holds the key to understand the continuum of events following the collapse of a massive star, from standard supernovae (no relativistic jet) to cosmic GRBs (highly energetic and relativistic jets); see section 3.3.

(2) Acceleration and composition of the relativistic ejecta, physical origin of the prompt emission. GRBs give unique opportunities to study the physics of relativistic astrophysical jets. The nature of the physical mechanism that launches GRB ultra-relativistic ejecta is not elucidated, and the composition of the jet (electromagnetic or matter dominated) is currently the subject of an intense debate, as well as the internal dissipation mechanism responsible for the prompt emission (photospheric emission vs internal shocks vs magnetic reconnection, Kobayashi et al. 1997; Daigne & Mochkovitch 1998; Mészáros et al. 2002a; Daigne & Mochkovitch 2002; Rees & Mészáros 2005; Beloborodov 2010; Spruit et al. 2001;

Zhang & Yan 2011). Many issues are also related to the microphysics in the emission regions, especially related to the acceleration of the electrons responsible for the non-thermal emission, and the identification of the associated radiative processes (synchrotron emission, inverse Compton scatterings, etc.). Progress in this field will require a better understanding of the prompt emission phase (energy reservoir and extraction mechanism, radiation processes) and especially to be able to observationally constrain the physical conditions in the jet when this emission is produced: radius, Lorentz factor, magnetization, magnetic field geometry, etc.

Since the launch of *Fermi*, knowledge of the high-energy part of the spectrum has increased. On the other hand, the prompt X-ray and optical emission remain poorly known. The prompt optical emission provides important clues about the emission region and the internal dissipation mechanism but has been detected only in a few cases: a larger sample, allowing a statistical description, is necessary to identify the underlying mechanisms. The prompt X-ray emission is important to better characterize the spectrum and identify the emission mechanism (related to the nature of the jet) and the dominant radiative processes. The identification of thermal components in the spectrum can be a signature of the photosphere of the relativistic jet and would therefore provide an important clue for its nature (Hascoët et al., 2013).

A better understanding of the physical origin of the prompt emission requires a sample of GRBs with well measured properties, with a good temporal resolution and the largest spectral range, from the optical to the high-energy gamma-rays, including X-rays and soft gamma-rays. Such a sample cannot be limited to the observation of the prompt emission, as the distance is mandatory to measure the radiated energy from the ejecta, and as the early X-ray afterglow contains important information about the end of the prompt phase (e.g. Hascoët et al., 2012).

Simultaneous detections of few GRBs with instruments providing a good description of the prompt emission and allowing the measurement of the distance, and instruments with polarization measurements capabilities, such as POLAR, would also provide a key GRB sample to study the nature of the relativistic outflow (e.g. Granot, 2003). In a similar way, the detection of high-energy neutrinos associated to a GRB would also provide important information on the composition of the jet and on the internal dissipation processes (see section 3.5).

(3) Interaction of the ejecta with the circumburst medium – The physical origin of the afterglow. *Swift* has brought much new and puzzling information on the afterglow phase, especially related to unexpected time variability (see the recent review by Gehrels & Razzaque, 2013). This led to the emergence of many variations of theoretical models accounting for these observations. Several emission regions are invoked: shocked external medium (forward shock), shocked ejecta (reverse shock), late internal shocks, etc. Some of these models have strong implications on the lifetime and energetics of the central engine as they imply late energy injection by the source or relativistic ejection at late times.

To distinguish between these models and better understand the physics of the interaction of the jet with its environment, and especially the different emission regions contributing to the afterglow and the nature of the circumburst medium, it is necessary to build a sample of GRBs where all information is available (a description of the afterglow at different wavelengths, but also the distance/redshift). A good description of the prompt emission in this sample is also necessary to put constraints on the lifetime and energetics of the central engine, and to test models linking some afterglow features with the prompt emission.

***SVOM* contributions.** To summarize, the understanding of the GRB physics requires observations in the largest spectral domain and in the largest temporal interval, from the possible precursor up to the transition between the prompt and afterglow emissions. Simultaneous observation of the prompt GRB event in the gamma-ray, X-ray and visible bands, combined with narrow field observations of the afterglow in X-rays, visible and near infrared immediately after the beginning of the event will enable a better understanding of mechanisms at work in such events. New measurements (gravitational wave, gamma-ray polarization, neutrinos) may also become possible in the future, and their impact on the

physical understanding of the GRB phenomenon will be maximized if these measurements are made for bursts whose "standard" properties, including the distance, are well measured.

The *SVOM* mission is well adapted to these objectives. Compared to previous missions, it offers *simultaneously* (i) the capacity to trigger on all types of GRBs (see section 3.3), (ii) an excellent efficiency of the follow-up and the redshift measurement; (iii) a good spectral coverage of the prompt emission by ECLAIRs+GRM allowing a detailed modeling, as illustrated in Fig. 6. For a significant fraction of *SVOM* GRBs, GWAC will provide in addition a measurement or an upper limit on the prompt optical emission; (iv) a good temporal and spectral coverage of the prompt and afterglow emission thanks to MXT, VT and the GFTs, as illustrated in Fig. 7.

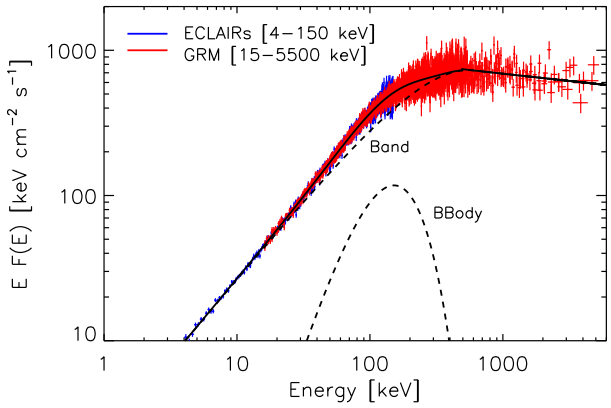

Figure 6: Simulation of the prompt spectrum of a long GRB in *SVOM*/ECLAIRs+GRM. The long GRB 100724B was detected by *Fermi*/GBM and shows a two components spectrum (Guiriec et al., 2011b). It has been simulated in ECLAIRs and GRM assuming that the burst is on-axis in ECLAIRs and therefore 30° offaxis in GRM. The resulting spectrum is plotted together with the best fit (solid line) by a combination of a non-thermal (BAND) and quasi-thermal (BBody) components. The recovered parameters are equal within 1σ to those published for the same spectral model by Guiriec et al. (2011b). This illustrates how well this complex shape is recovered by *SVOM* thanks to the broad spectral coverage of the prompt emission allowed by the ECLAIRs+GRM.

3.2 Classical long GRBs: characterization of the population

The association of long GRBs (LGRBs) with core-collapse SNe is a well established fact (see Hjorth & Bloom 2011; Cano et al. 2016, for a review). Through photometry and spectroscopy it is possible to look for SN signatures in the afterglow light-curves and spectra. The spectral features indicate that these SNe are broad-line type Ibc. For LGRBs close enough not to have the associated SN flux too faint to emerge from the afterglow ($z \lesssim 0.6$), all the searches for an associated SN have been successful, except for two LGRBs (GRB 060605 and GRB 060614; e.g.: Fynbo et al. 2006). Monitoring LGRB afterglows with the VT on board of *SVOM* will make possible the systematic search for SN signatures in the afterglow light-curves, together with the identification of the rise time of the SN, allowing an efficient spectroscopic follow-up.

A well sampled multi-wavelength coverage of the prompt and afterglow phases for a large fraction of GRBs, together with a high percentage of redshift determinations, are the conditions needed to make a step forward in the characterization of the LGRB population. *SVOM* will have a great impact on this topic, thanks of the unique synergy of the space and ground segments (see section 2). Not only will *SVOM* have a visible telescope onboard (the VT) capable to systematically follow the LGRBs detected by the higher energy instruments, but it will also benefit of the follow-up carried out by a dedicated network of telescopes included in the ground segment (GWAC, F-GFT and C-GFT).

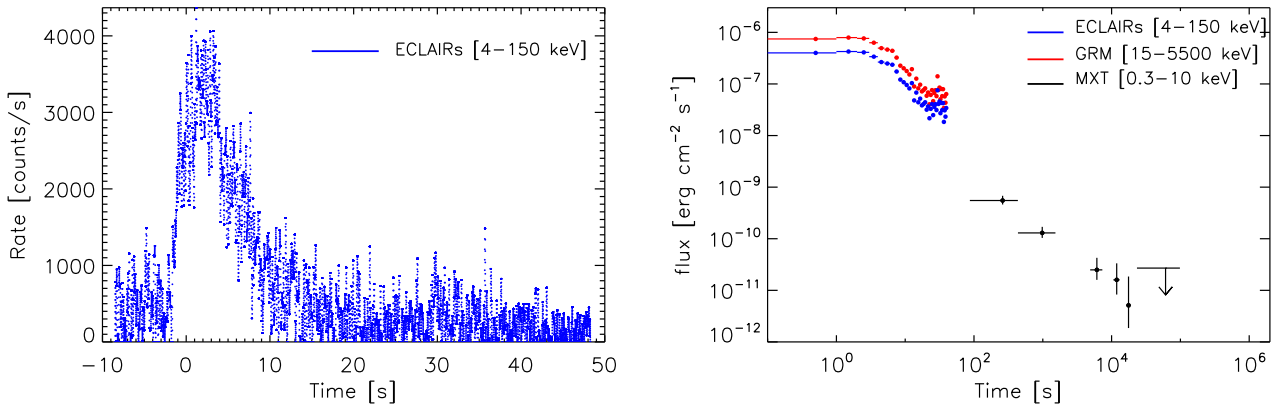

Figure 7: Simulation of the prompt and afterglow emission of a long GRB in *SVOM* instruments. GRB 091020 is a classical long GRB detected by *Swift* and *Fermi*/GBM. Using GBM data (Gruber et al., 2014b) for the prompt emission and *Swift*/XRT data for the X-ray afterglow (Evans et al., 2007, 2009), this GRB has been simulated in ECLAIRs and GRM, assuming that the GRB is on-axis for ECLAIRs and therefore 30° off-axis in GRM, and in MXT where the afterglow is detected up to $\sim 10^4$ s. *Left :* simulated prompt light curve in counts per seconds in ECLAIRs. *Right :* prompt and afterglow flux in log-log scale simulated in ECLAIRs, GRM and MXT.

Rapid identification of the LGRB counterparts in the optical and/or NIR frequencies in different filters will give a first redshift indication and ease the rapid spectroscopic follow-up by the larger telescopes. This is mandatory for the redshift determination of a significant fraction of the LGRB detected by *SVOM*. Nowadays only $\sim 30\%$ of LGRBs have an associated redshift. The goal of *SVOM* is to double this fraction. LGRB samples complete in redshift are the fundamental ingredient to determine the rest-frame properties of LGRBs and their evolution with cosmic time, characterizing the LGRB population in terms of redshift distribution, luminosity function, progenitors and being able to use it to trace star-formation.

To achieve these goals it is mandatory to have a sample not biased against *dark* GRBs (see Jakobsson et al. 2004; van der Horst et al. 2009). As *dark* GRBs are optically dim, the NIR camera on the F-GFT will be particularly helpful to identify their afterglows and provide their precise positions, needed for the spectroscopic observations allowing the redshift determination.

SVOM will operate from 2021, an epoch were facilities such as *SKA* (and its precursors) will be available (see section 1.2). Thanks to their improvement of sensitivity, *SKA* will make possible a detailed study of the afterglow in the radio domain for a much larger number of LGRBs. *SKA* should be able to detect all *SVOM* LGRB afterglows and, in addition to an amazing great leap forward on the study of the afterglow emission phases, it will allow the determination of the density of the environment and jet opening angle of *SVOM* LGRBs. This information will allow the characterization of the LGRB progenitors and a better determination of the true rate of LGRBs.

The jet opining angle and the redshift determination are also a fundamental information to test the correlations found between some quantities related to the gamma-ray prompt emission of LGRBs. Indeed, Amati (2006a), Yonetoku et al. (2004a) and Ghirlanda et al. (2004b), found a correlation between the peak energy (E_{peak}) and the isotropic energy (E_{iso}), isotropic luminosity (L_{iso}) and isotropic energy corrected by the jet collimation (E_γ) of the gamma-ray prompt emission, respectively. These correlations can in principle bring to the use of LGRBs to determine cosmological parameters (see section 3.9.1), but their physical explanations are still unknown and there is still an open debate on their robustness. A *SVOM* sample of LGRBs complete in redshift (and including the jet opening angle determination for the E_{peak} vs E_γ correlation), will make us able to test these relations.

3.3 The diversity of long GRBs: X-ray flashes, underluminous and ultralong GRBs

Long gamma-ray bursts exhibit a great diversity in their luminosities, spectral and temporal properties. The luminosity function of classical long GRBs covers a wide range in isotropic luminosity from $< 10^{50}$ erg s^{-1} to $> 10^{54}$ erg s^{-1} (e.g. Sun et al., 2015). But some nearby long GRBs have luminosities as low as a few 10^{47} erg s^{-1}. These underluminous GRBs must have a large event rate, and probably form a distinct population (e.g. Liang et al., 2007; Bromberg et al., 2011). The peak energy of the spectrum goes from a few keV in X-ray flashes to several MeV in hard bright bursts and the spectrum extends to several tens of GeV in some events detected by *Fermi*/LAT. GRB light curves can be simple, showing one single pulse or extremely complex with many pulses and spikes, often overlapping. The class of ultra-long GRBs extends the maximum observed burst duration to more than one hour.

SVOM will take advantage from its wide spectral coverage of the prompt emission (from X/γ with ECLAIRs and GRM to the optical with GWAC) to explore and better understand this diversity, which is a source of complexity but can also provide clues to decipher the various mechanisms at work during the prompt emission of GRBs. A few examples of expected *SVOM* contributions are given below.

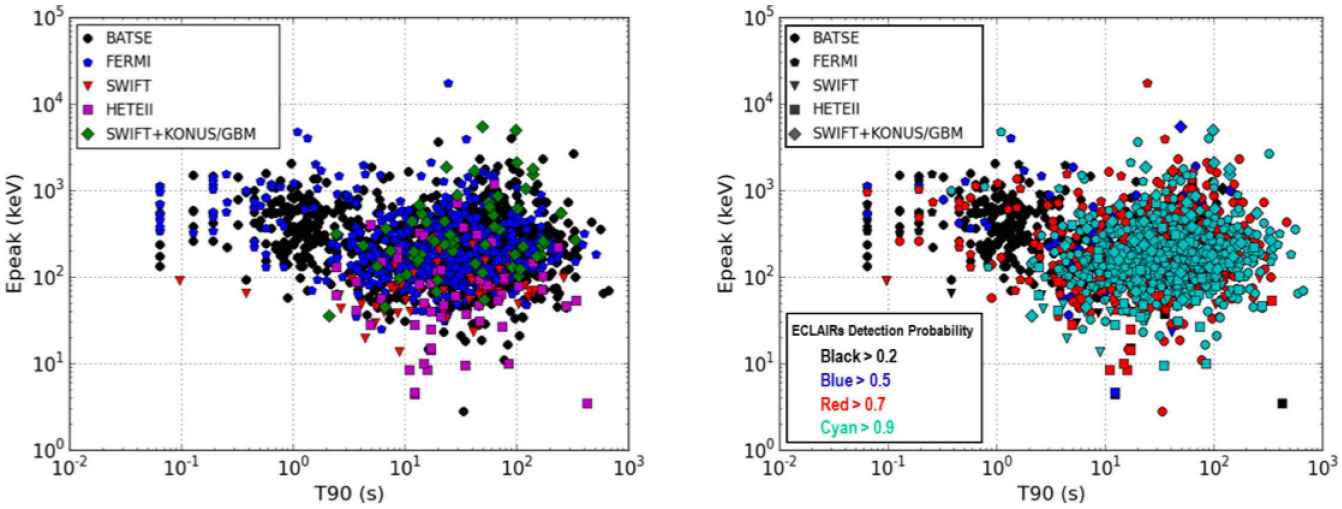

Figure 8: Exploration of the GRB diversity by *SVOM*. This figure illustrates the capacity of ECLAIRs to trigger on the various known classes of GRBs. *Left :* the sample of known GRBs with a prompt spectral measurement is plotted in the hardness (peak energy $E_{\rm peak}$) – duration (T_{90}) plane. Each symbol correspond to a different GRB catalog : *CGRO*/BATSE (Goldstein et al., 2013), *HETE2* (Sakamoto et al., 2005), *Swift* GRBs with a spectrum measured by either *Konus* or *Fermi*/GBM (sample taken from Heussaff et al. 2013) and *Fermi*/GBM (Gruber et al., 2014b). The classical long GRB population is well covered by all instruments but the number of GRBs with both an accurate prompt spectrum and an afterglow detection – corresponding approximatively to the *Swift*+*Konus*/GRB sample – remains relatively small. Short hard GRBs (small duration, high peak energy) are mainly detected by BATSE and GBM thanks to a broader spectral range of the trigger instrument. The artificial vertical line at $T_{90} = 64$ ms is due to the time-resolution of the sample and corresponds to the shortest GRBs. X-ray rich GRBs and X-ray flashes (long duration, small peak energy) belong mainly to the *HETE2* sample. *Right :* each GRB in the total sample of the left panel has been simulated in ECLAIRs. The resulting detection probability (averaged over the whole field of view, assuming an isotropic distribution in the sky) is color-coded. This illustrates the capacity of *SVOM* to trigger on all classes of GRBs. The detection probability is especially good for classical long GRBs, X-ray rich GRBs and X-ray Flashes. The efficiency for short GRBs may be improved using ECLAIRs+GRM trigger which is more sensitive to hard bursts.

Spectral diversity: X-ray rich GRBs and X-ray Flashes. Based on the peak energy distribution (E_p) or hardness ratio of GRBs, GRB-related high-energy transients are sometimes classified into several

sub-types (e.g. Sakamoto et al., 2005), including typical GRBs ($E_p > 50$ keV), X-ray rich GRBs (XRR, $30 \leq E_p \leq 50$ keV), and X-ray flashes (XRFs, $E_p < 30$ keV). The relatively narrow spectral coverage of *Swift* and the *Fermi* GBM trigger starting at 15 keV and 8 keV respectively have limited the ability of these two missions to efficiently observe soft events. Conversely ECLAIRs, with a trigger starting at 4 keV will increase the samples of X-Ray rich GRBs and X-Ray Flashes (see Fig. 8), providing redshifts and a detailed spectral information on these soft events.

Spectral diversity: spectral differences between various classes of GRBs. Apart from the class of XRR and XRFs, differences in spectral properties are also expected in relation with the luminosity, the temporal properties (highly variable vs smooth light curves, ultra-long events) or the source distance. The extended spectral coverage of *SVOM* and the image mode available with ECLAIRs will allow studying in details these spectral differences in e.g. the ratio between thermal and non thermal components or the level of additional power-laws contributing at low or/and high energy. In addition the ability to efficiently obtain the burst redshift from the same plateform will be extremely valuable for the physical interpretation of the results.

Temporal diversity: ultra-long GRBs. A new class of events, characterized by a very long duration, has recently been identified (e.g. Levan et al., 2014a). They have been detected via the image mode of *Swift*. Similarly the image trigger available on *SVOM* will detect ultra-long GRBs. *SVOM* will offer a very complete monitoring of these objects with the three onboard instruments and the GWAC on the ground. Together with its good localization capability *SVOM* will contribute shedding light on their physical origin.

Temporal diversity: various progenitors. Apart from the known separation between short and long GRBs expected to come respectively from compact star mergers and collapsars, other subtypes of events may have specific progenitors. For example, while typical long-duration GRBs may arise from successful jets from the core collapse of Wolf-Rayet stars, low-luminosity GRBs may be related to unsuccessful choked jets (e.g. Bromberg et al., 2011). Ultra-long GRBs have been suggested to probably have a blue supergiant progenitor (Levan et al., 2014a). The very complete spectral coverage available with *SVOM* will help identifying thermal and non thermal components (possibly peaking at widely separated energies) of different sub-types of GRBs, providing clues that will help to discriminate among various possible scenarios.

***SVOM* contributions.** By offering a broad spectral coverage and localization on a single plateform *SVOM* combines several *Swift* and *Fermi* capabilities and offers new ones, such as the continuous monitoring of the ECLAIRs FoV in the optical. *SVOM* is well designed to explore the GRB diversity and will fly when GW observatories and new facilities (*JWST*, *LSST*) will be fully operational.

3.4 Short GRBs

Short GRBs were discovered by Mazets & Golenetskii (1981), and are generally defined as those having $T_{90} < 2$ s (Kouveliotou et al., 1993). They appear to form a population distinct from the longer GRBs as they form a secondary peak in the burst duration distribution measured by high energy detectors; they also have generally harder prompt emission, have an energy output $\sim 1\%$ of long GRBs, and are seen to occur at closer distances than long GRBs (short $\langle z \rangle \sim 0.5$, long $\langle z \rangle \sim 2.0$). For a review see Berger (2014). In distinction to the long bursts, which occur in regions of high specific star formation rate, short GRBs occur in a broader range of environments, including elliptical galaxies; the short GRB rate is ten times higher per unit galaxy mass in late-type than in early-type galaxies. This variety of host galaxy types indicates a range of burst delay times since the initial star formation.

The distinction between long and short GRBs is not without problems however. It has been argued that the band-pass of the detector should be considered in setting the threshold T_{90} value (Bromberg et al., 2013), as bursts are known to last longer at lower energies. In addition, when the cosmological time dilation of the bursts is accounted for the durations of long and short bursts no longer appear distinct, and it seems as if short GRBs are rather like the first 0.3 rest-frame seconds of the long GRBs (Ghirlanda et al., 2015a). GRB060614 and GRB060505 were nearby bursts with $T_{90} > 2$ s but without the supernovae

characteristic of long GRBs, and are well-known examples of bursts that are difficult to assign to the short or long burst groups (Gal-Yam et al., 2006; Ofek et al., 2007; Zhang et al., 2007).

Physical classification schemes have been proposed based on the widely held view that short GRBs have a formation mechanism independent of that of the long GRBs (Zhang et al., 2007, 2009; Lü et al., 2010; Bloom et al., 2008): while long GRBs are considered to be the result of the collapse of a massive star, short GRBs are thought to be due to the collision of a neutron star and a black hole or a pair of neutron stars in a binary system due to orbital decay caused by the emission of gravitational radiation. Consistent with this picture, long bursts are seen to be accompanied by a type Ibc supernova if they are close enough, whereas no supernova occurs with short bursts (e.g. Kann et al., 2011), and short GRBs can occur at a significant distance from their host galaxy, as expected if their progenitors are the very long-lived NS-NS or NS-BH systems which have received a significant kick at the time of their creation. The merger of white dwarf binaries has also been proposed to be responsible for un-kicked short GRBs in both early and late-type galaxies (e.g. Levan et al., 2006). For both long and short GRBs a highly relativistic jet along the rotation axis is pointed in our direction; it is the emission from this that we see as the gamma-ray burst, and this common factor is likely responsible for the difficulties in classifying burst types.

The compact star merger model of short GRBs leads directly to two predictions: the simultaneous production of strong gravitational wave emission from the final stages of orbital decay and merger, and the substantial production of r-process elements in the neutron-rich merger ejecta. The recent detection of gravitational wave emission from a massive BH+BH binary by the advanced LIGO interferometers (Abbott et al., 2016a) gives great hope that the NS+NS predictions of (Abbott et al., 2016d), although uncertain, will eventually be realised at close to ∼40 detections per year. Decay of radioactive r-process elements in the rapid ejection of up to a few percent of a solar mass of neutron star material is expected to give rise to an unbeamed "kilonova" peaking in the near IR a few days after the merger (Li & Paczyński, 1998; Barnes & Kasen, 2013; Kawaguchi et al., 2016), a prediction apparently confirmed for the short GRB 130603B by Tanvir et al. (2013). X-ray heating may be a more efficient kilonova powering mechanism (Kisaka et al., 2016). Candidate kilonova emission has also been found in GRB 060614 (Yang et al., 2015) and GRB 050709 (Jin et al., 2016). The final stellar outcome is expected to be a black hole (Fryer et al., 2015), although a rapidly spinning magnetar may be formed (e.g. Rowlinson et al., 2013), perhaps as an intermediate product before final collapse, in which case the detectable electromagnetic signatures from the system can become much richer and brighter (Gao et al., 2015). (Fernández & Metzger, 2015) review the electromagnetic emission from colliding neutron star systems (see Fig. 9).

Swift has discovered just over 8 short GRBs per year, leading to substantial progress, for example by discovering the first short GRB afterglow (Gehrels et al., 2005). It has shown that ∼45% of short GRBs fade beyond observational limits in X-rays within ∼17 minutes. Median r-band AB magnitudes are ∼23 at 7 hours, an order of magnitude lower flux than from long GRB afterglows (in spite of their much closer distance). Because of their relative faintness short GRBs are hard to study.

SVOM has much to add, with its complementary wide-field and wide band-pass suite of sensitive instruments. The *SVOM* pointing scheme is optimised for ground-based follow-up, so it will enable the measurement of a much higher fraction of redshifts than has been possible so far, helping to overcome the selection effects evident in the current sample. Knowledge of the burst distance is key to establishing the energetics and physical mechanisms responsible for the emission. In addition, the large FoV of the *SVOM* GWAC is expected to provide the very first measurements of the prompt optical emission, while the GFTs may cover the so-called extended emission phase, so helping to constrain outflow and emission models. The VT on *SVOM* is more sensitive than the *Swift* UVOT, and so it will locate a much higher fraction of short GRB afterglows than has been possible so far. The combination of GRM and ECLAIRs is well suited to investigation of the prompt initial hard spike and the following softer extended emission which is observed in a significant fraction of short GRBs (see Fig. 10). This may be due to magnetar spin-down, or to accretion gating by a magnetic propeller and a signature of a significant mass ratio in the progenitor binary leading to a large ejecta mass and so a larger fall-back accretion disk (e.g. Fan &

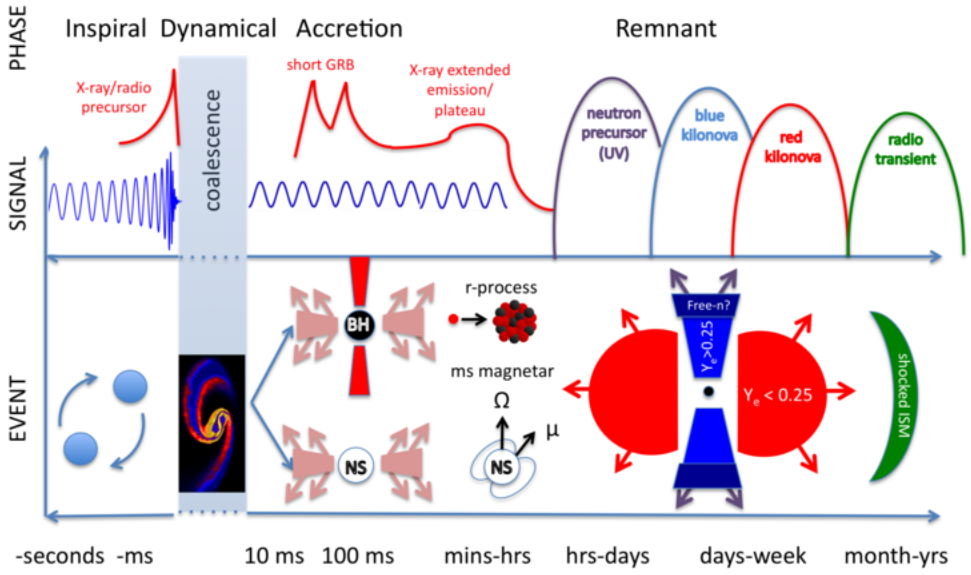

Figure 9: Expected electromagnetic counterparts to gravitational waves in a NS/NS or NS/BH merger. This figure, taken from the review by Fernández & Metzger (2015) illustrates the expected time sequence: gravitational wave emission during the inspiral, merger and post-merger phase, associated short GRB and its afterglow, kilonova and radio afterglow. The uncertainties related to the final state of the merger are also indicated: see Fernández & Metzger (2015) for a full description of the figure.

Xu, 2006; Gompertz et al., 2014). The relationship between the optical and X-ray emission in the minutes after the burst certainly require clarification. Rowlinson et al. (2013) show that the magnetar signature seen in X-rays is not necessarily seen in the optical.

The 50 keV - 5 MeV sensitivity of the 3 GRM modules provides a radical new capability compared to *Swift*, the combination of GRM and ECLAIRs is a powerful tool that will allow strong constraints on the low energy prompt spectrum. This will enable newly sensitive searches for optically thick thermal components in *SVOM* bursts, and also will strongly constrain the low energy part of the Band function, which has been shown to be a defining characteristic of short GRBs (Ghirlanda et al. 2015a, see however Guiriec et al. 2010b).

Kilonovae may be the most commonly found electromagnetic counterparts to gravitationally detected neutron star mergers. The frequency of these associations will allow the evaluation of contribution of mergers in the nucleosynthetis of the heaviest elements in the Universe (e.g. Vangioni et al., 2016). The red and blue bands of the VT will be useful in defining the early decay that will help in the identification of new kilonovae. Short GRBs are also expected from appropriately oriented mergers; the wide FoV of the MXT will be especially useful in searching the large error regions of the advanced LIGO and VIRGO gravitational wave interferometers (X-ray search strategies are proposed by Evans et al. (2016) and Gehrels et al. (2016)). The combination of gravitational wave signal and X-ray light curve from the MXT will be key driver of new science by identifying the EM counterpart, linking the NS equation of state to the X-ray light curve and establishing whether a mergernova or a magnetar phase exists in the collapse (Lasky et al., 2014; Dall'Osso et al., 2015; Li & Yu, 2016). Bloom et al. (2009); Metzger & Berger (2012) and Li et al. (2016); Chu et al. (2016) provide overviews of the multiple and important benefits of joint GW-EM short GRB measurements; these include increased detection sensitivity, more complete diagnosis of the binary parameters, establishment of the astrophysical evolutionary context, constraints on the equation of state of the neutron stars, cosmological constraints through the measurement of both redshift and luminosity distance, as well as a strong constraint on the speed of gravitational waves.

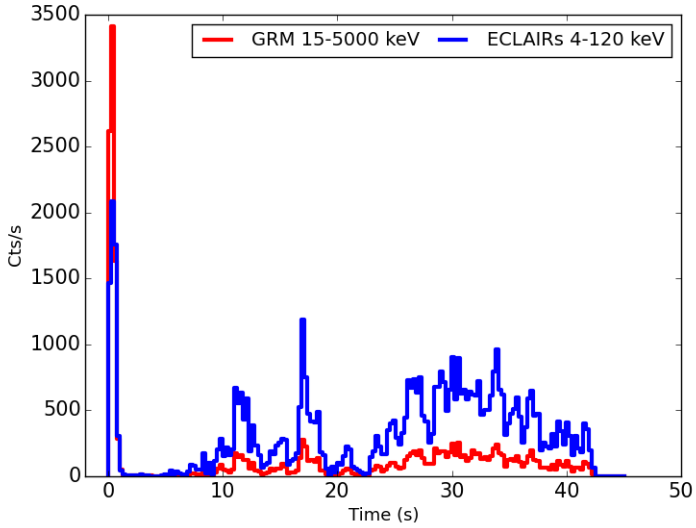

Figure 10: Simulation of the light curve of a short GRB with a soft extended emission in *SVOM*/ECLAIRs+GRM. GRB 990712A shows an initial short and hard spike, leading to the classification as a short hard GRB, followed by a soft extended emission (Norris & Bonnell, 2006). The simulated light curve is plotted in counts per second in ECLAIRs and GRM, based on the time-dependent spectral analysis published by Kaneko et al. (2006a) and assuming that the GRB is on-axis for ECLAIRs and therefore 30 off-axis in GRM. During the initial hard spike, GRM is more sensitive than ECLAIRs: it is detected at 62σ in GRM and 41σ in ECLAIRs. Therefore, in the case of weaker short GRBs, the detection by GRM may be used to increase confidence in a marginal ECLAIRs detection and to lower the slew threshold. During the soft extended emission, ECLAIRs becomes more sensitive: detection at 77σ in ECLAIRs and 15σ in GRM. Therefore the combination of the two instruments will allow to increase the sensitivity of *SVOM* to short GRBs and the capacity to slew and catch their early afterglow.

3.5 GRBs as particle accelerators

Electrons and hadrons are accelerated on a very short timescale at the shock fronts in the jets to ultra-relativistic speeds. In the standard framework, the gamma-ray emission is generaly explained by the synchrotron emission of the relativistic electrons. The origin of the high-energy gamma-ray emission ($\gtrsim$ 100 MeV) measured by *Fermi*/LAT is still debated: both leptonic and hadronic models can be invoked to explain the spectral shape of the extra-components. The combination of multi-wavelength and multi-messenger studies are required to answer to this question.

The observation by the *Fermi*/LAT of several GRB photons with energies reaching 10-100 GeV in the source frame (Ackermann et al., 2013b), as late as $\sim$ 1 day after the trigger in the case of GRB130427A, is encouraging for GRB detections at very high energies with the current ground-based imaging atmospheric Cherenkov telescopes and with synoptic detectors such as *HAWC* (Mészáros et al., 2015) and *LHAASO* (Di Sciascio & on behalf of the LHAASO Collaboration, 2016). None of the past and current experiments ever succeeded in capturing a high-energy signal from a GRB with their present operational threshold energies of $\sim 100-200$ GeV and the attenuation by the extragalactic background light (EBL) in this band at the typical distances of GRBs could be hindering their detection. The Cherenkov Telescope Array (*CTA*) (Inoue et al., 2013) is the next generation ground-based facility in the northern and southern hemispheres, which when combined will cover the entire sky over a broad energy range from tens of GeV up to $\sim$ 100 TeV, with a sensitivity considerably improved with respect to existing instruments. Moreover, the large field of view will maximize the chance to discover a GRB compared to present experiments.

The *Fermi*/LAT has detected an attenuation in the high-energy power-law component of some GRBs,

which has been attributed to internal gamma-ray opacity to pair production. Therefore, a simple extrapolation of the spectra to the VHE range is uncertain and makes the detections rate prediction difficult ($\sim$1 VHE GRB per year depending on the considered experiment (Abeysekara et al., 2012; Inoue et al., 2013; Gilmore et al., 2013; Taboada & Gilmore, 2014a). Joint time-resolved spectral analyses based on *SVOM*, *HAWC*, *LHAASO* and *CTA* data will help to pinpoint the nature and the origin of the acceleration and emission processes at high energies in GRB jets.

Such analyses are also crucial to study the most energetic photons from a burst. Precious information on the gamma-ray opacity has been provided by the detection of high-energy photons, allowing to set stringent limits on the jet bulk Lorentz factor. Similarly, variability studies and spectral shapes in the GRB prompt emission phase from MeV to TeV energies will help to distinguish between leptonic and hadronic models, and to answer the long-standing question of the origin of the cosmic rays observed on Earth with energies up to 10^{20} eV. The detection of *SVOM* GRBs at energies greater than $\sim$ 10 GeV will also provide crucial tests of the amount and of the origin of the EBL at high redshifts ($z > 2$), beyond the reach of blazar active galactic nuclei. It will bring additional constraints on the intergalactic magnetic fields through their impact on the propagation of the photon/pair cascades created by the interaction of VHE photons with the EBL. By studying the delay between the low and high energy emissions, *SVOM* GRBs will also be used as probes of the Lorentz invariance violation, which can manifest as a dependence of the speed of light in vacuum on its energy. *SVOM* will provide GRB alerts with very similar characteristics as *Swift* alerts at a rate of 60-70 GRBs/year and excellent localization well within the *CTA* field-of view. More generally, *SVOM* will provide the low-energy context which is fundamental for any broad-band multi-component spectral analysis, in particular for the understanding of GRB properties in the gamma-ray extreme energy range.

GRBs have been proposed as one of the potential sources for ultra-high energy cosmic rays (UHECRs) with energy up to 10^{20} eV (Vietri, 1995; Waxman, 1995). The baryon interactions with the fireball photons produce a burst of neutrinos with energies above 100 TeV in the standard internal shock model (Waxman & Bahcall, 1997; Hümmer et al., 2010). In the external shock region, GRBs may also produce neutrinos with even higher energies (Waxman & Bahcall, 2000; Li et al., 2002). A lower energy neutrino component (few TeV) may be also expected through hadronic interactions with the stellar envelope material (Mészáros & Waxman, 2001; Murase et al., 2006). The detection of an high-energy neutrino (HEN) signal in coincidence with GRBs would be a direct proof of the existence of an hadronic component in the jets. The ANTARES and the IceCube detectors are the current most sensitive neutrino telescopes in operations in the Northern and Southern hemispheres, respectively. During the *SVOM* operations, the KM3Net detector in the Mediterranean Sea will achieve an instantaneous sensitivity larger than the current IceCube telescope (Adrián-Martínez et al., 2016a). After 2025, the IceCube Collaboration also plans to extend its array to 10 km^3 (IceCube-Gen2 Collaboration et al., 2014). A first HEN signal has been detected by IceCube and found to be consistent with an isotropic flux (Aartsen et al., 2014a) with energies above few tens of TeV. The sources of these neutrinos are currently unknown. Their potential origins as GRBs have been discussed by several authors (see e.g. Liu & Wang, 2013; Murase & Ioka, 2013)

Searches for a neutrino signal from individual bright GRBs and/or through the stacking of a large number of GRBs have been unsuccesful so far (Abbasi et al., 2010; Adrián-Martínez et al., 2013). This non-detection suggests that the standard GRB population is not the major contributor to the diffuse HEN flux (IceCube Collaboration et al., 2016). Low-luminosity GRBs and chocked GRB jets, largely missed by current gamma-ray satellites (see section 3.3) may contribute significantly to the HEN diffuse (Wang et al., 2007). Less powerful jets or denser external material are more favorable for VHE production (Ando & Beacom, 2005; Gupta & Zhang, 2007; Murase et al., 2008). *SVOM* may be more efficient in the detection of such GRB populations thanks to the ECLAIRs low threshold energy of 4 keV (see Fig. 8), therefore providing a new sample to search for a correlated neutrino emission. Predictions for HEN emissions from GRBs are still uncertain. Improving the modeling requires gamma-ray spectra, multi-band afterglow light curves and redshift measurements. Thanks to the performance of its instruments, to their large multi-wavelength coverage and to the excellent space-ground synergy, *SVOM* will provide a

sample of well characterized GRBs, which is primordial for the search of their potential HEN counterpart.

3.6 *SVOM* and the high-redshift universe

Thanks to their extreme high luminosities and the spectroscopy of the optical afterglows, GRBs can be detected and studied up to high redshifts. Thus, high-z GRBs have been considered as a new powerful tool to explore the early Universe. *SVOM* will be ideal in that its capabilities are optimized to detect GRBs at high-redshifts. Indeed, because GRBs are associated with the death of massive stars, they are expected to be detected up to extremely high redshift, $z > 10$, where bright quasars may not have time to build up their central black hole. They are thus unique probes of the ISM of the first galaxies and of the reionization epoch. In this regard, there are potentially important gains from rapid response of follow-up telescopes, ideally getting on target in some tens of minutes.

In order to exploit the full potential of GRBs as a probe of the distant Universe, a larger sample of high-z GRBs is needed compared to what is available now. The detection of high-z GRBs is one of the essential goals driving the design of future GRB missions, including the forthcoming *SVOM* satellite. It has been suggested that the best strategy for detecting a large number of high-z GRBs is to design a facility operating in the soft X-ray band with a high sensitivity (Ghirlanda et al., 2015b; Salvaterra, 2015). ECLAIRs has a wide FoV of 2 sr ($89^\circ \times 89^\circ$). The sensitivity of ECLAIRs is expected to be 7.2×10^{-10} erg cm^{-2} s^{-1} ($\sim$ 30 mCrab, 5 σ detection level in 1000 s, Paul et al. 2011; Godet et al. 2014b; Cordier et al. 2015). It will be sensitive from 4 to 150 keV. Thanks to the low energy threshold of 4 keV, ECLAIRs will be sensitive to soft GRBs like X-ray Flashes and highly redshifted GRBs.

Our detailed simulations of the number of GRB detections expected with *SVOM*/ECLAIRs are described as follows (see Ghirlanda et al. 2015b, for more details):

(1). GRBs are distributed in redshift (up to $z = 20$) following a modified comoving star formation rate:

$$\psi(z) \propto (1+z)^{\delta} \psi_{\star}(z) \tag{1}$$

where $\psi_{\star}(z)$ denotes the cosmic star formation rate (Hopkins & Beacom, 2006; Li, 2008) in units of M$_{\odot}$ yr^{-1} Mpc^{-3}:

$$\psi_{\star}(z) = \frac{0.0157 + 0.118z}{1 + (z/3.23)^{4.66}}. \tag{2}$$

Salvaterra et al. (2012a) found that strong evolution in the GRB rate density ($\delta = 1.7 \pm 0.5(1\sigma)$) is required in order to account for the observed differential number counts of BATSE and the observed z distribution of the *Swift* complete sample. Here we adopt their value of δ.

(2). The GRB luminosity function (LF) has also been well constrained by Salvaterra et al. (2012a) through the BAT6 sample, which is a broken power law function,

$$\phi(L_{\rm iso}) \propto \begin{cases} (L_{\rm iso}/L_{\rm cut})^{x}, & L_{\rm iso} < L_{\rm cut} \\ (L_{\rm iso}/L_{\rm cut})^{y}, & L_{\rm iso} > L_{\rm cut}\ , \end{cases} \tag{3}$$

where $x = -1.50$, $y = -2.32$, $L_{\rm cut} = 3.8 \times 10^{52}$ erg s^{-1}, and $L_{\rm iso}$ is the peak isotropic luminosity.

(3). To calculate the peak flux of bursts in a given energy range, we need to assign a spectrum to each mock GRB. Assuming that all bursts are well fit with the Band function (Band et al., 1993) and the photon spectral indices in the energy bands lower and higher than the peak energy $E_{\rm peak}$ are -1 and -2.3, respectively (e.g., Kaneko et al. 2006b; Nava et al. 2011; Goldstein et al. 2012).

(4). The spectral peak energy $E_{\rm peak}$ for each burst is obtained through the Yonetoku relation (Yonetoku et al., 2004b). We adopt the $E'_{\rm peak} - L_{\rm iso}$ relation obtained with the complete BAT6 sample (Nava et al., 2012):

$$\log\left(E'_{\rm peak}\right) = -25.33 + 0.53 \log\left(L_{\rm iso}\right)\ , \tag{4}$$

where $E'_{\rm peak} = E_{\rm peak}(1+z)$ is the rest frame peak energy.

(5). With the assumptions above, the peak flux P of each simulated burst in a given energy range $\Delta E = [E_1, E_2]$ can be expressed as:

$$P_{\Delta E} = \frac{L_{\rm iso}}{4\pi d_L(z)^2} \cdot \frac{\int_{E_1}^{E_2} N(E)dE}{\int_{1{\rm keV}/(1+z)}^{10^4{\rm keV}/(1+z)} E\,N(E)dE} \ , \quad (5)$$

where $N(E)$ is the photon spectrum and $d_{\rm L}(z)$ is the luminosity distance of the GRB.

We normalize the simulated GRB population to the real population of bright *Swift*/BAT bursts, as Ghirlanda et al. (2015b) did. The BAT6 sample of Salvaterra et al. (2012a) is constructed by considering only bursts with favorable observing conditions, which are bright in the 15–150 keV *Swift*/BAT band, i.e., with peak photon flux $P \geq 2.6$ ph cm^{-2} s^{-1}. This sample is composed of 58 GRBs and reaches a completeness level of 95% in redshift. Among the current *Swift*/BAT sample (773 events detected up to 2014 July with duration exceeding $T_{90} \geq 2$ s)[10], 204 bursts with peak flux $P \geq 2.6$ ph cm^{-2} s^{-1} (i.e. the same flux threshold used to define the BAT6 sample) have been extracted. Considering the *Swift* FoV of 1.4 sr and the observational period of ∼9.5 years, a detection rate by *Swift*/BAT is estimated to be ∼15 events yr^{-1} sr^{-1} with peak flux $P \geq$2.6 ph cm^{-2} s^{-1} (Ghirlanda et al., 2015b). The simulated population of GRBs is normalized to this rate.

Using the fraction of observed sky per year (i.e., the ECLAIRs FoV of 2 sr) and the expected ECLAIRs sensitivity of $\sim 7.2 \times 10^{-8}$ erg cm^{-2} s^{-1} for an exposure of 10 s in the 4–150 keV energy range, our simulations show that ECLAIRs will detect 70–77 GRBs/yr depending on the exact assumptions on the GRB population (see the simulation procedures). Over the 3 yr lifetime of the mission, ECLAIRs is expected to be able to detect ∼ 200–230 GRBs. Fig. 11 shows the differential distribution of the GRBs expected to be detected by ECLAIRs as a function of redshift. One can see from this plot that nearly 4%–5% of ECLAIRs GRBs are expected to be high redshift GRBs ($z > 5$), which corresponds to a detection rate of about 3–4 GRBs/yr at $z > 5$, including ∼ 2–3 GRBs/yr at $5 < z < 6$ and ∼ 1 GRBs/yr at $6 < z < 7$. These results are in good agreement with the predictions from Godet et al. (2014b) and Cordier et al. (2015).

In the *SVOM* era we expect to rapidly identify candidate high-z bursts (VT non-detections), and benefit from the greatly enhanced imaging and spectroscopic capabilities of *JWST* and subsequently the 30 m class ground-based telescopes. This will mean not only much better redshift completeness at high-z than has been possible for the *Swift* sample, based on afterglow spectroscopy (and host spectroscopy if the afterglow was localised, but no spectrum secured), but also both extremely high signal-to-noise afterglow spectra in many cases, together with much deeper imaging to search for hosts in emission than is possible with current technology. Thus, in the three year core mission, we expect to roughly double the current known sample of $z \gtrsim 6$ GRBs, but, crucially, for most of these also to obtain much more precise measures of host luminosity, column density and metallicities.

3.6.1 GRBs to probe reionization

After the Big-Bang, expansion made the universe temperature decrease rapidly. After about 380,000 years, the universe became transparent, radiation and matter decoupled and hydrogen recombined. Under the action of gravitation, the first objects formed slowly and, either stars or quasars or both, started to reionized the universe. This phase change is a crucial period and GRBs offer a unique opportunity to probe the ionization state of the gas at that time.

Therefore, a very important observation to be made in the spectrum of high redshift ($z > 6$) GRB afterglows is to search for the red damping wing of the absorption trough produced by neutral hydrogen in the IGM. As it is known that reionization ends around $z \sim 6$ (Becker et al., 2007), this signature would be definite evidence for this crucial phase of the universe history. GRBs have the advantage that no large scale proximity effect is expected contrary to QSOs that ionize the IGM to a distance of several Mpc

[10] http://swift.gsfc.nasa.gov/docs/swift/archive/grb_table/

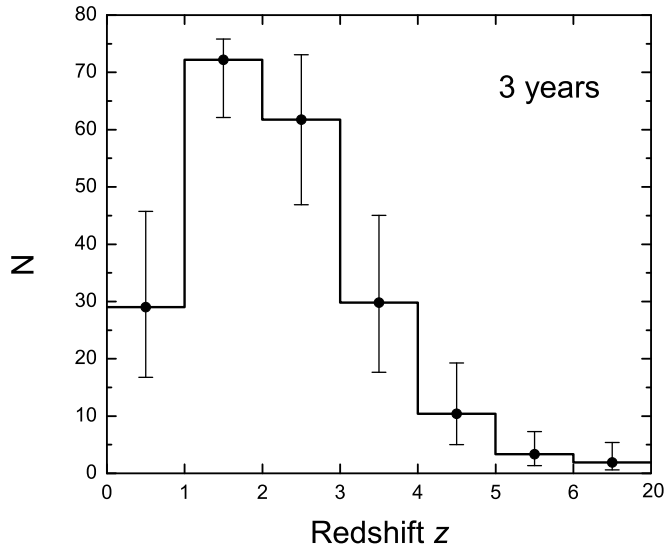

Figure 11: Simulated redshift distribution of GRBs to be detected by ECLAIRs during the 3 year mission lifetime. Error bars show the 2σ uncertainties of the assumptions on the GRB population (i.e., the 2σ uncertainties of the GRB rate density evolution, $\delta = 1.7 \pm 2\sigma$) in the redshift bin.

(Guimarães et al., 2007). Their disadvantage is that usually neutral gas from the host galaxy located in

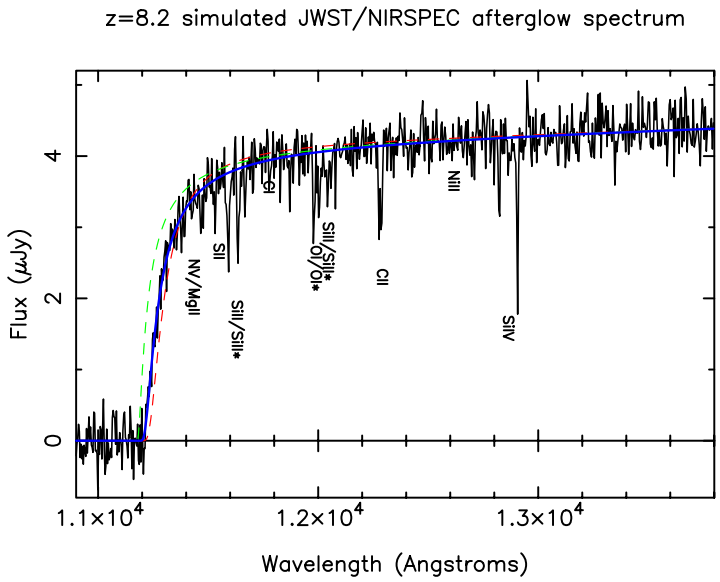

Figure 12: Simulated *JWST*/NIRSPEC spectrum of a GRB afterglow based on GRB 090423, as it would have been observed 4 days post-burst in a 5 hr exposure. This clearly shows that high S/N spectroscopy will be possible even for faint afterglows using *JWST*. The simulation assumed a 100% neutral IGM and a host HI column density of $\log(N_{\rm H}/{\rm cm}^{-2}) = 21$. The continuum cannot be fit by either a pure neutral IGM model (green line), or a pure host model with an ionized IGM (red line). Instead the two components can be decomposed, as illustrated with the blue fit.

front of the GRB already produces a damping wing which is difficult to disentangle from the IGM effect (Patel et al., 2010). This is possible however if a high SNR spectrum of the afterglow is available. At a redshift of $z = 8$, the contribution of the IGM is predominant as is shown in Fig. 12. At the time *SVOM* will be launched, *JWST* will be the best facility to perform such observations waiting for the advent of E-ELT.

It has long been suspected that the primary driver of reionization was extreme-UV radiation emitted from early generations of massive stars (Loeb & Barkana, 2001). This explanation requires both that sufficient star formation was occurring at $z \gtrsim 6$ and also that a sufficient proportion of the UV radiation that they produced escaped from their host galaxies into the surrounding medium. Establishing whether these combined requirements are met in reality is fraught with difficulties.

Determinations of the global star formation density at high-z generally relies on estimating the star formation rates in individual detected galaxies, and then extrapolating the luminosity function (LF) to account for galaxies below the detection threshold. Various studies have suggested that the galaxy luminosity function steepens at high redshift, to the point that the overall star formation is likely dominated by the faint galaxies, below the depth of *HST* deep field observations (Bouwens et al., 2015). This adds considerable uncertainty to the extrapolation since the form of the LF must be postulated (usually taken to be a Schechter function; Schechter, 1976), the faint end slope estimated from observations at the bright end, and some cut-off chosen below which it is assumed that the lower rates of star formation could not be sustained.

The average escape fraction, $f_{\rm esc}$, of ionizing radiation presents an even tougher problem. It is not feasible to measure directly at $z > 6$ because the high opacity of the intergalactic medium itself will absorb almost all the radiation that might escape any given galaxy. Most direct searches for Lyman continuum emission at lower redshift have suggested that the escape fraction is only a few percent, or even less, although, again, there are large uncertainties and potential systematics (Guaita et al., 2016). It is generally found that $f_{\rm esc}$ must increase to values of at least $\sim 10\%$ at $z \gtrsim 6$, for stars to have been the agents of reionization (e.g., Robertson et al., 2015).

Observations of high redshift gamma-ray bursts and their hosts provide powerful alternative routes to addressing both of these problems, and hence offer exciting opportunities for *SVOM*.

3.6.2 The galaxy luminosity function in the era of reionization

By conducting deep searches for the hosts of GRBs at high-z we can directly estimate the ratio of star-formation occurring in detectable and undetectable galaxies to some limiting magnitude. Thus, without fixing the luminosity function itself, we obtain the correction factor by which detected star formation must be multiplied to infer the total star formation. Note, this is an essentially independent route to the global star formation rate compared to that discussed in section 3.7, and does not suffer from uncertainties in the evolution of GRB properties with redshift. The sole assumptions are that GRB-rate is proportional to star-formation rate and that redshift incompleteness is independent of host star-formation rate. At high redshifts, where the large majority of star formation is at sub-solar metallicities, and most galaxies are relatively free of dust, these assumptions are likely to be valid (e.g., Perley et al., 2016).

Since the position and redshift of each host is known from the GRB afterglows, the follow-up observations can be much shorter than equivalent multi-filter deep field searches for Lyman-break galaxies. Early application of this technique to small samples high-z hosts, none of which were detected in deep *HST* or VLT imaging, confirmed that the majority of star formation above $z > 5$ occurred in galaxies below the effective detection limit of *HST* (Tanvir et al., 2012; Basa et al., 2012; Trenti et al., 2012). Subsequently, new *HST* observations have resulted in the first detections of $z \sim 6$ hosts (McGuire et al., 2015, see Fig. 13), although the total sample remains modest (9 *Swift* GRBs at $z \gtrsim 6$ at the time of writing).

3.6.3 The escape fraction of ionizing radiation

Ground-based spectra of afterglows at $z \gtrsim 2$ usually show prominent troughs due to Lyman-α absorption (in most cases resulting in a damped line) by neutral hydrogen in the host galaxy, the median column density being $\log(N_{\rm H}/{\rm cm}^{-2}) \sim 21.5$. Since column densities of $\log(N_{\rm H}/{\rm cm}^{-2}) \gtrsim 18$ are essentially opaque to ionizing radiation, we can already say that the large majority of sight-lines to GRBs would have $f_{\rm esc} = 0$. Of course, it is possible that in any given galaxy, another sight line would have lower column density, but by assuming that GRB progenitors are representative, in terms of their locations, of typical very massive stars (which are responsible for the bulk of UV production), we can infer statistically the average $f_{\rm esc}$ from a sample of GRBs (Chen et al., 2007). This has been performed for GRBs at $z = 2$–4, indicating an upper limit of $f_{\rm esc} < 7.5\%$ (Fynbo et al., 2009).

At higher redshifts, the flux blueward of the Lyman-α line becomes increasingly attenuated by absorption due to the Lyman-α forest. This begins to present a technical challenge, as the contribution of the neutral fraction of the IGM must be disentangled from the absorption due to the host, but this is possible given sufficiently high quality spectra (e.g., Hartoog et al., 2015). So far there are only hints of reducing HI column density in hosts at $z \gtrsim 5.5$ (Chornock et al., 2014, see Fig. 13) compared to lower redshifts, but the sample remains too small for firm conclusions, and still favours a low value of $f_{\rm esc}$.

3.6.4 Catching PopIII stars

Gamma-ray bursts also offer the exciting opportunity to search for the first stars (hereafter, Pop III-primordial metal-free) formed in the Universe. Numerical simulations show that Pop III stars form in primordial minihaloes at $z \sim 20$, with virial mass $M_{\rm vir} \sim 10^6$ M$_\odot$ and temperatures $T_{\rm vir} \leq 10^4$ K. These primordial stars are considered to have played a crucial role in the early cosmic evolution by emitting the first light and producing the first heavy elements.

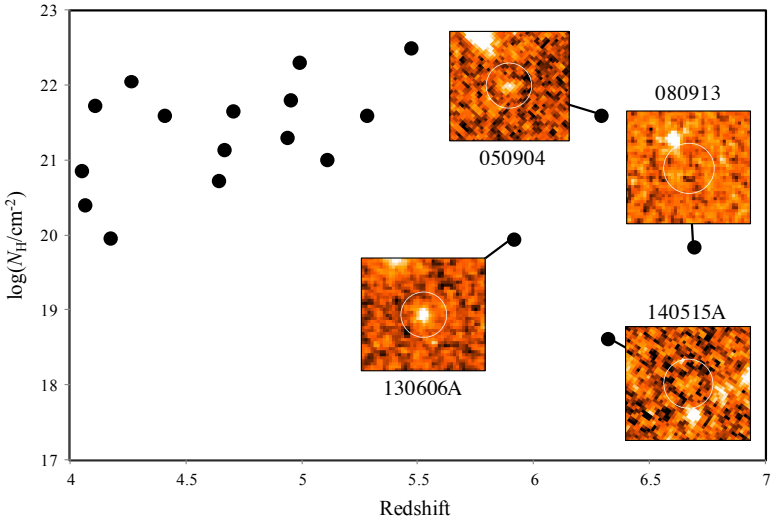

Figure 13: Plot of HI column density for the sample of *Swift* GRBs (taken from various sources, primarily Thöne et al., 2013; Chornock et al., 2014), showing marginal evidence for a decline at $z > 5.5$, potentially indicating an increase in the escape fraction of ionizing radiation. Deep *HST* imaging of the four highest redshift GRBs in this figure are shown as inset panels. Two hosts (of GRBs 130606A and 050904) are clearly detected, one (GRB 140515A) is marginally detected, and the last (GRB 080913) is undetected.

The theoretical efforts developed to explain the formation and fate of PopIII stars remain largely untested because there is no direct observation of these stars up to now. Different techniques may soon shed light on this important issue. For example the analysis of the morphology of 21cm spots could help discriminate the contribution of the different populations at different redshifts and carry wealth of information on Pop III stars. The *JWST* will also allow to directly observe the formation of the first galaxies, thus opening an amazing window for understanding the nature of the first stars and the evolution of populations at high redshift.

Another technique for observing these primordial stars may be to use GRBs. Indeed Pop III stars may also produce collapsar gamma-ray bursts whose total isotropic energy could be ∼2 orders of magnitude larger than average (Bromm & Loeb, 2006; Heger et al., 2003; Stacy et al., 2011). Even if the Pop III star has a supergiant hydrogen envelope, the GRB jet can break out of it because of the long-lasting accretion of the envelope itself. In this context the minimum energy expected for a GRB triggered by a Pop III star is near the maximum energy recorded for any GRB. Therefore, any GRB at $z \geq 6$ and $E_{\rm iso} \geq 8 \times 10^{54}$ erg would potentially have a Pop III progenitor.

Unfortunately it is not so easy to associate with certainty a distant GRB to a Pop III star. A promising method is to exploit the remarkable brightness of the GRB afterglow triggered by a Pop-III star. In the K band, the JWST will be able to detect GRBs, and to conduct spectroscopy on their afterglows out to $z \sim 16$, even after 1 day. In the M band, the redshift horizon is extended further still, to $z \sim 35$.

3.7 The cosmic Star Formation Rate evolution

Long-duration GRBs triggered by the collapse of massive stars, provide a complementary method for measuring the global star formation rate density (Totani, 1997; Wijers et al., 1998; Bromm et al., 2002; Vangioni et al., 2015; Wang et al., 2015; Petitjean et al., 2016). The short life-time of such stars makes them natural tracers of the recent star formation. As a result, the rate of long GRBs ($\dot{N}$) is linked to the star formation rate (SFR):

$$\dot{N}(z) = \epsilon \times \dot{\rho}_*(z) \tag{6}$$

ϵ is the efficiency with which GRBs occur (and are detected) by unit of star formation rate $\dot{\rho}_*(z)$. Since long GRBs can be detected up to very high redshift (at $z \gtrsim 6$), if ϵ was perfectly known, we could use equation 6 to measure the cosmic SFR in the very early history of the universe. However, several works have shown that the rate of GRBs does not strictly follow the SFR history (Le & Dermer, 2007; Salvaterra & Chincarini, 2007; Kistler et al., 2008; Yüksel et al., 2008; Wang & Dai, 2009; Robertson & Ellis, 2012; Wang, 2013). For example, the SFR density inferred from high-redshift ($z > 6$) GRBs has consistently been significantly higher than obtained through galaxy studies (Bouwens et al., 2009, 2011), although the finding of a very steep faint end of the galaxy luminosity function has begun to ease this tension (Trenti et al., 2013). It is however still possible to use GRBs to measure the evolution of the cosmic SFR by assuming an evolution of the efficiency with redshift:

$$\epsilon = \epsilon_0 (1+z)^\delta. \tag{7}$$

By combining this form with a cosmic SFR history, GRB detector efficiency, and luminosity function, it is possible to fit simultaneously for the various parameters (see e.g. the review of Wang et al., 2015, and references therein). The redshift dependence (δ) can be constrained at $z < 4$ where other tracers of the cosmic SFR are available. The GRB rate at $z > 4$ then provides a measurement of the cosmic SFR in the first galaxies (see Fig. 14 for an example). Some variants of this method were used e.g. in Daigne et al. (2006b); Lapi et al. (2008); Kistler et al. (2009); Robertson & Ellis (2012); Salvaterra et al. (2012b); Wang (2013); Trenti et al. (2015) finding δ in the range 0.5 to 1.5. Some studies suggest however a perfect correspondence of the GRB rate and SFR, i.e. $\delta \sim 0$ (Elliott et al., 2012, e.g.).

Possible reasons for the over-production of long GRBs at high redshift are discussed in details in Wang et al. (2015). This issue is interesting to investigate as this may yield astrophysical requirements for GRB production. The metallicity evolution of the universe may well play an important role since theory and

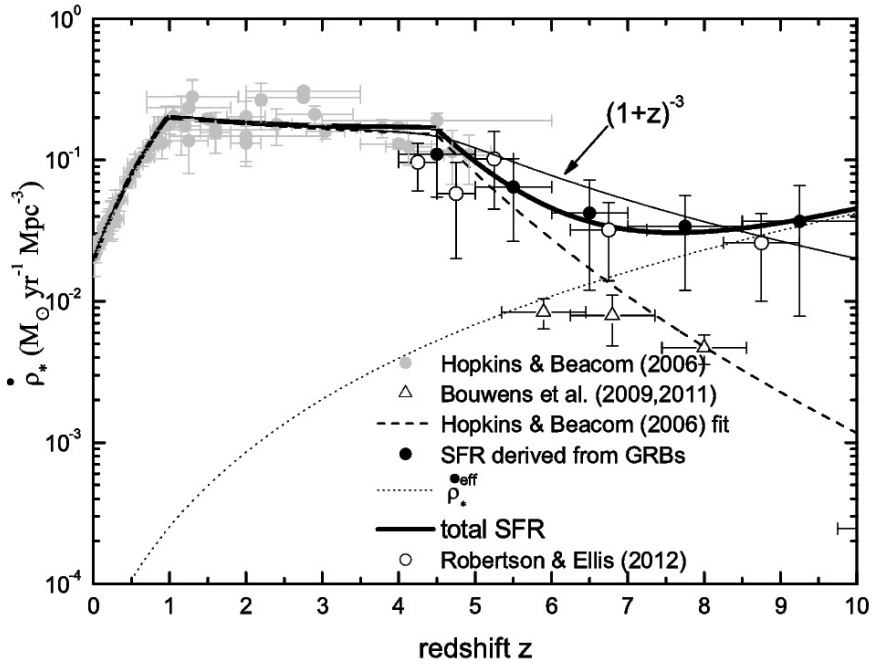

Figure 14: The cosmic star formation history. The grey points are taken from Hopkins & Beacom (2006), the dashed line shows their fit. The triangles are from Bouwens et al. (2009, 2011). The open circles are taken from Robertson & Ellis (2012). The filled circles are the SFR derived from GRBs in Wang (2013). Adapted from Wang (2013).

observation both support that long GRBs prefer low-metallicity environments. However, a few GRB hosts have high metallicity, so that the role of metallicity is still debated (Wolf & Podsiadlowski, 2007; Kocevski et al., 2009; Graham et al., 2009; Svensson et al., 2010). Other possibilities are the evolution of the stellar initial mass function (IMF), whose effect on the GRB rate are studied in Wang & Dai (2011) ; the evolution of the break in the luminosity function of long GRBs (Virgili et al., 2011) ; or even cosmic strings (linear topological defects formed in very early universe) serving as GRB central engines (Cheng et al., 2010).

The relation between GRB rate and SFR is also discussed at redshift lower than 1. Several selection effects affect the observed redshift distribution of GRBs (Coward, 2007), and so their intrinsic rate. The most important one is the flux sensitivity of detectors. To correct for this effect, the Lynden-Bell's c^- method (Lynden-Bell, 1971) has been applied to the *Swift* long GRBs (Yonetoku et al., 2004a; Kocevski & Liang, 2006; Wu et al., 2012; Yu et al., 2015a). The obtained trend suggests that the formation rate of GRBs does not directly trace SFR at low redshift $z < 1.0$ (see however Pescalli et al., 2016).

Finally some insight on the relation between SFR and GRBs can come from the study of GRB host galaxies. A strong dependence of the GRB rate on host-galaxy properties out to $z \sim 1$ is found by Perley et al. (2013). Vergani et al. (2015) found that the mass distribution of long GRB host galaxies is different than the expected one for star-forming galaxies at $z < 1.0$. In the same redshift range, Boissier et al. (2013) found that ϵ depends on the SFR or stellar mass of the host galaxy (and is possibly related to a metallicity effect). Such a trend is also found in other works (Vergani et al., 2015; Krühler et al., 2015), but questions remain due to the possibility of biases, the unknown nature of dark bursts, sample sizes (e.g. Hunt et al., 2014). Other studies argue that GRBs trace star formation without any bias (e.g. Michałowski et al., 2012). At higher redshift ($3 < z < 5$), Greiner et al. (2015) argues for a good correspondence between GRB rate and SFR, i.e. a constant ϵ (see also Perley et al., 2016). On the other hand, Schulze et al. (2015) still argue for a metallicity varying ϵ in the redshift range ($0 < z < 4.5$).

SVOM will allow us to improve over the legacy of *Swift* observations on several aspects:
• The error-bars at redshift larger than 5 will simply diminish owing to the number of GRBs that will be detected during the nominal mission (see header of this section).
• Based on the predictions for the *SVOM* mission, Wei et al. (2016) performed Monte Carlo simulations of a sample of 450 GRBs (5 yr observations). Using simulated GRBs with $z < 4$ and $L_{\rm iso} > 1.8 \times 10^{51}$ erg s^{-1}, they show it is possible to better constrain δ in equation 7 and other parameters than with the current *Swift* sample.
• While the study of host galaxies could bring important insight, they have yielded up to now to conflicting results (see above). This is likely due to the small statistics and biases affecting the current samples.

Owing to its quick follow-up in the optical and in the near infrared, *SVOM* will allow us to construct large, complete, and unbiased samples of long GRBs. The comparison of the their host galaxies with the usual population of galaxies will allow us to constrain how ϵ varies with physical properties of the host galaxy, and more generally to learn about the long GRB progenitors (e.g. to confirm or not a metallicity effect). This will help us to better understand the connection between star formation and long GRBs, so that the cosmic SFR can be studied from the long GRB rate on a sound basis.

3.8 Studies of GRB host galaxies

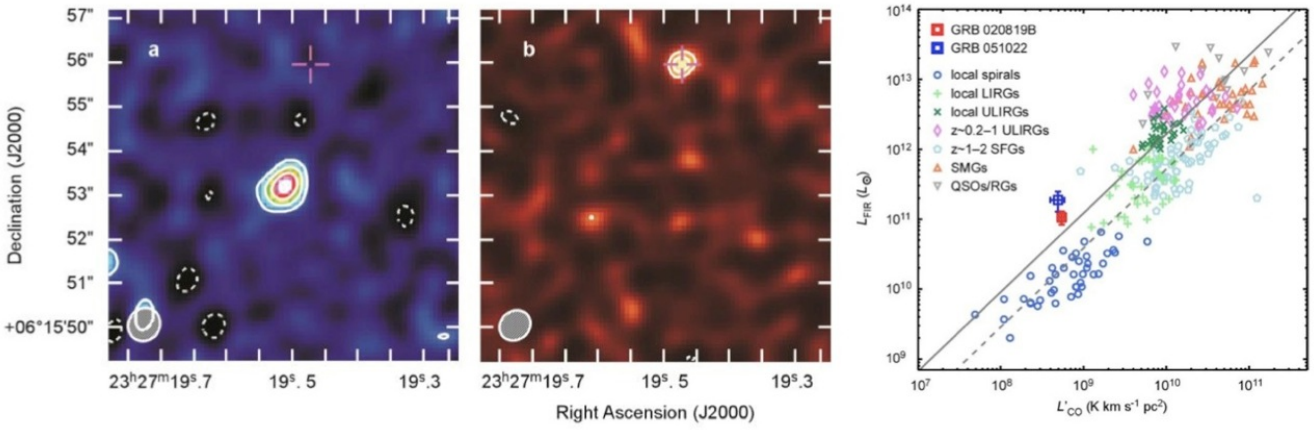

Figure 15: The cold dust (*left panel*) and CO molecular gas (*central panel*) emission maps of the GRB 020819B host galaxy at z=0.4. The star-forming region where the GRB was discovered is indicated by the cross symbol and shows very low gas-to-dust ratio compared to the central region of the galaxy. *Right panel*: CO versus total Infrared luminosities for 2 GRB hosts, compared to a variety of galaxy samples at low and high redshift. The Schmidt-Kennicutt law for star-forming disks is represented by the dashed line, while the solid line depicts the relation followed by starburst sources. For their CO luminosities, the 2 GRB hosts discussed here display more intense star-forming activity than disk galaxies, pointing to more efficient processes at converting gas into stars. Adapted from Hatsukade et al. (2014).

3.8.1 GRBs as probes of star-forming processes and physical conditions in very young stellar environments

Studying the host-galaxies of GRBs supplements in a very original way what is being learned from the deep cosmological surveys of galaxies selected by their continuum emission. First, the selection of cosmic sites with LGRBs is done independently of the properties of their underlying host galaxies, hence yielding an identification of star-forming sources that is not affected by galaxy continuum detection limits. Besides, their redshift can be measured from absorption lines detected in the spectrum of the afterglow, even when the host is too faint to be followed-up with 8m-class telescope spectroscopy. LGRBs thus allow probing the very faint end of the galaxy distribution with accurate spectroscopic redshifts, which can not be performed

with other techniques. Finally, because of the very short lifetime of their progenitor, the selection of star-forming environments with LGRBs can be sensitive to much shorter time-scales (typically $\sim$10 Myrs) than what is typically probed with continuum-selected galaxy surveys (e.g., $\gtrsim$100 Myrs at Ultraviolet and far-Infrared wavelengths). In fact, high resolution imaging obtained with the *HST* has shown that the localization of LGRB afterglows within their host galaxies is more closely connected to the highest surface brightness regions than what can be observed from the spatial distribution of more ordinary core-collapsed Supernovae (Fruchter et al., 2006). Although it could be simply due to increased star formation density leading to a higher probability for producing long GRBs (Kelly et al., 2014; Blanchard et al., 2016), it may also be explained by an aging effect if LGRBs have progenitors with shorter lifetimes than SNe and explode in young and luminous regions where the bulk of massive stars has not yet vanished (Raskin et al., 2008). Irrespective of these possible interpretations, LGRBs offer an original view on high-redshift sources, enabling the census of star-forming environments with markedly different properties than those characterizing the bulk of galaxies selected with other techniques.

In this regard, the most exciting aspect making the use of GRBs unique is the possibility to combine constraints on the neutral gas obtained from absorption spectroscopy on the line of sight of the afterglow (see next section) with constraints on the ionized gas obtained with subsequent spectroscopic follow-up of the host galaxy in emission. This has proven to be technically difficult so far, not only because LGRB host galaxies tend to be generally faint but also because long-slit spectroscopy of distant sources do not resolve emission line properties on the scale of individual star-forming regions, unlike the information encoded in absorption on the line of sight of the GRB. In the near future, *SVOM* will yet benefit from a unique synergy with facilities like *JWST* and possibly the Extremely Large Telescopes, which will allow us to constrain at sub-kpc scales the ionized gas properties (density, temperature, ...) of GRB-selected star-forming environments thanks to spatially-resolved IFU spectroscopy. Such analysis has already been carried for few GRB host galaxies restricted to the low redshift Universe (e.g., GRB 980425: Christensen et al., 2008). Beyond $\sim$2020, it will be possible to extend these studies with larger GRB samples up to $z \sim 2$, probing sources at the peak of galaxy formation history. Besides, with the future generation of large millimeter and radio interferometers available in the *SVOM* era (e.g., ALMA, SKA), it will also be possible to measure the atomic and molecular gas masses as well as the dust luminosity in the close vicinity of GRBs. Combining all these follow-up campaigns will provide a unique opportunity to characterize both the ionized and neutral gas phases, the local gas conditions, the metal enrichment and the nature of star formation processes within individual star-forming regions.

In the case of LGRB sites experiencing very young star formation, this will allow us to quantify the efficiency of converting the gas into stars, especially in the early phases of star formation just when the gas is undergoing its first gravitational collapse. Hydrodynamical simulations of gas-rich disk galaxies at intermediate redshifts indeed suggest that this very early phase could be characterized by very high star formation efficiency during the first $\sim$ 15 Myrs, before evolving to a more quiescent mode of star formation following the standard Schmidt law (e.g., Bournaud et al., 2014). However, observational constraints supporting this scenario are still missing, not only because of the difficulty of identifying such environments of early star formation in the distant Universe, but also for the limited performance of current facilities at long wavelengths. Similarly, models suggest that the relative velocity dispersions of the ionized and molecular gas phase components can put tight constraints on the strength of stellar feedback, which still remains today a key but unconstrained ingredient in our understanding of galaxy formation. Combining the properties derived in absorption using the *SVOM* GRB afterglows with the host galaxy follow-ups carried with JWST, SKA and ALMA will thus produce spatially-resolved constraints on stellar feedback and star formation efficiency that will not be rivaled by any other methods.

Finally, recent observations of CO emission carried out at (sub)millimeter wavelengths have suggested that galaxies hosting LGRBs, or at least the star-forming regions where they are produced, could be deficient in molecular gas (Hatsukade et al., 2014; Stanway et al., 2015). This was directly observed in the host of GRB 020819B at $z \sim 0.4$, where the GRB occurred in a star-forming region with low gas-to-dust mass ratio (see Fig. 15). Similarly, the amount of molecular gas inferred from the very few H_2 absorption

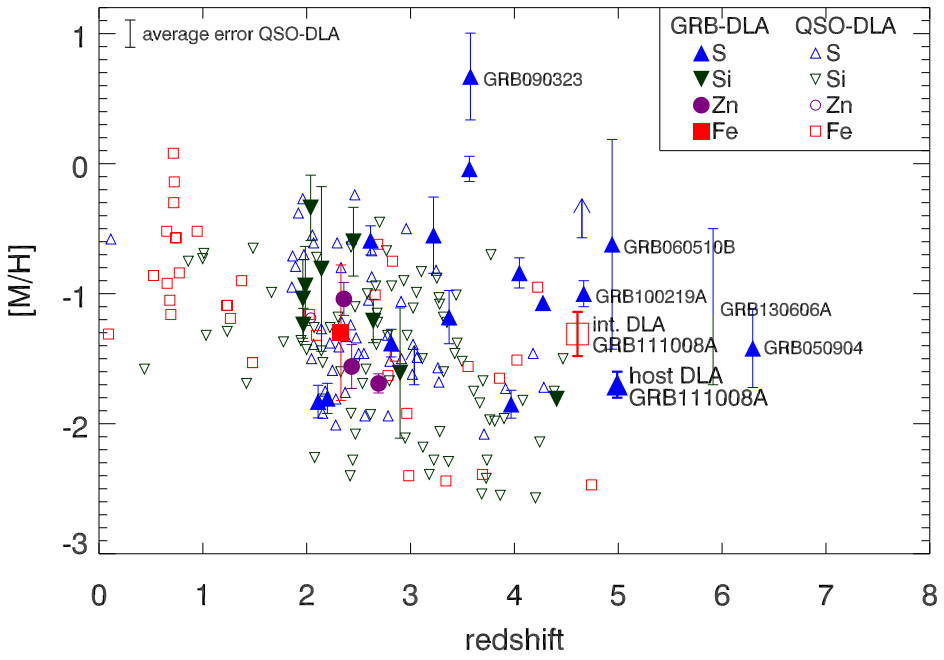

Figure 16: Metallicities measured in DLAs versus redshift. Red squares are for intervening DLAs observed along the line of sight to quasars (see Rafelski et al. 2012) and blue squares are for GRB-DLAs (Figure from Sparre et al. 2014).

lines detected so far in the spectra of GRB afterglows appears to be weak with respect to the neutral gas content (Ledoux et al., 2009). This apparent lack of gas in the molecular phase within LGRB hosts is far from being understood at this stage. It could be due to an extremely high efficiency in turning molecular gas into stars in the close environment (~ 100 pc) of GRBs, but why these conditions are specifically found among GRB hosts is not clear. Interestingly, 21cm observations of nearby LGRB hosts have revealed high levels of neutral HI gas, typical of ordinary star-forming galaxies with comparable stellar mass and star formation rate (Michałowski et al., 2015). Given recent evidence for metallicities below solar in GRB host environments, this could indicate either a much shorter timescale for gas cooling and star formation than the timescale needed for the conversion from HI to H_2, or that star formation in these sources is directly fueled by large reservoirs of atomic gas from the intergalactic medium (Krumholz, 2012). This interpretation is however based on a limited number of GRB hosts at low redshifts, and it is also not clear if this small sub-sample is fully representative of the whole LGRB host population, especially for sources at higher redshifts. *SVOM* will provide a more homogeneous sample of long GRBs with accurate localizations and spectroscopic identifications, which will be perfectly suited for follow-up with ALMA and SKA (at least up to $z \sim 1$) to characterize their gas and dust content at the scale of individual star forming regions. In parallel, the more rapid and more systematic identification of GRB afterglows with *SVOM* will also lead to more uniform constraints on the metal and gas content seen in absorption, which will result in a better understanding of the physical processes triggering star formation in the distant Universe.

3.8.2 Absorptions in afterglow spectra

Afterglows of GRBs can be very bright and therefore are ideal targets to study the ISM of high-redshift galaxies. Since long GRBs are produced by the deaths of massive stars, the spectrum of the afterglow yields unique information on the host galaxy and possibly the star-forming region where the afterglow explodes. The most prominent absorption line seen in most high-redshift GRB afterglow spectra is a strong Lyman-α H I absorption associated with a wealth of metal absorption lines from which it is possible to

derive accurate metallicities (see Fig. 16). H I column densities are much larger than in most Damped Lyman-α (DLAs) systems observed on the line of sight to quasars often reaching log $N(\mathrm{cm}^{-2}) > 22$. It can be seen that GRB DLAs probe higher redshifts. The fact that metallicities seem to be higher toward GRBs indicates as well that the two populations do not probe the same gas. Since GRBs are located close to the region of star formation, one can expect to probe higher column densities and thus higher metallicities. Recent searches for high-column density QSO-DLAs show that at higher column densities, metallicity are on average higher (Noterdaeme et al., 2015). GRBs are thus ideal beacons with which it is possible to study the physical conditions, formation of molecules and properties of dust in the inter-stellar medium for different environments (star formation activity, low-metallicities etc...). All this information gathered along the line of sight can be combined with the properties of the host-galaxy gathered once the afterglow has faded.

In addition, the powerful UV flash following the GRB ionizes and excites the gas in the circumburst environment and the interstellar medium surrounding the GRB up to 200 pc from the GRB (Vreeswijk et al., 2013). Absorption from excited levels of species like Fe II, Ni II, Cr II are detected in afterglow spectra taken just after the burst. Since the GRB afterglow fades rapidly, recombination prevails and the populations of these levels change (most of the time decrease but sometimes can increase for a while). This induces these absorptions in the afterglow spectrum to vary and at the end to disappear. Detection of these time-dependent processes, with timescales ranging from seconds to days in the observer frame can lead very interesting information on the burst itself and the ISM of the host (Vreeswijk et al., 2007; De Cia et al., 2012).

Finally, one could search for absorption signatures from the relics of gas expelled by the GRB progenitor. However, the task seems difficult and no clear and robust signature has been found yet probably because of the high ionization state of this gas (Fox et al., 2008).

3.9 Cosmology and fundamental physics

3.9.1 Could GRBs be used as standard rulers ?

The isotropic energy outflow from GRBs, estimated using the redshift and the integrated gamma-ray fluence, is enormous, up to $E_{\rm iso} \sim 10^{54}$ ergs, and even if the outflow is collimated in jets the total energy involved is still huge, $E_\gamma \sim 10^{51}$ ergs. The possibility that GRBs tap a standard energy reservoir to provide this prodigious output has been pursued by many authors following the initial suggestion from Frail et al. (2001). If the total energy available were roughly constant or predictable by some means and we could reliably estimate the collimation, then GRBs could be used as a cosmological probe to very high redshifts, (Bloom et al., 2003; Ghirlanda et al., 2004a). Early analysis of *BATSE* data revealed a correlation between the characterisic photon energy $E_{\rm p}$, the peak of observed $E.F(E)$ spectrum, and the fluence (Mallozzi et al., 1995; Lloyd et al., 2000). When redshifts became available for long bursts the isotropic energy, $E_{\rm iso}$, could be estimated from the fluence and the peak photon energy could be transformed into the source frame, $E_{\rm pz}$ and the so-called Amati relation, a correlation between $E_{\rm iso}$ and $E_{\rm pz}$ in the sense that more energetic bursts have a higher $E_{\rm pz}$, was discovered using data from *BeppoSAX* (Amati et al., 2002). This correlation has subsequently been confirmed and extended although there remain many significant outliers, including all short bursts, Fig. 17. The physical origin of the correlation may be associated with the emission mechanisms operating in the fireball but the theoretical details are far from settled (see the discussion by Amati (2006b) and references therein). More recently a tighter correlation between $E_{\rm iso}$, $E_{\rm pz}$ and the jet break time, $t_{\rm break}$, measured in the optical afterglow has been reported by Ghirlanda et al. (2004a), see Fig. 17. This is explained in terms of a modification to the Amati relation in which $E_{\rm iso}$ is corrected to a true collimated energy, E_γ, using an estimate of the collimation angle derived from $t_{\rm break}$. The details of the collimation correction depend on the density and density profile of the circumburst medium, Nava et al. (2006) and references therein. Multivariable regression analysis was performed by Liang & Zhang (2005) to derive a model-independent relationship, $E_{\rm iso} \propto E_{\rm pz}^{1.94} t_{\rm zbreak}^{-1.24}$, indicating that the rest-frame break time of the optical afterglow, $t_{\rm zbreak}$ was indeed correlated with the prompt emission

parameters.

Other studies have concentrated on the properties of the isotropic peak (maximum) luminosity of the GRB, $L_{\rm iso}$ ergs s^{-1}, measured over some short time scale ≈ 1 s, rather than the time integrated isotropic energy, $E_{\rm iso}$. Schaefer (2003) noted a possible correlation between $L_{\rm iso}$ and $E_{\rm pz}$ and later Yonetoku et al. (2004b) published such a correlation for 16 GRBs with firm redshifts. A correlation between $L_{\rm iso}$ and the spectral lag was first identified by Norris et al. (2000) and explained in terms of the evolution of $E_{\rm peak}$ with time. The shocked material responsible for the gamma-ray emission is expected to cool at a rate proportional to the gamma-ray luminosity and it has been suggested that $E_{\rm peak}$ traces the cooling (Schaefer, 2004). A similar correlation between $L_{\rm iso}$ and the variability of the GRB (V) was described by Ramirez-Ruiz & Fenimore (2000), and Reichart et al. (2001) and a related correlation between $E_{\rm pz}$ and V was described by Lloyd-Ronning & Ramirez-Ruiz (2002). The origin of the $L_{\rm iso} - V$ relation is likely to be related to the physics of the relativistic shocks and the bulk Lorentz factor of the outflow. It could be that high $\Gamma_{\rm outflow}$ results in high $L_{\rm iso}$ and V while lower luminosity and variability are expected if $\Gamma_{\rm outflow}$ is low (Mészáros et al., 2002b). A rather bizzare correlation involving $L_{\rm iso}$, $E_{\rm pz}$ and duration was found by Firmani et al. (2006). They employed the "high signal" time, T_{45}, as formulated by Reichart et al. (2001) in their study of variability, and showed that $L_{\rm iso} \propto E_{\rm pz}^{1.62} T_{45}^{-0.49}$ for 19 GRBs with a spread much narrower than that of the Amati relation. There is currently no explanation for such a correlation although, if it is not simply an artifact of the small sample size, it may be connected with the spectral lag and variability correlations and the Amati relation.

The correlation between $E_{\rm iso}$ and $E_{\rm pz}$ supplemented by additional empirical information can be used in pseudo redshift indicators, as for example Atteia (2003), but the intrinsic spread in the correlation and uncertainty about the underlying physical interpretation introduce large errors, typically of a factor ~ 2. It may be possible to reduce the errors by simultaneous application of several independent luminosity/energy correlations, and an extension of the Hubble Diagram to high redshifts using GRBs has been attempted (Schaefer, 2007). However, it is not clear that the correlations briefly described above are truly independent and there may be some underlying principle or mechanism which connects them all together. Recently, and more controversially, Butler et al. (2007) have raised serious doubts about the validity of these correlations suggesting that it is likely that they are introduced by observational/instrumental bias and have nothing to do with the physical properties of the GRBs and hence they conclude that GRBs are probably useless as cosmological probes. At very least their arguments suggest that selection effects must be carefully accounted for if these relations are applied in practice.

In order to estimate the cosmological parameters, these correlations must be calibrated in a cosmological model independent way to avoid the obvious circular argument problem. This could be done in two ways; using a solid physical interpretation of these relations to determine the slope independently from cosmology or calibration of the relations using many low redshift GRBs (Ghirlanda et al., 2006). Furthermore it is likely that the physical mechanism which gives rise to the correlations yields parameters which are dependent on the redshift. The luminosity, total energy, characteristic photon energy and temporal lags etc. may well depend on metallicity, the circumburst environment and the structure of the progenitor stars all of which evolve with time. Analysis of *BATSE* and more recently *Swift* data indicates that the luminosity function of GRBs evolves with time (Salvaterra et al., 2012a; Petrosian et al., 2015; Pescalli et al., 2015).

Independent of whether we can use GRBs as a probe of high redshift cosmology or not, a better understanding of the luminosity evolution of GRBs is crucial if we are to use them in the study of the cosmic star formation rate, the period of reionisation and other properties of the high-z Universe. What is required to make progress in our understanding of the correlations and the physics which lies behind them is simultaneous multiwavelength observations of the prompt and afterglow phases of GRBs. The combination of the GRM, ECLAIRs, MXT, VT and GWAC on *SVOM* can provide excellent spectral and temporal coverage significantly superior to previously available instrumentation. They will provide a large sample of GRBs for which we know the redshift, the prompt spectrum from gamma rays to soft X-rays and in some cases extending to the optical, the spectral-temporal structure of the prompt and soft

X-ray and optical coverage extending from the end of the prompt into the later stages of the X-ray and optical afterglow. These data will greatly improve our understanding of the presently known correlations and the physical mechanisms behind them.

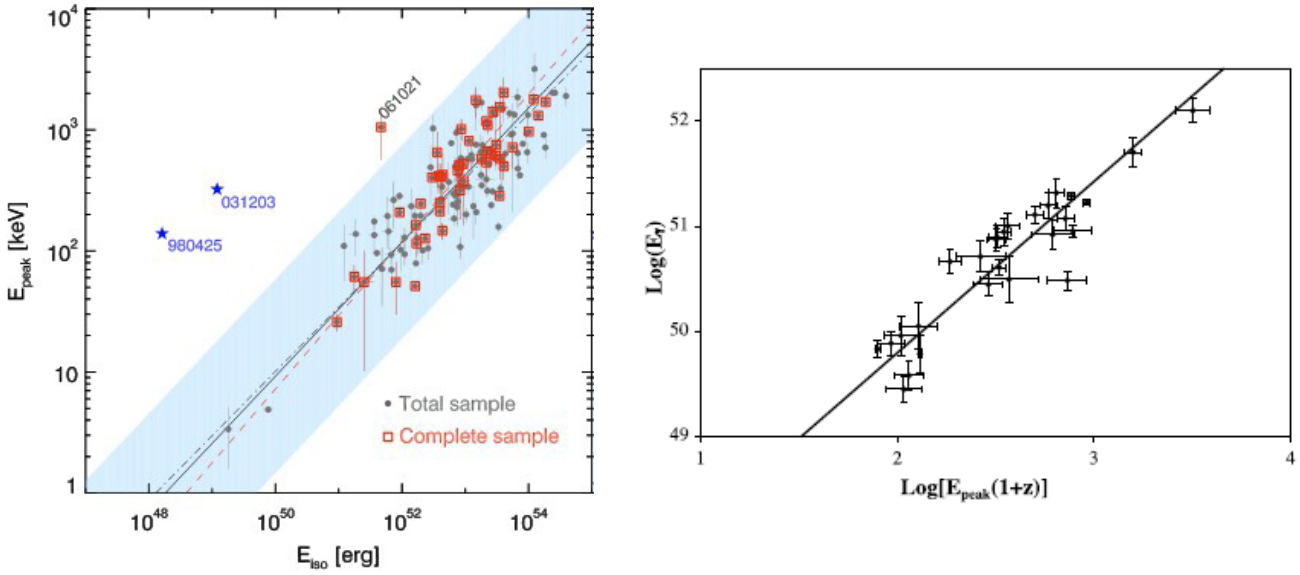

Figure 17: *Left-hand panel*: The Amati relation (Nava et al., 2012) showing the spread in the bulk correlation and obvious outlier including short bursts. *Right-hand panel*: The so-called Ghirlanda relation for 27 GRBs (Schaefer, 2007). E_γ is the burst energy calculated using the jet-angle, estimated from the so-called jet-break time in the optical afterglow, and $E_{\rm iso}$.

3.9.2 Variation of fundamental constants

Metal lines of absorption systems due to intervening galaxies along the line of sight towards distant sources provide insight into the atomic structure at the cosmic time and location of the intervening object. All atomic transitions depend on the fine-structure constant, offering a way to probe possible variations in its value in space and time (Rahmani et al. 2013 and references therein). These absorption lines are readily observed in the spectra of GRB afterglows and could be used to probe these possible variations. In case of the detection of H_2, the variations of the electron to proton mass ratio can be probed as well. Both measurements could be performed at the same time.

GRB afterglows, if well selected, can be unique targets in this field after the advent of extremely large telescopes (TMT and ELT) since GRB afterglows can be very bright even at high redshift and yield spectra of the highest SNR. The key here is that the probability that the line-of-sight intersects a diffuse molecular cloud is much higher in the case of GRBs compared to QSOs. Even though detection of H_2 in GRB afterglows has been rare up to now, it may be due to a selection effect because only bright afterglows can be followed up at high spectral resolution when the presence of H_2 implies the presence of dust and thus attenuation of the afterglow (Petitjean et al., 2006). The situation may change with the advent of larger telescopes, and with the VT on *SVOM* giving quicker identification of potentially obscured bursts.

Note that these studies will be possible only if a fast response mode on a high resolution spectrograph is available (e.g. Vreeswijk et al. 2007) but also if wavelength calibration is controlled to a very high level of precision.

4 *SVOM* Advances on Rapid Follow-Up Observations (*SVOM* ToO program)

4.1 Introduction

SVOM will become a premier time-domain machine in the early part of the next decade, an era when time domain astronomy will truly come of age in terms of multi-wavelength, wide-field sky coverage plus multi-messenger information. The advent of SKA (radio), LSST (optical) and CTA and HAWC (very high energy) on the ground, for example, will provide a very large increase in the number of rapidly available triggers for a wide variety of source types. Other electromagnetic facilities, such as the *SVOM* GWAC, will also find many transients.

The launch of *SVOM* will also coincide with an era where there will be a significant improvement in the capability of multi-messenger observatories. The gravitational wave observatories will have improved sensitivity and provide localisations of size 5-10 square degrees (Aasi et al., 2013) compared to the current several hundred square degrees. *SVOM* can tile such regions quickly and efficiently. The first phase of the new KM3NeT neutrino facility will complement IceCube and also provide much improved localisations which the *SVOM* narrow-field instruments can observe in a single pointing (for track events).

The much larger volume of triggers will provide a challenging scientific opportunity for *SVOM* which will have the on-board capability to obtain multi-wavelength follow-up observations.

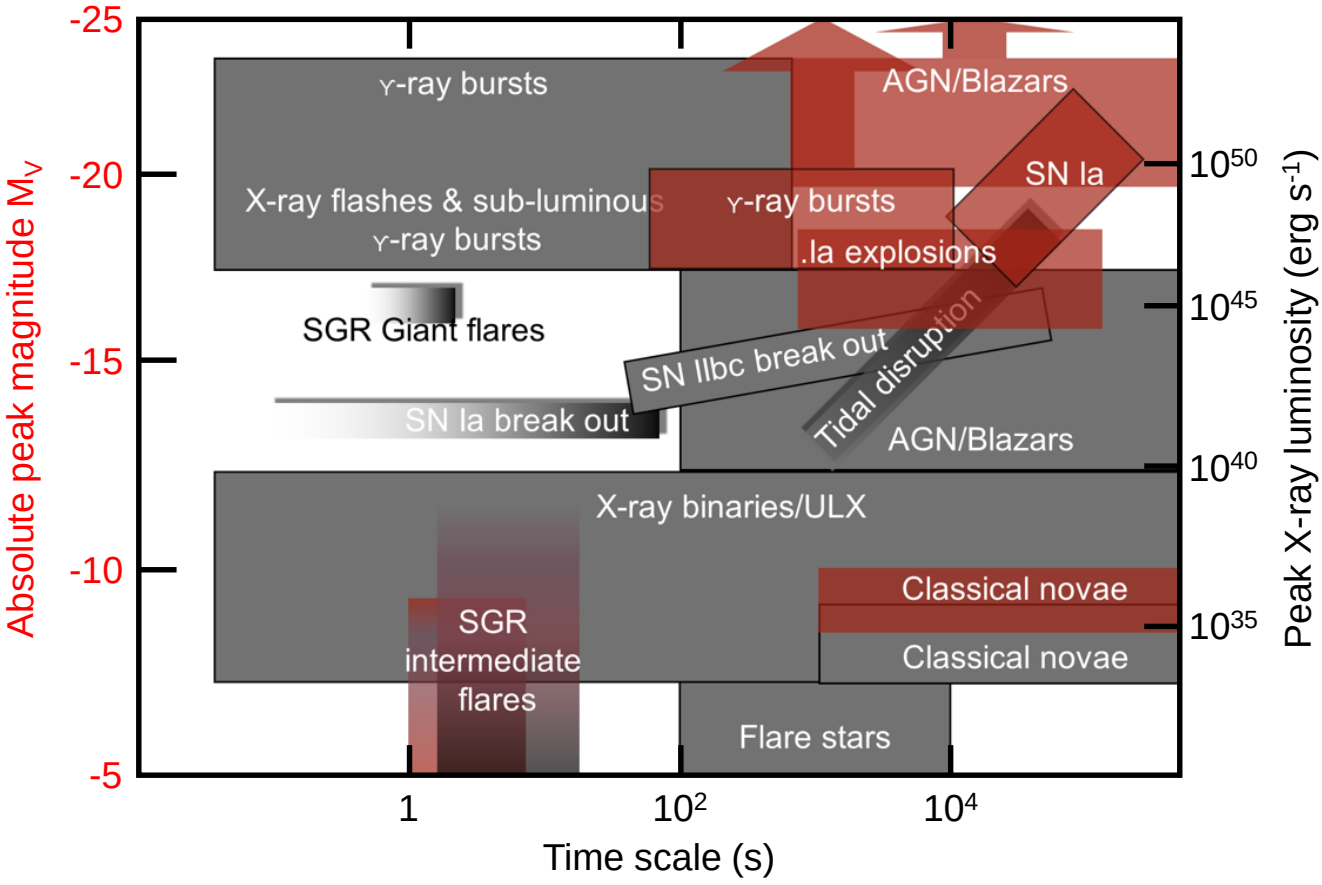

Figure 18: The characteristic absolute optical magnitude (red) and X-ray luminosity (grey) versus characteristic timescale for various classes of object which could be studied by *SVOM*. The optical/X-ray scales are on the left/right axes. Sources/phenomena that have been relatively poorly studied are plotted without border and with fading shading. Some object classes have a large range in characteristic timescales due to different physical processes. Adapted from Jonker et al. (2013).

4.2 Search for *SVOM* counterparts to multi-wavelength triggers

SVOM has multiple roles to play in the new era. It can: (1) follow-up triggers from other facilities, including multi-messenger facilities, and any candidate counterparts found by other electromagnetic facilities; (2) trigger multi-wavelength follow-up of *SVOM* triggers, including faint sources found in ground analysis which did not result in an on-board trigger and sources found with the ground-based *SVOM* facilities; (3) monitor sources likely to undergo a transient; and (4) survey classes of transients to provide population information. These types of observation will in some cases require MoUs for mutual benefit but will also require detailed planning to avoid overwhelming the observational limits of *SVOM* given the sheer number of triggers that will emerge from the wide-field transient machines. The latter issue is perhaps the greatest challenge facing astronomy – how to decide what to observe?

In terms of likely (known) classes of source there are several of particular importance well suited to the sensitivity of *SVOM*. Some of the explosive transient event types available for *SVOM* are shown in Fig. 18. Example classes of object include:

- Gamma-Ray Bursts: *SVOM* can localise and provide prompt follow-up for GRBs not automatically triggered on board, including those from other facilities and those found in *SVOM* ground analysis which may be of particular interest (low luminosity, high redshift etc.).
- Supernova: LSST and other optical facilities will find very large numbers of supernova, including rare classes demanding prompt follow-up. *SVOM* can observe in the optical and X-ray to look for information on the environment and progenitor, such as observing luminous supernova that may be powered by a central engine possibly in analogy with GRBs.
- Tidal Disruption Events: *SVOM* can probe the physical properties of TDEs which have emission which is either relativistic jet or accretion flow dominated. *Swift* has found a few jet-dominated cases raising the probability of discovery across the electromagnetic spectrum, but the rate of discovery should rapidly increase with the new survey facilities.
- Active Galactic Nuclei: *SVOM* can target AGN undergoing a flaring event, including Seyfert galaxies and quasars where the combination of optical and X-ray data can constrain synchrotron versus synchrotron-self-Compton emission.
- Blazars: *SVOM* can provide crucial information on the spectral energy distribution of blazars. Future facilities will increase the number of high-redshift blazar candidates and provide many potential events with large variability amplitudes possibly due to state changes.
- Galactic transients: Many types of transients in the Milky Way are potential *SVOM* targets, such as flaring magnetars (rare but provide crucial insight into emission mechanisms), X-ray binaries and ULX sources (constrain jet and disk emission) and accreting white dwarfs (probe novae). *SVOM* itself will find some of these in outburst but can also follow-up triggers from other facilities.
- Unknown: The most exciting discoveries will come from transients which are poorly understood, such as fast radio bursts, and those yet to be found. For example, CTA will probe the very high energy sky in much greater depth and over larger areas than currently achievable and likewise SKA in the radio and LSST in the optical.

4.3 Search for *SVOM* counterparts to multi-messenger triggers

Multi-messengers astronomy has been discussed for a long time for its ability to shed light on the physical process giving birth to GRBs in the case of gravitational waves (section 3.4) or on the acceleration mechanisms in the jets for neutrinos and gamma-rays (section 3.5). In the very first moments following the explosion, the photons do not escape the dense medium, we will have to rely on some new messengers to

get some information. The detectors for those messengers are becoming mature. Gravitational waves have finally been discovered and astrophysical neutrinos have been observed. The multi-messenger astronomy era has really begun.

SVOM with its ground and space instruments will offer a large and complementary follow-up capability through ToOs (Target of Opportunity). GWAC with its 5000 sq. deg. coverage can start the observation since the alert reception. The GFTs with their small field of view will confirm GWAC candidates and will be able to do follow-up for well localized events. To activate the satellite instruments, we will rely on a specific ToO program to send the observation program using S-band stations. This program guarantees less than 12 hours between the alert and the start of space observations (less can be expected for most cases) and can be activated around 20 times per year. From space, MXT and its 1 sq. deg. field of view will have the possibility to cover larger sky portion using a specific tiling procedure.

4.3.1 Gravitational waves

On September 14, 2015 at 09:50:45 UTC the two detectors of the Laser Interferometer Gravitational-Wave Observatory LIGO simultaneously observed a transient gravitational-wave signal (Abbott et al., 2016c). The signal matches the waveform predicted by general relativity for the merger of a black hole binary. This first detection, followed by a second one in december 2015, opens new prospects and the beginning of an exciting new era of astronomy.

While an electromagnetic emission is not expected from binary black hole mergers, it is not completely excluded yet. However, one of the most promising sources for joint electromagnetic-gravitational wave observations are coalescing binaries including at least a neutron star. Those sources are considered to be good progenitor candidates for GRB of short duration (section 3.4).

In 2020 there will be five active gravitational-wave detectors on Earth including Virgo in Italy. This world-wide network is expected to observe few to hundreds gravitational-wave events per year associated to neutron-star binary mergers during the future science runs.

The long baseline of the intercontinental network will yield a much more accurate localisation of the source (below tens of square degrees) than the one obtained by LIGO alone (Aasi et al., 2013). As shown in Fig. 19, the GWAC will be able to cover rapidly the sky error region from the ground. From space, MXT will be able to cover a significant amount of the error box with the help of multiple tilings.

4.3.2 Neutrinos

IceCube has demonstrated the existence of neutrinos of astrophysical origin using the outer layer of the IceCube detector as a veto and searching for events starting inside the inner volume (HESE sample) (IceCube Collaboration (2013), Aartsen et al. (2014b)). Two event topologies are detected with such detectors: track and cascade event resulting for the muon neutrino charged current interaction and the electron/tau neutrino interaction and muon neutrino neutral current interaction, respectively. Due to the different topologies of the events, the angular resolution is roughly 10-15 deg. for cascades and 0.5 deg. for muons. Since 2008, a follow-up of multiplet events, two times per month, is working with optical and X-ray telescope (IceCube Collaboration, 2013). The HESE events are now also sent to follow-up facilities through the GCN network (Kowalski & Mohr (2007), Aartsen et al. (2015b)). The typical rate of the HESE events is around 5 track events and 10 cascade events per year. The IceCube Collaboration is planning an expansion of the current detector, IceCube-Gen2, including the aim of instrumenting volume of clear glacial ice of the order of 10 km^3 at the South Pole (IceCube-Gen2 Collaboration et al., 2014)

The KM3NeT collaboration is building the second generation neutrino telescope in the Mediterranean Sea (Adrián-Martínez et al., 2016a). Above 10 TeV, muon tracks have a typical angular resolution lower than 0.2 deg. while showers, the most promising events, have a 2 deg. localisation error. The expected event rates are indicated in Fig. 19. The existing multi-wavelength follow-up program of ANTARES (Ageron et al. (2012), Adrián-Martínez et al. (2016b)) will be extended to KM3NeT.

Ultra-high energy earth-skimming neutrinos can be detected by the large cosmic-ray arrays such as the Pierre Auger Observatory in Argentina (Aab et al., 2015) and the large radio neutrino telescope GRAND in China (Martineau-Huynh et al., 2016). Finding the source of these high energy neutrinos would have a huge impact on the astrophysical community since they are both related with the acceleration processes in the jets (section 4.5). As seen in Fig. 19, the performances of *SVOM* are perfectly tailored to follow neutrino alerts with the MXT and VT instruments on-board and the ground-based telescopes (GFTs and GWAC).

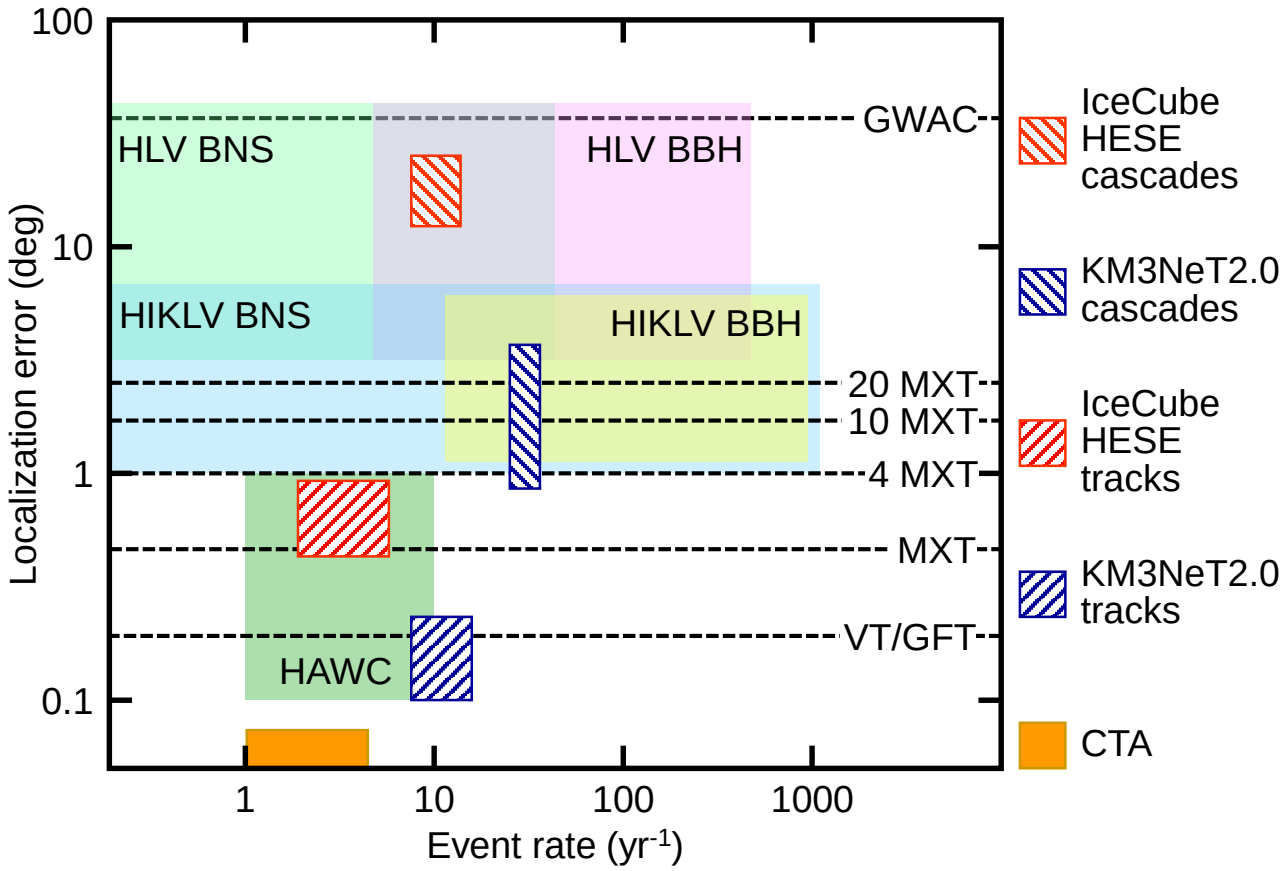

Figure 19: Anticipated event rate and localization error for some forthcoming detectors operating in the field of multi-messenger astronomy. Predictions are shown for two configurations of gravitational-wave detectors: Hanford-Livingston-Virgo (HLV) and Hanford-India-Kagra-Livingston-Virgo (HIKLV) and two sources: binary neutron stars (BNS) and binary black-holes (BBH). Predictions are also shown for two phase 2 high-energy neutrinos detectors: IceCube for high-energy starting events (HESE) detected as cascades or tracks and KM3NeT, again for events detected as cascades or tracks. Predictions are finally shown for two high-energy gamma-ray detectors, HAWC and CTA. Horizontal dotted lines indicate the *SVOM* follow-up instrument capabilities with 4 MXT, 10 MXT and 20 MXT corresponding to different MXT tilings with 4, 10 and 20 tiles.

4.3.3 High Energy Photons

The scientific return of the *SVOM* mission will be further enhanced by its synergy with other space missions or ground-based telescopes providing external electromagnetic triggers. Gamma-ray space detectors operating in the MeV range with poor localisation capabilities, e.g. similarly to the *Fermi*/GBM (Connaughton et al., 2015), might be operating at the time of *SVOM*, providing numerous alerts with relatively small error boxes that can be scanned by the MXT or GFT. At very high energies ($>10-100$

GeV), the main data acquisition system of the HAWC experiment will distribute GRB trigger times and positions to the world-wide GRB community, with an accuracy of 1 deg or less (Taboada & Gilmore, 2014b). In addition, a fraction of CTA observations might be performed in a wide-field mode, where several telescopes are offset to maximize the solid angle, with a corresponding rate of 2-3 GRBs observable per year (Inoue et al., 2013).

In both cases, the position accuracy will be small enough to initiate follow-up observations with the MXT in one single tile. The GFTs small field of view will be wide enough in some cases to cover the localisation error box in a single pointing.

5 *SVOM* Advances on Observatory Science (*SVOM* general program)

The wide field surveys with ECLAIRs and the GRM will permit to detect transient activity from many different types of sources other than GRBs, while the narrow FoV instruments (MXT, VT, GFTs) will allow to extend the scientific analysis of dedicated sources to a wider spectral window. This "general program" can cover and bring relevant information on a wide range of sources and scientific topics. With a minimum observing time of one orbit (effective time of $\sim$ 3000 s with the MXT), the 0.3–6 keV 5σ detection limit of the MXT is 2 10^{-12} erg cm^{-2} s^{-1}($\sim$ 0.1 mCrab). Extrapolation of the XMM-Newton high precision Log N–Log S indicates a source density of $\sim 0.2/\mathrm{deg}^2$ at high galactic latitudes (Mateos et al., 2008) which shows the high potential of MXT for dedicated studies of specific sources. For the wide field surveys, we estimated a total exposure time as low as $\sim$ 200 ks over one year on the galactic centre region. This leads to a 4–150 keV sensitivity limit of $\sim$ 7 mCrab, roughly 2 10^{-10}erg cm^{-2} s^{-1}. Such a limiting sensitivity permits to survey a large number of sources : the 17–60 keV *INTEGRAL* Log N–Log S indicates a density of 0.02 (resp. 2 10^{-4}) source/deg^2 at $|b|<5^\circ$ (resp. $|b| >5^\circ$)] (Krivonos et al., 2007b).

5.1 Active Galactic Nuclei

Active Galactic Nuclei (AGNs) are the most luminous persistent objects in the Universe. An important part of the observatory science of *SVOM* will certainly include studies of persistent and transient AGNs at high energies with ECLAIRs, MXT, and, in the optical domain, with the VT, the GWACs, and the GFTs. Photons emitted by the disk around the central super massive black hole are inverse Compton up-scattered on relativistic electron plasmas in the vicinity, e.g. in a corona partially covering the disk. Some AGNs develop powerful jets rising perpendicular to the accretion disk accelerating particles up to relativistic speeds. Thus they are divided into different classes, based on the angle of the line of sight with respect to the accretion disk and intrinsic absorption, and whether or not they exhibit a jet (Beckmann & Shrader, 2012).

ECLAIRs is going to open a new window on AGN large area surveys, as it will cover the 4–150 keV energy range with unprecedented sensitivity. Although there will be more sensitive all-sky surveys below 10 keV (e.g. eROSITA) and above 20 keV (*Swift*/BAT, *INTEGRAL*/IBIS), the ECLAIRs sensitivity between 10 and 20 keV (a gap not covered by any current and future missions) will be crucial to study the inverse Compton scattering spectra of the accretion disk in AGNs. The capabilities of the narrow field instruments will be used to study AGN in outburst, in multi-wavelength (hereafter MWL) campaigns, or to clarify the nature of an object.

Within a typical year of operations, *SVOM*/ECLAIRs is going to detect 250 AGN. For the majority of these mainly Seyfert type galaxies, the GWACs are going to provide detailed lightcurves. After a 5 year mission life time, ECLAIRs will provide crucial information on about 700 AGN. For the brightest 30 of the persistent AGN, which are mainly absorbed Seyfert type galaxies, ECLAIRs data will allow to derive precise measurements of the continuum slope, determining the Compton reflection contribution to the flux. One example is the Seyfert 1.9 galaxy MCG-05-23-16 as shown in Fig. 20. The whole survey sample will give us the average Compton reflection fraction and thus will be an important input to determine the sources of the cosmic X-ray background in this energy range (Ueda et al., 2014). It has to be noted that missions like NuSTAR are determining the contribution of AGN to the CXB in a similar energy range (6-70 keV), but only in pencil-beam surveys and thus at higher redshifts. The study of the CXB in the local Universe can only be done using wide field surveys like the one performed by ECLAIRs.

SVOM's all-sky survey will also allow to pick up transient AGNs, such as blazars, Seyfert galaxies in high state, and tidal disruption events (TDEs, section 5.2). The on-board processing will allow to predefine a list of interesting AGN with individual trigger thresholds for automatic repointing of the satellite. The narrow field X-ray instrument MXT on-board *SVOM* will allow to follow-up on AGN outbursts and also to provide a means of identification of X-ray counterparts to optical AGN candidates as they will be seen in the VT. This will be vital in view of the deep all-sky survey telescopes operating during the *SVOM*

mission lifetime, such as the LSST and Euclid. Their multi-band photometric data will allow to pick out candidates for so far unknown transient X-ray AGNs. These can be either blazars in outburst or Seyfert galaxies, which show type changes (Risaliti et al., 2011), spectral variability (Hernández-García et al., 2015), and/or significant brightening (Soldi et al., 2014), as we have seen for several Seyfert 2 galaxies, and also from radio galaxies like Pictor A and Centaurus A (Steinle, 2010). The GFT network will be able to provide simultaneous optical spectra with information about the broad and narrow line regions and the underlying continuum from the accretion disk of the AGNs.

Since the emission from blazars is often found to vary simultaneously across the spectrum, wide-field instruments like those provided by *SVOM* are particularly useful in their study because they can be used to trigger MWL campaigns when a blazar enters a flaring state (e.g. for 3C 454.3; Wehrle et al. 2012). This is of particular interest to observers at very-high energies. Blazars are known to be extremely variable in the gamma-ray regime and most very high energy (VHE) observatories reserve significant fractions of their telescope time to follow-up blazar flares. In this way, MWL campaigns can be triggered when a known blazar enters into an active state. In addition to triggering such MWL campaigns, the *SVOM* instruments and the GFT will be used to provide accurate measurements of the spectral energy distribution of high-state blazars. Recent studies have shown that blazars at high redshifts ($z > 4$) can be extremely bright, up to $L_{\rm X} > 10^{47}\,{\rm erg\,s^{-1}}$ in ECLAIRs' hard X-ray band (Ajello et al., 2009). This makes them ideal targets to study the early accretion (and emission) history of the Universe, and opens a window for *SVOM* to study the early formation of relativistic jets Ghisellini et al. (2015).

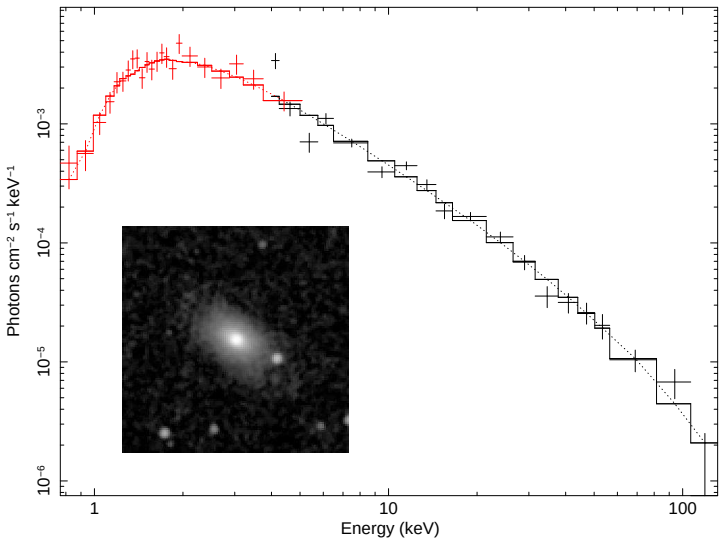

Figure 20: Simulated 10 ksec *SVOM*/MXT observation of the absorbed Seyfert 1.9 galaxy MCG-5-23-16 ($f_{4-150{\rm keV}} \simeq 8\,{\rm mCrab}$), combined with the expected 1-year spectrum (effective exposure time of 300 ks) from ECLAIRs. The cut-off in the spectrum at $E_{\rm cut} = 72\,{\rm keV}$ and the absorption in the line of sight can be determined with an accuracy of 10%. The optical image gives an impression of a *SVOM*/VT observation of this source (based on a 2MASS image; Skrutskie et al. 2006).

5.2 Ultra Luminous X-ray Sources and Tidal Disruption Events

Ultra-luminous X-ray sources (ULXs) are X-ray objects located outside the galaxy nucleus, with luminosities that exceed the Eddington luminosity (L_{Edd}) for a stellar mass black hole, where $L_{Edd} = 1.3 \times 10^{38}\,(M/M_{\odot})$ erg s^{-1}. First discovered with the *Einstein* observatory (1978-1981, Fabbiano, 1989) almost 40 years ago, many questions about these sources remain to be answered. Firstly, what is the nature and the mass of the compact object? Until recently the compact objects were assumed to be black

holes, but Bachetti et al. (2014) demonstrated that the ULX M82 X-2 (L_{max} $\sim$1.8 $\times$ 10^{40} erg s^{-1}, 0.3-10.0 keV), hosts a neutron star accretor, with $L_x \sim 100 L_{Edd}$. This not only implies that the compact objects could be neutron stars, but also demonstrates that long term super-Eddington accretion appears possible. How a source can continuously accrete above the Eddington limit has yet to be discovered. Elucidating the accretion mechanism in ULXs requires observations at different luminosities/spectral regimes. Many ULXs are either transient (e.g. Middleton et al., 2013) or variable, like M 82 X-2.

A rather large number of known ULXs can be detected with the MXT ($F_{[0.3-10keV]} > 10^{-12}$ erg $s^{-1}cm^{-2}$) during a one orbit observation time. Several suitable targets are located in the following galaxies with good visibility throughout the year (> 100 days): NGC 55, NGC 253, NGC 5204, NGC 5408, NGC 5907, NGC 6946, NGC 7793. An X-ray monitoring of these sources will allow us to trigger observations with other X-ray and multi-wavelength observatories when they are observed to show spectral transitions at different flux levels.

For those ULXs with bright and isolated optical counterparts ($M_V < 23$), the VT will allow us to search for periodicities in the lightcurve of these objects. This in turn could reveal the orbital period of these systems, allowing us to gain a handle on the mass of the two stars (thanks to Kepler's laws) and provides further constraints on the accretion regime. An excellent example of such a study was done for the X-ray source P 13 in NGC 7793 (Motch et al., 2014).

Other events that *SVOM* will lend itself well to discovering are tidal disruption events (TDEs). These occur when a star in a galaxy wanders too close to the central massive black hole. The star disrupts when the tidal forces exceed the self-gravity of the star and a previously undetected massive black hole will become extremely bright, allowing it to be studied. The detection of three candidate relativistic tidal disruption flares (rTDFs) within 12 years of *Swift* operations (e.g. Levan et al. 2011) at initial X and hard X-ray fluxes ($F_{[0.3-10keV]} \sim F_{[15-50keV]} \sim 10^{-9}$ erg $s^{-1}cm^{-2}$) suggest that up to one such event could be detectable with ECLAIRs within *SVOM* initial lifetime. Another possible prospect to find non-relativistic TDEs would be to survey galaxies with large globular cluster populations, those being in addition prime targets to hide the extremely rare intermediate mass black holes (IMBH, $\sim 10^{2-5}$ $M_\odot$). This would be done with dedicated MXT observations. Without violating the B1 law, the Virgo cluster is an obvious candidate due to its close proximity and number density of galaxies. Regular monitoring of the cluster (i.e every one/two weeks for 10 ksec in a 3x3 tiling mode) should lead to the detection of 6 TDEs within *SVOM* initial lifetime, with fluxes down to 10^{41-43} erg s^{-1} that we can expect for a 10^5 $M_\odot$ BH.

5.3 Galactic sources

The lower energy threshold and broader spectral coverage of *SVOM* (compared to *RXTE*, *Swift* or *INTEGRAL*) will permit to detect high energy galactic sources and unexpected events (outbursts, flares from binaries, thermonuclear explosion, ...) easily, thanks to the ECLAIRs sensitivity of 50 mCrab in one orbit.

5.3.1 Accreting systems

Cataclysmic variables (CVs) and X-ray binaries (XRBs) are systems that are powered by the accretion of matter onto the compact object (CO). The former systems contain a white dwarf (WD) and the latter either a neutron star (NS) or a black hole (BH). The compactness of the CO will affect the peak of the thermal emission of the disc, but also how accretion proceeds in the innermost regions when a significant magnetic field and/or a rigid surface enter into the game. By monitoring these sources from the early stages of their outbursts, one can better constrain models of disk instabilities and how they trigger outburst, but also how the different media (CO surface, accretion disk, "corona") interact and lead to the spectral state transitions. The *SVOM* wide 0.1–5000 keV spectral coverage will permit to precisely measure the local absorption, probe the spectral shape of the high energy emission (black body and/or

bremsstrahlung temperature, power law photon index Γ, cut-off energy, reflection component, iron line, ...) while removing the degeneracy between kT, N_H and Γ thanks to the large "lever arm" brought by the 4–5000 keV band. The high temporal resolution of ECLAIRs and the GRM will also permit timing studies (pulsations, level of variability, quasi-periodic oscillations, ...) to be performed. Here we mention a few specific points for each systems that can be studied with *SVOM*.

The intermediate polars (IP), a sub-type of CVs containing intermediately magnetized white dwarf, are of particular relevance for the multi-wavelengths capabilities of *SVOM*. These systems have been detected with both *Swift* and *INTEGRAL* (e.g. Revnivtsev et al., 2008). Many lie at high galactic latitude, and are easily observable within the B1 law. Optical/IR and X-ray follow-up have shown levels above the limits of the MXT ($F_{IGR-CVs,2-10keV} > 10^{-12}$ erg/cm^2/s), the VT, and the GWAC ($M_R \sim 14-17$). Serendipitous activity (outburst, nova-like phenomenon) will easily be detected within the large ECLAIRs and GRM's FoV.

Neutron star high mass XRBs are thought to be young systems hosting pulsars with rather large magnetic fields ($B \sim 10^{12}$ G). Here the detection of resonant cyclotron scattering features can permit to measure the value of B, since $\frac{B}{10^{12}\ \mathrm{G}} = \frac{E_{cycl}}{11.6} \times (1+z)$ where E_{cycl} is the centroid of the line, and z the gravitational redshift near the NS. ECLAIRs has the capabilities to detect these lines during the brightest phases of outburst in sources such as A0535−26, and also to search for coherent pulsations giving access to the pulsar spin, and eventually the spin derivative. GWAC and GFTs will, simultaneously, permit to study the companion, and/or the potential optical flaring activity and its possible relation with X-ray flares.

The evolution of BH and NS XRBs (and CVs in some respect) along their outbursts show a similar phenomenology of spectral transitions between states dominated by the accretion disk and those dominated by hard X-ray "coronae". The mechanisms that drive the evolutions (smooth vs large flaring activity, and/or limit cycle oscillations), and the hysteresis (the fact that the hard to soft transition is always brighter than the soft to hard one) are, however, still not understood. In addition, many of these sources are also known as jet-emitting sources (as seen in the radio domain) and thus dubbed micro-quasars. While the association of jets with particular states of activity is now clear (e.g. Corbel et al., 2003; Rodriguez et al., 2008; Coriat et al., 2011, to cite just a few), the exact interplay between accretion and ejection, and how jets influe on the source evolution (self-regulation of outburst, energy and material feedback in the ISM or interaction with the local environment) is largely unknown. Recent activity of some sources (e.g. IGR J17091−2624 or V404 Cyg) have also shown that some objects largely depart from the "standard" behavior (Fig. 21), with short (10–15 days) outburst and huge level of emission (up to 50 Crab) on very short (hour) time scales. While these sources are mostly outside the B1 law, systematics (spectral and temporal) surveys of outbursts, during the 10% allowed time can thus be used to better understand the physics driving the evolution of these sources, their impact on their surrounding and eventually the Galaxy. The right panels of Fig. 21 show spectral MXT+ECLAIRs simulations of a moderately bright state with a cold disk, and a faint hard state.

5.3.2 Pulsars and magnetars

Magnetars (either Anomalous X-ray Pulsars, AXPs, and Soft Gamma Repeaters, SGRs) are a small class of isolated NS that are, contrary to standard NS, powered by the decay of their huge magnetic field (B$\sim 10^{14-15}$ G). They can emit short (< 1 s) bursts, intermediate flares lasting for a few tens of seconds, and giant flares. The latter peak at a luminosity of 10^{47} erg s^{-1}. A spectral measurement by ECLAIRs (at least before eventual instrumental saturation, or during the decaying tail) will permit to characterize these events. Giant flares in nearby (< 100 Mpc) galaxies could be discovered by ECLAIRs mimicking short-hard bursts, and followed with MXT. The < 10 keV spectrum of the more common magnetar

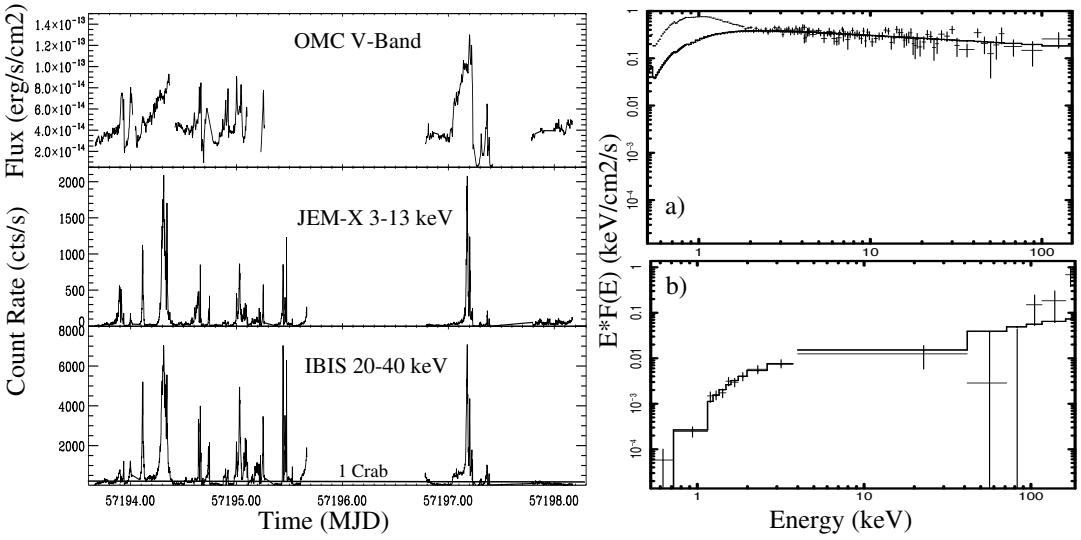

Figure 21: **Left:** *INTEGRAL* light curves of V404 Cyg during part of its 2015-July outburst. From top to bottom optical V-band, soft (3–13 keV), and hard (20–40 keV) X-rays. Adapted from Rodriguez et al. (2015). **Right:** a)10 ks MXT-ECLAIRs simulated spectra of a moderately bright soft state (75 and 32 mCrab in the 1-10 and 20-200 keV ranges). b) Same for a 1 mCrab (1–10 keV)/ 5 mCrab (20–200 keV) hard state.

bursts is not well known. Olive et al. (2004) used a double black body to describe an intermediate flare of SGR 1900+14, whereas Israel et al. (2008) showed that a Comptonized spectrum could represent the *Swift*/XRT–BAT spectra of the same source well. Hence, the correct spectral modelling and consequent physical interpretation of short bursts at a few keV is not settled yet and requires further observations, and *SVOM* with its unique multi-wavelength coverage can bring new diagnostics in this field.

Recent results tend to show relatively low dipolar magnetic fields in at least two objects (SGR 0418+5729, and *Swift* J1822−1606) with B close to standard pulsar values. This may imply that the magnetar population includes many more X-ray dim (outside outbursts) members than previously thought, and that can be studied only using prompt follow-up observations by sensitive high-energy observatories like *SVOM*.

In addition, the first direct measurement of a magnetar magnetic field (Tiengo et al., 2013) through a proton cyclotron feature at $\sim$ 2 keV in SGR 0418+5729 confirms a high magnetic field value (B$\sim$ $2 - 20 \times 10^{14}$ G) mainly stored in multi-pole components at the surface. This variable feature seen at still a high flux (5×10^{-12} erg cm^{-2} s^{-1}) may be accessible to MXT thanks to its good spectral resolution and sensitivity with a 10 ks observation (sensitivity limit 7×10^{-13} erg cm^{-2} s^{-1}). The frontier between pulsars and magnetars appears more tenuous than previously thought, objects belonging to one class being able to reproduce – during some special periods of activity– the behavior of the other family. The timing and spectral capabilities of the instruments on board *SVOM* will help to study the link between the two classes of objects, having interesting consequences on their formation.

5.3.3 Flaring stars

ECLAIRs will also be sensitive to flaring M and K stars that could produce huge flares. This could provide information on non-thermal processes happening in the stellar corona. This could help constraining particle acceleration mechanisms. Detection of X-ray lines in emission could also provide some clues on the shape/geometry of the magnetic loop reconnection leading to these events (Osten et al., 2010). Observations of super-flares from such small stars have also implications for astrobiology.

5.4 Exoplanets and Solar System bodies

As of today only a handful of stars having soft X-ray luminosity between 10^{-13}–10^{-10} erg cm^{-2} s^{-1} are known to have planets in their habitable zones. In one case (HD187933), the transit of the hot Jupiter orbiting around the star has been observed in X-ray with *Swift*/XRT (Lecavelier des Etangs et al., 2012). The sensitivity of the MXT instrument onboard *SVOM* would make the observation of exoplanets feasible only in the case of higher luminosity stars, by averaging several transits to obtain light curves where amplitude variations of a few percent could be detected. However, it can be expected that more stellar systems hosting planets will be discovered in the next years, therefore the search for exoplanets and the study of their atmospheres with *SVOM* can be considered at this stage as a potential application.

Many solar system bodies emit X-rays like planets, moons, comets etc and simultaneous *SVOM* X-ray and optical observations will be very promising for Solar System studies as shown by the *Swift* mission that could study several comets.

5.5 Additional science opportunities

The *SVOM* mission will also bring new insights to a number of other important high-energy science topics for which its specific operation strategy, with frequent Earth passes in the instrument FoVs, will favor accurate measurements.

The Cosmic X-ray Background (CXB) is a uniform, isotropic component of the sky X-ray emission, which is likely due to a population of unresolved weak point-sources. Indeed, the observed CXB surface brightness at more than few keV is likely provided by accreting super-massive black holes (SMBH) in galactic nuclei at various distances from us and it is therefore an overall measure of the growth of all SMBHs in the history of the Universe (Soltan, 1982; Fabian & Iwasawa, 1999). Combining accurate CXB measurements with detailed AGNs population synthesis models can provide the characteristics of this population and then trace the long term history of the SMBH formation, growth and evolution in the Universe (Ueda et al., 2014).

Unlike at lower energies, above 7 keV most of the CXB is unresolved (only 2.5 % in 20-60 keV) and will remain so in the near future (*NuStar* is expected to resolve at most 30 % of it). This range traces the highly absorbed Compton thick AGN population, not visible at low energies, and an accurate CXB measurement here is needed for evaluating the role of this population. A recent compilation of CXB measurements (Revnivtsev, 2014) shows that in the crucial range of the peak of the spectrum, the 10-50 keV band, the uncertainties in the absolute intensity are still of the order of 20-30 %, which has a large impact on the computation of the Compton thick AGN demography.

In the determination of the CXB an important problem is the estimation of the intrinsic particle-induced background and of the other celestial components that contribute to the recorded flux. One of the most effective techniques to evaluate the background is to perform measurements during Earth occultation of the sky (Churazov et al., 2007; Revnivtsev, 2014).

Due to the *SVOM* pointing strategy, ECLAIRs will suffer from a large rate of partial Earth occultation and it will therefore provide unprecedented statistics for accurate CXB measurements in the range 4-150 keV. Given the high galactic latitudes of these observations, galactic point-sources and diffuse emission contamination will also be low, reducing the errors in the CXB estimations.

Likewise, the Galactic plane is known to be an intense source of continuum high-energies emission. At gamma-ray energies, this emission is mainly of diffuse nature and is well understood, while in the X-ray band it is referred as Galactic Ridge X-ray Emission (GRXE) and its origin is still debated.

At energies below 50 keV, recent observations from the *RXTE* and *INTEGRAL* satellites showed that the global morphology of the GRXE reproduces the distribution of stars in the Milky Way, which points to a GRXE stellar origin where accreting WDs are the main contributors (Krivonos et al., 2007a).

However, the various source populations responsible of the emission are not precisely known (Morihana et al., 2013). In addition, the spectrum region around 50 keV is poorly constrained and the few recent measurements are dominated by systematics and modeling biases. Similarly, accurate measurements are needed to fix the characteristics of the power-law continuum below 100 keV, thought to be due to the interstellar radiation field interaction with the cosmic-ray electrons.

Again, Earth occultation observations in which the Galactic plane is occulted by the Earth can be used. Such a technique has been successfully applied to the data obtained with *INTEGRAL*/IBIS using few dedicated Earth occultation observations and obtaining a GRXE spectrum with a good accuracy in hard X-rays (Türler et al., 2010). As mentioned above, the number of such Earth modulated observations is expected to be substantially higher for ECLAIRs, this will lead to a high signal-to-noise ratio measurement of the GRXE spectrum in the hard X-ray energy range and will help to resolve the issues above mentioned.

Other topics that will be studied with *SVOM* also thanks to observations pointed towards the Earth are solar and terrestrial events involving particle acceleration, confinement and interaction like in solar flares, south Atlantic anomaly, aurorae and terrestrial gamma-ray flashes (TGF). The TGF are extremely rapid (< 10 ms) bursts of photons in the range 20 keV – 20 MeV associated with tropical thunderstorms in the atmosphere for which physical mechanisms are not yet understood. ECLAIRs will provide localisation of these events and help to resolve the open questions about TGFs in synergy with the future dedicated CNES mission *Taranis* and the ESA experiment to be flown on the ISS.

Acknowledgements

Financial support for this work was provided by the CNES (French Space Agency), the PNHE (French National High Energy Program), the European Research Group (Exploring the Dawn of the Universe with Gamma-Ray Bursts) and the UnivEarthS Labex program at Sorbonne Paris Cité (ANR-10-LABX-0023 and ANR-11-IDEX-0005-02).

References

Aab, A., et al. 2015, Phys. Rev., D91, 092008

Aartsen, M. G., Ackermann, M., Adams, J., et al. 2014a, Physical Review Letters, 113, 101101

—. 2014b, Physical Review Letters, 113, 101101

Aartsen, M. G., Abraham, K., Ackermann, M., et al. 2015a, Physical Review Letters, 115, 081102

—. 2015b, ApJ, 811, 52

Aasi, J., et al. 2013, arXiv:1304.0670, [Living Rev. Rel.19,1(2016)]

Abbasi, R., Abdou, Y., Abu-Zayyad, T., et al. 2010, ApJ, 710, 346

Abbott, B. P., Abbott, R., Abbott, T. D., et al. 2016a, Physical Review Letters, 116, 131102

—. 2016b, Physical Review Letters, 116, 061102

—. 2016c, Physical Review Letters, 116, 061102

—. 2016d, Living Reviews in Relativity, 19, arXiv:1304.0670

Abdo, A. A., Ackermann, M., Ajello, M., et al. 2009, ApJL, 706, L138

Abeysekara, A. U., Aguilar, J. A., Aguilar, S., et al. 2012, Astroparticle Physics, 35, 641

Ackermann, M., Asano, K., Atwood, W. B., et al. 2010, ApJ, 716, 1178

Ackermann, M., Ajello, M., Allafort, A., et al. 2013a, ApJS, 209, 34

Ackermann, M., Ajello, M., Asano, K., et al. 2013b, ApJS, 209, 11

Adrián-Martínez, S., Albert, A., Samarai, I. A., et al. 2013, A&A, 559, A9

Adrián-Martínez, S., Ageron, M., Aharonian, F., et al. 2016a, ArXiv e-prints, arXiv:1601.07459

Adrián-Martínez, S., Ageron, M., Albert, A., et al. 2016b, JCAP, 2, 062

Ageron, M., Aguilar, J. A., Al Samarai, I., et al. 2012, Astroparticle Physics, 35, 530

Ajello, M., Costamante, L., Sambruna, R. M., et al. 2009, ApJ, 699, 603

Amati, L. 2006a, MNRAS, 372, 233

—. 2006b, MNRAS, 372, 233

Amati, L., Frontera, F., Tavani, M., et al. 2002, A&A, 390, 81

Ando, S., & Beacom, J. F. 2005, Physical Review Letters, 95, 061103

Angel, J. R. P. 1979, ApJ, 233, 364

Antier, S., Schanne, S., Cordier, B., et al. 2015, ArXiv e-prints, arXiv:1508.05505

Atteia, J.-L. 2003, A&A, 407, L1

Bachetti, M., Harrison, F. A., Walton, D. J., et al. 2014, Nature, 514, 202

Band, D., Matteson, J., Ford, L., et al. 1993, ApJ, 413, 281

Barnes, J., & Kasen, D. 2013, ApJ, 775, 18

Barthelmy, S. D., Barbier, L. M., Cummings, J. R., et al. 2005, Space Science Reviews, 120, 143

Basa, S., Cuby, J. G., Savaglio, S., et al. 2012, A&A, 542, A103

Becker, G. D., Rauch, M., & Sargent, W. L. W. 2007, ApJ, 662, 72

Beckmann, V., & Shrader, C. R. 2012, Active Galactic Nuclei

Beloborodov, A. M. 2010, MNRAS, 407, 1033

Berger, E. 2014, Annual Review of Astronomy and Astrophysics, 52, 43

Blanchard, P. K., Berger, E., & Fong, W.-f. 2016, ApJ, 817, 144

Blandford, R. D., & Znajek, R. L. 1977, MNRAS, 179, 433

Bloom, J. S., Butler, N. R., & Perley, D. A. 2008, in American Institute of Physics Conference Series, Vol. 1000, American Institute of Physics Conference Series, ed. M. Galassi, D. Palmer, & E. Fenimore, 11–15

Bloom, J. S., Frail, D. A., & Kulkarni, S. R. 2003, ApJ, 594, 674

Bloom, J. S., Holz, D. E., Hughes, S. A., et al. 2009, ArXiv e-prints, arXiv:0902.1527

Bode, M. 2015, ASTRONET, `http://www.astronet-eu.org`

Boissier, S., Salvaterra, R., Le Floc'h, E., et al. 2013, A&A, 557, A34

Bournaud, F., Perret, V., Renaud, F., et al. 2014, ApJ, 780, 57

Bouwens, R. J., Illingworth, G. D., Franx, M., et al. 2009, ApJ, 705, 936

Bouwens, R. J., Illingworth, G. D., Labbe, I., et al. 2011, Nature, 469, 504

Bouwens, R. J., Illingworth, G. D., Oesch, P. A., et al. 2015, ApJ, 803, 34

Bromberg, O., Nakar, E., & Piran, T. 2011, ApJL, 739, L55

Bromberg, O., Nakar, E., Piran, T., & Sari, R. 2013, ApJ, 764, 179

Bromm, V., Coppi, P. S., & Larson, R. B. 2002, ApJ, 564, 23

Bromm, V., & Loeb, A. 2006, ApJ, 642, 382

Bucciantini, N., Quataert, E., Metzger, B. D., et al. 2009, MNRAS, 396, 2038

Butler, N. R., Kocevski, D., Bloom, J. S., & Curtis, J. L. 2007, ApJ, 671, 656

Campana, S., Lodato, G., D'Avanzo, P., et al. 2011, Nature, 480, 69

Cano, Z., Wang, S.-Q., Dai, Z.-G., & Wu, X.-F. 2016, ArXiv:1604.03549, arXiv:1604.03549

Castro-Tirado, A. J., Møller, P., García-Segura, G., et al. 2010, A&A, 517, A61

Chen, H.-W., Prochaska, J. X., & Gnedin, N. Y. 2007, ApJL, 667, L125

Cheng, K. S., Yu, Y.-W., & Harko, T. 2010, Physical Review Letters, 104, 241102

Chornock, R., Berger, E., Fox, D. B., et al. 2014, ArXiv e-prints, arXiv:1405.7400

Christensen, L., Vreeswijk, P. M., Sollerman, J., et al. 2008, A&A, 490, 45

Chu, Q., Howell, E. J., Rowlinson, A., et al. 2016, MNRAS, 459, 121

Churazov, E., Sunyaev, R., Revnivtsev, M., et al. 2007, A&A, 467, 529

Committee for a Decadal Survey of Astronomy and Astrophysics. 2010, National Academies Press

Connaughton, V., et al. 2015, Astrophys. J. Suppl., 216, 32

Corbel, S., Nowak, M. A., Fender, R. P., Tzioumis, A. K., & Markoff, S. 2003, A&A, 400, 1007

Cordier, B., Desclaux, F., Foliard, J., & Schanne, S. 2008, in American Institute of Physics Conference Series, Vol. 1000, American Institute of Physics Conference Series, ed. M. Galassi, D. Palmer, & E. Fenimore, 585–588

Cordier, B., Wei, J., Atteia, J.-L., et al. 2015, ArXiv e-prints, arXiv:1512.03323

Coriat, M., Corbel, S., Prat, L., et al. 2011, MNRAS, 414, 677

Coward, D. 2007, NewAR, 51, 539

Dai, Z. G., Wang, X. Y., Wu, X. F., & Zhang, B. 2006, Science, 311, 1127

Daigne, F., & Mochkovitch, R. 1998, MNRAS, 296, 275

—. 2002, MNRAS, 336, 1271

Daigne, F., Rossi, E. M., & Mochkovitch, R. 2006a, MNRAS, 372, 1034

—. 2006b, MNRAS, 372, 1034

Dall'Osso, S., Giacomazzo, B., Perna, R., & Stella, L. 2015, ApJ, 798, 25

De Cia, A., Ledoux, C., Fox, A. J., et al. 2012, A&A, 545, A64

Di Sciascio, G., & on behalf of the LHAASO Collaboration. 2016, ArXiv e-prints, arXiv:1602.07600

Elliott, J., Greiner, J., Khochfar, S., et al. 2012, A&A, 539, A113

Evans, P. A., Beardmore, A. P., Page, K. L., et al. 2007, A&A, 469, 379

—. 2009, MNRAS, 397, 1177

Evans, P. A., Osborne, J. P., Kennea, J. A., et al. 2016, MNRAS, 455, 1522

Fabbiano, G. 1989, Annual Review of Astronomy and Astrophysics, 27, 87

Fabian, A. C., & Iwasawa, K. 1999, MNRAS, 303, L34

Fan, Y.-Z., & Xu, D. 2006, MNRAS, 372, L19

Fernández, R., & Metzger, B. D. 2015, ArXiv e-prints, arXiv:1512.05435

Firmani, C., Ghisellini, G., Avila-Reese, V., & Ghirlanda, G. 2006, MNRAS, 370, 185

Fox, A. J., Ledoux, C., Vreeswijk, P. M., Smette, A., & Jaunsen, A. O. 2008, A&A, 491, 189

Frail, D. A., Kulkarni, S. R., Sari, R., et al. 2001, ApJL, 562, L55

Fruchter, A. S., Levan, A. J., Strolger, L., et al. 2006, Nature, 441, 463

Fryer, C. L., Belczynski, K., Ramirez-Ruiz, E., et al. 2015, ApJ, 812, 24

Fryer, C. L., & New, K. C. 2011, Living Reviews in Relativity, 14, doi:10.1007/lrr-2011-1

Fynbo, J. P. U., Watson, D., Thöne, C. C., et al. 2006, Nature, 444, 1047

Fynbo, J. P. U., Jakobsson, P., Prochaska, J. X., et al. 2009, ApJS, 185, 526

Gal-Yam, A., Fox, D. B., Price, P. A., et al. 2006, Nature, 444, 1053

Gao, H., Ding, X., Wu, X.-F., Dai, Z.-G., & Zhang, B. 2015, ApJ, 807, 163

Gehrels, N., Cannizzo, J. K., Kanner, J., et al. 2016, ApJ, 820, 136

Gehrels, N., & Razzaque, S. 2013, Frontiers of Physics, 8, 661

Gehrels, N., Chincarini, G., Giommi, P., et al. 2004, ApJ, 611, 1005

Gehrels, N., Sarazin, C. L., O'Brien, P. T., et al. 2005, Nature, 437, 851

Gendre, B., Stratta, G., Atteia, J. L., et al. 2013, ApJ, 766, 30

Ghirlanda, G., Bernardini, M. G., Calderone, G., & D'Avanzo, P. 2015a, Journal of High Energy Astrophysics, 7, 81

Ghirlanda, G., Celotti, A., & Ghisellini, G. 2003, A&A, 406, 879

Ghirlanda, G., Ghisellini, G., & Firmani, C. 2006, New Journal of Physics, 8, 123

Ghirlanda, G., Ghisellini, G., & Lazzati, D. 2004a, ApJ, 616, 331

—. 2004b, ApJ, 616, 331

Ghirlanda, G., Salvaterra, R., Ghisellini, G., et al. 2015b, MNRAS, 448, 2514

Ghisellini, G., Tagliaferri, G., Sbarrato, T., & Gehrels, N. 2015, MNRAS, 450, L34

Gilmore, R. C., Bouvier, A., Connaughton, V., et al. 2013, Experimental Astronomy, 35, 413

Godet, O., Nasser, G., Atteia, J.-, et al. 2014a, in Proc. SPIE, Vol. 9144, Space Telescopes and Instrumentation 2014: Ultraviolet to Gamma Ray, 914424

Godet, O., Nasser, G., Atteia, J.-, et al. 2014b, in Proceedings of the SPIE, Vol. 9144, Space Telescopes and Instrumentation 2014: Ultraviolet to Gamma Ray, 914424

Goldstein, A., Preece, R. D., Mallozzi, R. S., et al. 2013, ApJS, 208, 21

Goldstein, A., Burgess, J. M., Preece, R. D., et al. 2012, ApJS, 199, 19

Gompertz, B. P., O'Brien, P. T., & Wynn, G. A. 2014, MNRAS, 438, 240

Götz, D., Osborne, J., Cordier, B., et al. 2014, in Proc. SPIE, Vol. 9144, Space Telescopes and Instrumentation 2014: Ultraviolet to Gamma Ray, 914423

Graham, J. F., Fruchter, A. S., Kewley, L. J., et al. 2009, in American Institute of Physics Conference Series, Vol. 1133, American Institute of Physics Conference Series, ed. C. Meegan, C. Kouveliotou, & N. Gehrels, 269–272

Granot, J. 2003, ApJL, 596, L17

Greiner, J., Fox, D. B., Schady, P., et al. 2015, ApJ, 809, 76

Gruber, D., Goldstein, A., Weller von Ahlefeld, V., et al. 2014a, ApJS, 211, 12

—. 2014b, ApJS, 211, 12

Guaita, L., Pentericci, L., Grazian, A., et al. 2016, A&A, 587, A133

Guimarães, R., Petitjean, P., Rollinde, E., et al. 2007, MNRAS, 377, 657

Guiriec, S., Briggs, M. S., Connaugthon, V., et al. 2010a, ApJ, 725, 225

—. 2010b, ApJ, 725, 225

Guiriec, S., Connaughton, V., Briggs, M. S., et al. 2011a, ApJL, 727, L33

—. 2011b, ApJL, 727, L33

Guiriec, S., Daigne, F., Hascoët, R., et al. 2013, ApJ, 770, 32

Guo, H., & Wu, J. 2010, Springer-Verlag

Gupta, N., & Zhang, B. 2007, Astroparticle Physics, 27, 386

Hartoog, O. E., Malesani, D., Fynbo, J. P. U., et al. 2015, A&A, 580, A139

Hascoët, R., Daigne, F., & Mochkovitch, R. 2012, A&A, 542, L29

—. 2013, A&A, 551, A124

Hatsukade, B., Ohta, K., Endo, A., et al. 2014, Nature, 510, 247

Heger, A., Fryer, C. L., Woosley, S. E., Langer, N., & Hartmann, D. H. 2003, ApJ, 591, 288

Hernández-García, L., Masegosa, J., González-Martín, O., & Márquez, I. 2015, A&A, 579, A90

Heussaff, V., Atteia, J.-L., & Zolnierowski, Y. 2013, A&A, 557, A100

Hjorth, J., & Bloom, J. S. 2011, Chapter 9 in "Gamma-Ray Bursts", eds. C. Kouveliotou, R. A. M. J. Wijers, S. E. Woosley, Cambridge University Press, ArXiv:1104.2274, arXiv:1104.2274

Hopkins, A. M., & Beacom, J. F. 2006, ApJ, 651, 142

Hu, Y.-D., Liang, E.-W., Xi, S.-Q., et al. 2014, ApJ, 789, 145

Hümmer, S., Rüger, M., Spanier, F., & Winter, W. 2010, ApJ, 721, 630

Hunt, L. K., Palazzi, E., Michałowski, M. J., et al. 2014, A&A, 565, A112

IceCube Collaboration. 2013, Science, 342, 1242856

IceCube Collaboration, Aartsen, M. G., Abraham, K., et al. 2016, ArXiv e-prints, arXiv:1601.06484

IceCube-Gen2 Collaboration, :, Aartsen, M. G., et al. 2014, ArXiv e-prints, arXiv:1412.5106

Inoue, S., Granot, J., O'Brien, P. T., et al. 2013, Astroparticle Physics, 43, 252

Inoue, S., et al. 2013, Astropart. Phys., 43, 252

Israel, G. L., Romano, P., Mangano, V., et al. 2008, ApJ, 685, 1114

Jakobsson, P., Hjorth, J., Fynbo, J. P. U., et al. 2004, ApJL, 617, L21

Jin, Z.-P., Hotokezaka, K., Li, X., et al. 2016, ArXiv e-prints, arXiv:1603.07869

Jonker, P., et al. 2013, arXiv:1306.2336

Kaneko, Y., Preece, R. D., Briggs, M. S., et al. 2006a, ApJS, 166, 298

—. 2006b, ApJS, 166, 298

Kann, D. A., Klose, S., Zhang, B., et al. 2011, ApJ, 734, 96

Kawaguchi, K., Kyutoku, K., Shibata, M., & Tanaka, M. 2016, ArXiv e-prints, arXiv:1601.07711

Kelly, P. L., Filippenko, A. V., Modjaz, M., & Kocevski, D. 2014, ApJ, 789, 23

Kisaka, S., Ioka, K., & Nakar, E. 2016, ApJ, 818, 104

Kistler, M. D., Yüksel, H., Beacom, J. F., Hopkins, A. M., & Wyithe, J. S. B. 2009, ApJL, 705, L104

Kistler, M. D., Yüksel, H., Beacom, J. F., & Stanek, K. Z. 2008, ApJL, 673, L119

Kluźniak, W., & Ruderman, M. 1998, ApJL, 505, L113

Kobayashi, S., Piran, T., & Sari, R. 1997, ApJ, 490, 92

Kocevski, D., & Liang, E. 2006, ApJ, 642, 371

Kocevski, D., West, A. A., & Modjaz, M. 2009, ApJ, 702, 377

Kouveliotou, C., Meegan, C. A., Fishman, G. J., et al. 1993, ApJL, 413, L101

Kowalski, M., & Mohr, A. 2007, Astroparticle Physics, 27, 533

Krivonos, R., Revnivtsev, M., Churazov, E., et al. 2007a, A&A, 463, 957

Krivonos, R., Revnivtsev, M., Lutovinov, A., et al. 2007b, A&A, 475, 775

Krühler, T., Malesani, D., Fynbo, J. P. U., et al. 2015, A&A, 581, A125

Krumholz, M. R. 2012, ApJ, 759, 9

Kumar, P., & Zhang, B. 2015, PhR, 561, 1

Lacombe, K., Pons, R., Amoros, C., et al. 2014, in Proc. SPIE, Vol. 9144, Space Telescopes and Instrumentation 2014: Ultraviolet to Gamma Ray, 914451

Lapi, A., Kawakatu, N., Bosnjak, Z., et al. 2008, MNRAS, 386, 608

Lasky, P. D., Haskell, B., Ravi, V., Howell, E. J., & Coward, D. M. 2014, Physical Review D, 89, 047302

Le, T., & Dermer, C. D. 2007, ApJ, 661, 394

Le Provost, H., Schanne, S., Flouzat, C., et al. 2014, ArXiv e-prints, arXiv:1412.0481

Lebrun, F., Leray, J. P., Lavocat, P., et al. 2003, A&A, 411, L141

Lecavelier des Etangs, A., Bourrier, V., Wheatley, P. J., et al. 2012, A&A, 543, L4

Ledoux, C., Vreeswijk, P. M., Smette, A., et al. 2009, A&A, 506, 661

Levan, A. J., Wynn, G. A., Chapman, R., et al. 2006, MNRAS, 368, L1

Levan, A. J., Tanvir, N. R., Cenko, S. B., et al. 2011, Science, 333, 199

Levan, A. J., Tanvir, N. R., Starling, R. L. C., et al. 2014a, ApJ, 781, 13

Levan, A. J., Tanvir, N. R., Fruchter, A. S., et al. 2014b, ApJ, 792, 115

Li, L.-X. 2008, MNRAS, 388, 1487

Li, L.-X., & Paczyński, B. 1998, ApJL, 507, L59

Li, S.-Z., & Yu, Y.-W. 2016, ApJ, 819, 120

Li, X., Hu, Y.-M., Fan, Y.-Z., & Wei, D.-M. 2016, ArXiv e-prints, arXiv:1601.00180

Li, Z., Dai, Z. G., & Lu, T. 2002, A&A, 396, 303

Liang, E., & Zhang, B. 2005, ApJ, 633, 611

Liang, E., Zhang, B., Virgili, F., & Dai, Z. G. 2007, ApJ, 662, 1111

LIGO Scientific Collaboration, Aasi, J., Abbott, B. P., et al. 2015, Classical and Quantum Gravity, 32, 074001

Liu, R.-Y., & Wang, X.-Y. 2013, ApJ, 766, 73

Lloyd, N. M., Petrosian, V., & Mallozzi, R. S. 2000, ApJ, 534, 227

Lloyd-Ronning, N. M., & Ramirez-Ruiz, E. 2002, ApJ, 576, 101

Loeb, A., & Barkana, R. 2001, Annual Review of Astronomy and Astrophysics, 39, 19

Lorimer, D. R., Bailes, M., McLaughlin, M. A., Narkevic, D. J., & Crawford, F. 2007, Science, 318, 777

LSST Science Collaboration, Abell, P. A., Allison, J., et al. 2009, ArXiv e-prints, arXiv:0912.0201

Lü, H.-J., Liang, E.-W., Zhang, B.-B., & Zhang, B. 2010, ApJ, 725, 1965

Lynden-Bell, D. 1971, MNRAS, 155, 95

MacFadyen, A. I., & Woosley, S. E. 1999, ApJ, 524, 262

Mallozzi, R. S., Paciesas, W. S., Pendleton, G. N., et al. 1995, ApJ, 454, 597

Martineau-Huynh, O., Kotera, K., Bustamente, M., et al. 2016, in European Physical Journal Web of Conferences, Vol. 116, European Physical Journal Web of Conferences, 03005

Mateos, S., Warwick, R. S., Carrera, F. J., et al. 2008, A&A, 492, 51

Mazets, E. P., & Golenetskii, S. V. 1981, Astrophysics and Space Science, 75, 47

McGuire, J. T. W., Tanvir, N. R., Levan, A. J., et al. 2015, ArXiv e-prints, arXiv:1512.07808

Meidinger, N., Andritschke, R., Hälker, O., et al. 2006, Nuclear Instruments and Methods in Physics Research A, 568, 141

Mészáros, P., Asano, K., Murase, K., et al. 2015, ArXiv e-prints, arXiv:1506.02707

Mészáros, P., Ramirez-Ruiz, E., Rees, M. J., & Zhang, B. 2002a, ApJ, 578, 812

—. 2002b, ApJ, 578, 812

Mészáros, P., & Rees, M. J. 1993, ApJL, 418, L59

Mészáros, P., & Waxman, E. 2001, Physical Review Letters, 87, 171102

Metzger, B. D., & Berger, E. 2012, ApJ, 746, 48

Michałowski, M. J., Kamble, A., Hjorth, J., et al. 2012, ApJ, 755, 85

Michałowski, M. J., Gentile, G., Hjorth, J., et al. 2015, A&A, 582, A78

Middleton, M. J., Miller-Jones, J. C. A., Markoff, S., et al. 2013, Nature, 493, 187

Morihana, K., Tsujimoto, M., Yoshida, T., & Ebisawa, K. 2013, ApJ, 766, 14

Motch, C., Pakull, M. W., Soria, R., Grisé, F., & Pietrzyński, G. 2014, Nature, 514, 198

Murase, K., & Ioka, K. 2013, Physical Review Letters, 111, 121102

Murase, K., Ioka, K., Nagataki, S., & Nakamura, T. 2006, ApJL, 651, L5

—. 2008, Physical Review D, 78, 023005

Nasser, G., Godet, O., Atteia, J.-L., et al. 2014, in Proc. SPIE, Vol. 9144, Space Telescopes and Instrumentation 2014: Ultraviolet to Gamma Ray, 91443X

Nava, L., Ghirlanda, G., Ghisellini, G., & Celotti, A. 2011, A&A, 530, A21

Nava, L., Ghisellini, G., Ghirlanda, G., Tavecchio, F., & Firmani, C. 2006, A&A, 450, 471

Nava, L., Salvaterra, R., Ghirlanda, G., et al. 2012, MNRAS, 421, 1256

Norris, J. P., & Bonnell, J. T. 2006, ApJ, 643, 266

Norris, J. P., Marani, G. F., & Bonnell, J. T. 2000, ApJ, 534, 248

Noterdaeme, P., Srianand, R., Rahmani, H., et al. 2015, A&A, 577, A24

Ofek, E. O., Cenko, S. B., Gal-Yam, A., et al. 2007, ApJ, 662, 1129

Olive, J.-F., Hurley, K., Sakamoto, T., et al. 2004, ApJ, 616, 1148

Osten, R. A., Godet, O., Drake, S., et al. 2010, ApJ, 721, 785

Patel, M., Warren, S. J., Mortlock, D. J., & Fynbo, J. P. U. 2010, A&A, 512, L3

Paul, J., Wei, J., Basa, S., & Zhang, S.-N. 2011, Comptes Rendus Physique, 12, 298

Perley, D. A., Levan, A. J., Tanvir, N. R., et al. 2013, ApJ, 778, 128

Perley, D. A., Tanvir, N. R., Hjorth, J., et al. 2016, ApJ, 817, 8

Perna, R., & Belczynski, K. 2002, ApJ, 570, 252

Pescalli, A., Ghirlanda, G., Salafia, O. S., et al. 2015, MNRAS, 447, 1911

Pescalli, A., Ghirlanda, G., Salvaterra, R., et al. 2016, A&A, 587, A40

Petitjean, P., Ledoux, C., Noterdaeme, P., & Srianand, R. 2006, A&A, 456, L9

Petitjean, P., Wang, F. Y., Wu, X. F., & Wei, J. J. 2016, Space Science Reviews, arXiv:1601.04279

Petrosian, V., Kitanidis, E., & Kocevski, D. 2015, ApJ, 806, 44

Piran, T. 1999, , 314, 575

Qin, Y., Liang, E.-W., Liang, Y.-F., et al. 2013, ApJ, 763, 15

Racusin, J. L., Karpov, S. V., Sokolowski, M., et al. 2008, Nature, 455, 183

Rafelski, M., Wolfe, A. M., Prochaska, J. X., Neeleman, M., & Mendez, A. J. 2012, ApJ, 755, 89

Rahmani, H., Wendt, M., Srianand, R., et al. 2013, MNRAS, 435, 861

Ramirez-Ruiz, E., Celotti, A., & Rees, M. J. 2002, MNRAS, 337, 1349

Ramirez-Ruiz, E., & Fenimore, E. E. 2000, ApJ, 539, 712

Raskin, C., Scannapieco, E., Rhoads, J., & Della Valle, M. 2008, ApJ, 689, 358

Rees, M. J., & Mészáros, P. 1994, ApJL, 430, L93

—. 2005, ApJ, 628, 847

Reichart, D. E., Lamb, D. Q., Fenimore, E. E., et al. 2001, ApJ, 552, 57

Revnivtsev, M., Sazonov, S., Krivonos, R., Ritter, H., & Sunyaev, R. 2008, A&A, 489, 1121

Revnivtsev, M. G. 2014, Astronomy Letters, 40, 667

Risaliti, G., Nardini, E., Salvati, M., et al. 2011, MNRAS, 410, 1027

Robertson, B. E., & Ellis, R. S. 2012, ApJ, 744, 95

Robertson, B. E., Ellis, R. S., Furlanetto, S. R., & Dunlop, J. S. 2015, ApJL, 802, L19

Rodriguez, J., Hannikainen, D. C., Shaw, S. E., et al. 2008, ApJ, 675, 1436

Rodriguez, J., Cadolle Bel, M., Alfonso-Garzón, J., et al. 2015, A&A, 581, L9

Rowlinson, A., O'Brien, P. T., Metzger, B. D., Tanvir, N. R., & Levan, A. J. 2013, MNRAS, 430, 1061

Sakamoto, T., Lamb, D. Q., Kawai, N., et al. 2005, ApJ, 629, 311

Salvaterra, R. 2015, Journal of High Energy Astrophysics, 7, 35

Salvaterra, R., & Chincarini, G. 2007, ApJL, 656, L49

Salvaterra, R., Campana, S., Vergani, S. D., et al. 2012a, ApJ, 749, 68

—. 2012b, ApJ, 749, 68

Schaefer, B. E. 2003, ApJL, 583, L71

—. 2004, ApJ, 602, 306

—. 2007, ApJ, 660, 16

Schanne, S., Cordier, B., Atteia, J.-L., et al. 2015, ArXiv e-prints, arXiv:1508.05851

Schanne, S., Le Provost, H., Kestener, P., et al. 2014, ArXiv e-prints, arXiv:1411.7810

Schechter, P. 1976, ApJ, 203, 297

Schulze, S., Chapman, R., Hjorth, J., et al. 2015, ApJ, 808, 73

Skrutskie, M. F., Cutri, R. M., Stiening, R., et al. 2006, , 131, 1163

Soldi, S., Beckmann, V., Baumgartner, W. H., et al. 2014, A&A, 563, A57

Soltan, A. 1982, MNRAS, 200, 115

Sparre, M., Hartoog, O. E., Krühler, T., et al. 2014, ApJ, 785, 150

Spruit, H. C., Daigne, F., & Drenkhahn, G. 2001, A&A, 369, 694

Stacy, A., Bromm, V., & Loeb, A. 2011, MNRAS, 413, 543

Stanway, E. R., Levan, A. J., Tanvir, N. R., Wiersema, K., & van der Laan, T. P. R. 2015, ApJL, 798, L7

Steinle, H. 2010, , 27, 431

Sun, H., Zhang, B., & Li, Z. 2015, ApJ, 812, 33

Svensson, K. M., Levan, A. J., Tanvir, N. R., Fruchter, A. S., & Strolger, L.-G. 2010, MNRAS, 405, 57

Taboada, I., & Gilmore, R. C. 2014a, Nucl. Instrum. Meth., A742, 276

—. 2014b, Nucl. Instrum. Meth., A742, 276

Tanvir, N. R., Levan, A. J., Fruchter, A. S., et al. 2013, Nature, 500, 547

—. 2012, ApJ, 754, 46

Thöne, C. C., Fynbo, J. P. U., Goldoni, P., et al. 2013, MNRAS, 428, 3590

Tiengo, A., Esposito, P., Mereghetti, S., et al. 2013, Nature, 500, 312

Tierney, D., McBreen, S., Preece, R. D., et al. 2013, A&A, 550, A102

Totani, T. 1997, ApJL, 486, L71

Trenti, M., Perna, R., & Jimenez, R. 2015, ApJ, 802, 103

Trenti, M., Perna, R., Levesque, E. M., Shull, J. M., & Stocke, J. T. 2012, ApJL, 749, L38

Trenti, M., Perna, R., & Tacchella, S. 2013, ApJL, 773, L22

Türler, M., Chernyakova, M., Courvoisier, T. J.-L., et al. 2010, A&A, 512, A49

Ueda, Y., Akiyama, M., Hasinger, G., Miyaji, T., & Watson, M. G. 2014, ApJ, 786, 104

van der Horst, A. J., Kouveliotou, C., Gehrels, N., et al. 2009, ApJ, 699, 1087

van Haarlem, M. P., Wise, M. W., Gunst, A. W., et al. 2013, A&A, 556, A2

Vangioni, E., Goriely, S., Daigne, F., François, P., & Belczynski, K. 2016, MNRAS, 455, 17

Vangioni, E., Olive, K. A., Prestegard, T., et al. 2015, MNRAS, 447, 2575

Vergani, S. D., Salvaterra, R., Japelj, J., et al. 2015, A&A, 581, A102

Vestrand, W. T., Wren, J. A., Panaitescu, A., et al. 2014, Science, 343, 38

Vietri, M. 1995, ApJ, 453, 883

Vietri, M., & Stella, L. 1999, ApJL, 527, L43

Virgili, F. J., Zhang, B., Nagamine, K., & Choi, J.-H. 2011, MNRAS, 417, 3025

Virgili, F. J., Mundell, C. G., Pal'shin, V., et al. 2013, ApJ, 778, 54

Vreeswijk, P. M., Ledoux, C., Smette, A., et al. 2007, A&A, 468, 83

Vreeswijk, P. M., Ledoux, C., Raassen, A. J. J., et al. 2013, A&A, 549, A22

Wang, F. Y. 2013, A&A, 556, A90

Wang, F. Y., & Dai, Z. G. 2009, MNRAS, 400, L10

—. 2011, ApJL, 727, L34

Wang, F. Y., Dai, Z. G., & Liang, E. W. 2015, NewAR, 67, 1

Wang, X.-Y., Razzaque, S., Mészáros, P., & Dai, Z.-G. 2007, Physical Review D, 76, 083009

Waxman, E. 1995, Physical Review Letters, 75, 386

Waxman, E., & Bahcall, J. 1997, Physical Review Letters, 78, 2292

Waxman, E., & Bahcall, J. N. 2000, ApJ, 541, 707

Wehrle, A. E., Marscher, A. P., Jorstad, S. G., et al. 2012, ApJ, 758, 72

Wei, J.-J., Hao, J.-M., Wu, X.-F., & Yuan, Y.-F. 2016, Journal of High Energy Astrophysics, 9, 1

Wheeler, J. C., Yi, I., Höflich, P., & Wang, L. 2000, ApJ, 537, 810

Wijers, R. A. M. J., Bloom, J. S., Bagla, J. S., & Natarajan, P. 1998, MNRAS, 294, L13

Wolf, C., & Podsiadlowski, P. 2007, MNRAS, 375, 1049

Woosley, S. E. 1993, ApJ, 405, 273

Wu, S.-W., Xu, D., Zhang, F.-W., & Wei, D.-M. 2012, MNRAS, 423, 2627

Yang, B., Jin, Z.-P., Li, X., et al. 2015, Nature Communications, 6, 7323

Yonetoku, D., Murakami, T., Nakamura, T., et al. 2004a, ApJ, 609, 935

—. 2004b, ApJ, 609, 935

Yu, H., Wang, F. Y., Dai, Z. G., & Cheng, K. S. 2015a, ApJS, 218, 13

Yu, Y. B., Huang, Y. F., Wu, X. F., Xu, M., & Geng, J. J. 2015b, ApJ, 805, 88

Yüksel, H., Kistler, M. D., Beacom, J. F., & Hopkins, A. M. 2008, ApJL, 683, L5

Zhang, B. 2006, Nature, 444, 1010

Zhang, B., Fan, Y. Z., Dyks, J., et al. 2006, ApJ, 642, 354

Zhang, B., & Yan, H. 2011, ApJ, 726, 90

Zhang, B., Zhang, B.-B., Liang, E.-W., et al. 2007, ApJL, 655, L25

Zhang, B., Zhang, B.-B., Virgili, F. J., et al. 2009, ApJ, 703, 1696

Zhang, B.-B., Zhang, B., Murase, K., Connaughton, V., & Briggs, M. S. 2014, ApJ, 787, 66

Zhang, W., Woosley, S. E., & MacFadyen, A. I. 2003, ApJ, 586, 356

Zhao, D., Cordier, B., Sizun, P., et al. 2012, Experimental Astronomy, 34, 705